

Chemical Habitability: Supply and Retention of Life's Essential Elements During Planet Formation

Sebastiaan Krijt

School of Physics and Astronomy, University of Exeter, Stocker Road, Exeter EX4 4QL, UK (s.krijt@exeter.ac.uk)

Mihkel Kama

Department of Physics and Astronomy, University College London, Gower Street, London, WC1E 6BT, UK
Tartu Observatory, University of Tartu, Observatooriumi 1, Tõravere, 61602, Estonia

Melissa McClure

Leiden Observatory, Leiden University, 2300 RA Leiden, the Netherlands

Johanna Teske

Earth and Planets Laboratory, Carnegie Institution for Science, 5241 Broad Branch Road, NW, Washington, DC 20015, USA

Edwin A. Bergin

Department of Astronomy, University of Michigan, 323 West Hall, 1085 S. University Avenue, Ann Arbor, MI 48109, USA

Oliver Shorttle

Institute of Astronomy & Department of Earth Sciences, University of Cambridge, UK

Kevin J. Walsh

Department of Space Studies, Southwest Research Institute, 1050 Walnut St., Boulder, CO 80302, USA

Sean N. Raymond

Laboratoire d'Astrophysique de Bordeaux, Univ. Bordeaux, CNRS, B18N, All. Geoffroy Saint-Hilaire, 33615 Pessac, France

Carbon, Hydrogen, Nitrogen, Oxygen, Phosphorus and Sulfur (CHNOPS) play key roles in the origin and proliferation of life on Earth. Given the universality of physics and chemistry, not least the ubiquity of water as a solvent and carbon as a backbone of complex molecules, CHNOPS are likely crucial to most habitable worlds. To help guide and inform the search for potentially habitable and ultimately inhabited environments, we begin by summarizing the CHNOPS budget of various reservoirs on Earth, their role in shaping our biosphere, and their origins in the Solar Nebula. We then synthesize our current understanding of how these elements behave and are distributed in diverse astrophysical settings, tracing their journeys from synthesis in dying stars to molecular clouds, protoplanetary settings, and ultimately temperate rocky planets around main sequence stars. We end by identifying key branching points during this journey, highlighting instances where a forming planets' distribution of CHNOPS can be altered dramatically, and speculating about the consequences for the chemical habitability of these worlds.

1. INTRODUCTION

Almost three decades have passed since the discovery of the first exo-planet around a main sequence star. Children born after the publication of *Mayor and Queloz* (1995) are now finishing their PhDs in rapidly evolving and maturing fields like astrobiology and exoclimatology. It will be up to them to use the next generation of ground-based and space-

based observatories to search for and identify existing biospheres on nearby planets and provide a satisfactory answer to the question that has been on everyone's mind since 1995 (and before): *Are we alone in the universe?*

This next generation of scientists has evolved from organisms that first appeared on Earth perhaps within a few 100 Myr of the Moon-forming impact, arguably the last step in the assembly of Earth some 4.56 Gyr ago. All life on

Earth requires a solvent (water), energy (light from the Sun and redox chemical energy), and a series of bio-essential elements (carbon, hydrogen, nitrogen, oxygen, phosphorus, sulfur – hereafter “CHNOPS” – to construct molecules and polymers with a range of shapes, properties, and uses (Baross et al. 2020; Sasselov et al. 2020). Given the abundance of these elements in the Galactic disk, it can be argued that life originating elsewhere will make use of similar ingredients (Hoehler et al. 2020).

To help guide and inform the search for potentially habitable and ultimately inhabited environments, it is then useful to consider where these similar ingredients can come together as the result of planet formation and planet evolution (Des Marais et al. 2008; Zahnle and Carlson 2020). A lot of attention has been given to the (classical) Habitable Zone (Kasting et al. 1993), the region around a star where a planet (with some assumed properties and atmospheric make-up) could host liquid water on its surface. Even though the boundaries depend on the properties of said hypothetical planet (e.g. Kopparapu et al. 2013), the habitable zone is primarily an attribute of the central star. See Kaltenegger (2017) for a recent discussion of what properties of stars and mature planets define their habitable zones.

Here, we synthesize the state-of-the-art in understanding how universal cosmic processes form worlds with potentially habitable compositions. We use the term *chemical habitability*, an inherent property of planets distinct from the largely externally-constrained classical habitable zone concept. A world that is chemically habitable has: 1) a supply of carbon, hydrogen, nitrogen, oxygen, phosphorus, sulfur (“CHNOPS”), and other bio-essential elements that are accessible to prebiotic chemistry (Rimmer and Shorttle 2019; Sasselov et al. 2020), and 2) is capable of maintaining the availability of the CHNOPS elements over relevant geologic timescales. So defined, the chemical habitability of a world is built upon the distribution and cycling of its CHNOPS elements; features of a planet that are conditional upon the earliest phases of planet formation, right through to its present tectonic state.

State-of-the-art remote sensing observations of increasingly smaller exo-planets can be combined to provide information about their bulk densities, atmospheric properties, and orbital parameters. Architectures of multi-planet systems can be studied and compared, and planet occurrence rates can be estimated and improved, especially for the most easy-to-spot planets (Currie et al.; Lissauer et al.; Weiss et al., this volume). However, at present challenges arising from the presence of clouds and hazes (e.g., Crossfield and Kreidberg 2017; Gao et al. 2021; Barstow 2021), stellar activity (e.g., Dumusque et al. 2017; Rackham et al. 2018; Collier Cameron 2018; Cegla 2019; Iyer and Line 2020; Mayorga et al. 2021), and degeneracies associated from fitting interior models to a single bulk density (e.g., Dorn et al. 2015; Grimm et al. 2018; Plotnykov and Valencia 2020) prevent the detailed characterisation of the CHNOPS budget on/in terrestrial planet analogs.

Important additional context comes from an increasingly

sophisticated view of how planetary systems form. Much of the progress since *Protostars & Planets VI* has been driven by observations. Apart from the discovery of new exoplanet classes that had to be explained (Hot Jupiters, Mini-Neptunes, etc.), facilities like Herschel and ALMA have revolutionized our understanding of the reservoirs of atoms, molecules, and dust grains in protostellar and protoplanetary systems on spatial scales comparable to the size of the solar system (Manara et al.; Miotello et al.; Benisty et al., this volume). Indirect (Pinte et al., this volume) and direct (Keppler et al. 2018; Haffert et al. 2019) evidence of accreting giant planets embedded in young gas-rich disks has been found. High-resolution observations of dozens of systems can be arranged to outline evolutionary sequences (Garufi et al. 2018; Cieza et al. 2021) and compared to exoplanet demographics (van der Marel and Mulders 2021; Mulders et al. 2021). Driven by these observations, new ideas in planet formation theory have rapidly been developed and embraced. Modern planet formation theory now presents an unbroken chain of processes connecting the raw materials (e.g. dust, gas) in protostellar systems to fully-formed planets (e.g. Drażkowska et al., Lesur et al., Paardekooper et al. this volume).

In some cases, findings may appear to alienate our Earth and Solar System from the rest of the Galaxy. For example, cold Jupiters are fairly rare, even amongst FGK stars (Raymond et al. 2018b), and super Earths, the planet type most common in the Galaxy (Fulton et al. 2017), is absent here. At the same time, many perhaps unexpected connections between astronomical observations/theory and Solar System studies have appeared: the idea of Jupiter separating material reservoirs in the early solar nebula (Kruijer et al. 2017) resembles closely the planetary interpretation of abundant substructures seen with ALMA (Andrews 2020); convincing evidence for the streaming instability route to planetesimal formation (Johansen et al. 2014) was found in our own Kuiper Belt (Nesvorný et al. 2019; McKinnon et al. 2020); and pebble accretion models are now frequently invoked to explain the rapid growth of the Solar System’s giant (Johansen and Lambrechts 2017; Alibert et al. 2018) and even terrestrial planets (Johansen et al. 2021). In-person visits from interloping interstellar planetesimals/comets like 1I/Oumuamua (Meech et al. 2017) and 2I/Borisov (Jewitt and Luu 2019) are perhaps the most poetic examples of overlap between planet formation at home and abroad.

We begin this review of chemical habitability by discussing the distribution and origin of CHNOPS on Earth (Sect. 2), and the origin and variation of CHNOPS in other stars (Sect. 3). In Sect. 4 we highlight observed links between exo-planet properties and host star properties related broadly to chemical habitability, and in Sects. 5 and 6 discuss the varied behavior of CHNOPS en route to and during planet formation. Finally, in Sect. 7 we summarize and assess what we view as key branching points in the formation of chemically habitable terrestrial planets. Our focus is on temperate rocky worlds near the habitable zones of (single)

main sequence stars, but as we will see understanding these planets' CHNOPS budgets requires a holistic treatment of the formation of entire planetary systems.

2. TRACING THE EARTH'S INGREDIENTS BACK THROUGH TIME

The Earth provides a key constraint on how planets may attain chemical habitability. Here is a planet where, in principle, we can do the accounting: CHNOPS fluxes between reservoirs can be measured, and the reservoirs themselves probed directly, or indirectly, for budgetary estimates (Sect. 2.1). Reaching further back in time, fossil evidence places earliest life as being older than 3.5 Ga (Schopf 2006), with more controversial observations from the rock record and molecular clock analysis placing it even earlier, perhaps 3.7–4.1 Ga (Bell et al. 2015; Nutman et al. 2016; Betts et al. 2018). These older ages push the emergence of life into the Hadean eon and by necessity then also the point in time when Earth's chemical habitability was established. Only a few hundred million years earlier than this was the moon forming impact (Jacobson et al. 2014; Maurice et al. 2020), and Earth's history grades into that of the wider solar system (Sect. 2.2), as the remnants of planet formation were swept up by the larger planets. This is a key period in which the earlier CHNOPS losses, from the tenuous atmospheres of precursory planetary embryos, may have been made up for in the 'late accretion' of undifferentiated (i.e., only mildly heated) objects. Earlier still and Earth's history fragments into its innumerable building blocks and ultimately back to the nebular processes that set the stage for planet formation (Sect. 2.3).

2.1. The importance and distribution of CHNOPS on Earth

Much of what makes Earth the precious 'pale blue dot' (Sagan 1997) can be attributed to the CHNOPS elements. Clearly these elements are of central importance to the biosphere – at an elemental level these elements *are* the biosphere. However, CHNOPS also play a fundamental role in the abiotic dynamics of the modern Earth, from processes at the top of the atmosphere into our planet's core. This is evident from Tables 1 & 2, which list estimates for the budgets of CHNOPS in terrestrial reservoirs from the surface atmosphere-biosphere-hydrosphere, into the planet's silicate crust-lithosphere-mantle, and finally in the core. With the exception of P in the atmosphere, CHNOPS are pervasively distributed throughout the Earth system, and are capable of having a major impact on planetary dynamics at even part per million concentrations (e.g., as with carbon and greenhouse warming of the atmosphere). The chemical properties of CHNOPS (less so P) distinguish them from the major Fe-O-Mg-Si-Ca-Al elemental building blocks of the Earth (where O is a special case; McDonough and Sun 1995), which are bound in mineral form. Properties of the biotic and abiotic Earth therefore have a common dependence on CHNOPS, a dependence that is likely to be

replicated on habitable and inhabited planets throughout the Galaxy (e.g., Cockell et al. 2021). In this section we review some of the non-biological planetary processes CHNOPS are involved in that are key for setting planetary habitability (section 2.1.1), before moving onto the distribution and history of CHNOPS redistribution on Earth (section 2.1.2).

2.1.1. Why being 'Earth-like' requires CHNOPS

Earth is unique in a solar system context and, given what we know presently, in an exoplanetary context (Lissauer et al., this volume). Indeed, our knowledge of Earth is so detailed and specific that the concept of 'Earth-like' requires generalisation to be of any use to exoplanetary sciences (Shorttle et al. 2021). The minimalist definition captured by η_{\oplus} in Bryson et al. (2020) (orbital period and radius within 20% of Earth's) implies maybe 1 in 50 GK stars host an 'Earth'. However, a planet being 'Earth-like' still allows much room for non-Earth-like conditions on and inside the planet, differences that will very likely be rooted in a planet's divergent history of CHNOPS gain and distribution. Here, we emphasise two standout aspects of the modern Earth, its geodynamic mode of plate tectonics and its carbon cycle, phenomena habitable planets may be universally required to possess (Ehlmann et al. 2016), and which both are intimately coupled to CHNOPS.

Plate tectonics: This is an elegant theory that emerged in the mid-twentieth century to describe the long-term motions of Earth's surface, that the surface moves as rigid 'plates', being destroyed at trenches (subduction zones) and formed at mid-ocean ridges (McKenzie and Parker 1967; Morgan 1968). Despite this apparent simplicity, plate tectonics is the beating heart of our planet, connecting the evolution of the deepest mantle to the atmosphere and biosphere. It does this by enabling the cycling of huge masses of material, $\sim 10^{15} \text{ kg yr}^{-1}$, through mid-ocean ridge melting regions and subduction zones, allowing CHNOPS fluxes out of (at mid-ocean ridges and arc volcanoes) and into (at subduction zones) the Earth's interior (Fig. 1). This plate tectonic flux of material is large enough that, if sustained over 4.5 Gyr, it will process the entire silicate portion of the planet. Crucially for habitability, plate tectonics allows CHNOPS elements to be removed from the surface environment for hundred-million-year timescales by sequestration into our planet's interior, *and* allows for their restoration by degassing during mountain building and magmatism (Fig. 1). This provides a mechanism whereby accumulation of e.g., CO_2 , O_2 , SO_2 , and H_2O at the Earth's surface can be regulated by their drawdown into mineral form for longterm storage, but with the potential for re-release if their reservoir is subsequently embroiled in mountain building or magmatism: high temperature processes that drive volatile elements like C, H, N, O, and S, and elements like P with chemical affinity for melts, back to the surface.

The cycling of CHNOPS, sustained by plate tectonics on Earth, may be very different under other planetary geodynamic regimes (Fig. 1, left vs. right). On stagnant lid plan-

TABLE 1
THE C-H-N BUDGET OF THE EARTH¹

Reservoir ²	Reservoir mass			C		H			N		
	(kg)	(M _⊕)	(kg)	%C _{BE}	(M _{atm})	(kg)	%H _{BE}	(M _{ocean})	(kg)	%N _{BE}	(M _{atm})
Atmosphere	5.2×10^{18}	10^{-6}	8.8×10^{14}	10^{-5}	1	1.3×10^{14}	10^{-5}	10^{-6}	4.0×10^{18}	14	1
Biosphere	1.1×10^{16}	10^{-9}	5.5×10^{15}	10^{-4}	6.3	2.8×10^{12}	10^{-7}	10^{-8}	9.7×10^{14}	10^{-4}	10^{-4}
Hydrosphere	1.6×10^{21}	10^{-4}	3.8×10^{17}	10^{-2}	430	1.8×10^{20}	14	1	2.4×10^{16}	10^{-2}	10^{-2}
Crust	2.0×10^{22}	10^{-3}	7.1×10^{19}	1	10^5	3.5×10^{19}	3	0.19	2.3×10^{18}	1	0.58
Lithosphere	1.4×10^{23}	0.02	$\approx 6.0 \times 10^{19}$	1	10^5	$\approx 3.9 \times 10^{17}$	10^{-2}	10^{-3}	$\approx 6.0 \times 10^{18}$	2	1.5
Shallow mantle	9.4×10^{23}	0.16	3.5×10^{19}	10^{-1}	10^4	1.6×10^{19}	1	0.09	7.2×10^{18}	3	1.8
Deep mantle	2.9×10^{24}	0.49	$\approx 2.9 \times 10^{21\dagger}$	39	10^6	$\approx 3.3 \times 10^{20\dagger}$	26	1.8	$\approx 1.7 \times 10^{19\dagger}$	6	4.3
Core	1.9×10^{24}	0.33	$\approx 4.4 \times 10^{21\dagger}$	59	10^7	$\approx 7.2 \times 10^{20\dagger}$	56	4	$\approx 2.4 \times 10^{20\dagger}$	87	60
<i>Totals</i>											
BSE	4.03×10^{24}	0.675	3.1×10^{21}	41	3×10^6	5.6×10^{20}	44	3	3.7×10^{19}	13	9
Bulk Earth	5.97×10^{24}	1	7.5×10^{21}		9×10^6	1.3×10^{21}		7	2.8×10^{20}		70

¹BSE = Bulk silicate Earth. \approx indicate mass estimates with significant uncertainty, \dagger indicating those that also impact our understanding of the total CHNOPS budget of the Earth, and by implication the processes that will distribute the elements among planetary reservoirs more generally. References for compiling reservoir estimates, C: *Bar-On et al.* (2018); *Sleep and Zahnle* (2001); *Sleep* (2009); *Le Voyer et al.* (2017); *Marty* (2012); *Dasgupta* (2013); H: *Lécuyer et al.* (1998); *Hirschmann and Kohlstedt* (2012); *Wu et al.* (2018); and N: *Johnson and Goldblatt* (2015)

²The crust represents the sum of the oceanic and continental crust. The lithosphere is the sub-continental lithospheric mantle, i.e., the long-lived and non-convecting part of the mantle reservoir. The ‘shallow mantle’ represents the convecting mantle sampled by mid-ocean ridge volcanism, the mantle above the mantle transition zone at 670 km depth. The ‘Deep mantle’ is then all the silicate Earth below the transition zone. The bulk silicate Earth is all terrestrial reservoirs outside of the core, i.e., that are ultimately accessible to life and the surface environment.

TABLE 2
THE O-P-S BUDGET OF THE EARTH¹

Reservoir	O ²			P			S		
	(kg)	%O _{BE}	(M _{atm})	(kg)	%P _{BE}	(M _{ocean})	(kg)	%S _{BE}	(M _{atm})
Atmosphere	1.2×10^{18}	10^{-4}	1	—	—	—	4.8×10^9	10^{-11}	10^{-9}
Biosphere	4.4×10^{15}	10^{-6}	10^{-3}	1.3×10^{14}	10^{-6}	1	1.1×10^{13}	10^{-8}	10^{-5}
Hydrosphere	2.5×10^{18}	10^{-3}	2	1.3×10^{14}	10^{-6}	1	1.3×10^{18}	10^{-3}	1
Crust	8.2×10^{19}	10^{-2}	70	6.3×10^{18}	10^{-1}	10^4	8.4×10^{18}	10^{-2}	6.5
Lithosphere	$\approx 4.8 \times 10^{19}$	10^{-2}	40	$\approx 9.1 \times 10^{18}$	10^{-1}	10^5	2.1×10^{19}	10^{-1}	16
Shallow mantle	3.9×10^{20}	10^{-1}	300	4.6×10^{19}	1	10^5	1.4×10^{20}	10^{-1}	100
Deep mantle	$\approx 1.2 \times 10^{21}$	10^{-1}	10^3	3.0×10^{20}	6	10^6	8.4×10^{20}	3	600
Core	-4.8×10^{23}	10^2	-10^5	$\approx 4.9 \times 10^{21\dagger}$	93	10^7	$\approx 2.9 \times 10^{22\dagger}$	97	10^4
<i>Totals</i>									
BSE	1.7×10^{21}	10^{-1}	1×10^3	3.6×10^{20}	7	3×10^6	1×10^{21}	3	800
Bulk Earth	-4.8×10^{23}		-4×10^5	5.2×10^{21}		4×10^7	3×10^{22}		2×10^4

¹BSE = Bulk silicate Earth. \approx indicate mass estimates with significant uncertainty, \dagger indicating those that also impact our understanding of the total CHNOPS budget of the Earth, and by implication the processes that will distribute the elements among planetary reservoirs more generally. References for compiling reservoir estimates, O: *Lécuyer and Ricard* (1999); *Workman and Hart* (2005); *Hirose et al.* (2013); *McDonough and Sun* (1995); P: *Rudnick and Gao* (2014); *White et al.* (2014); *Rudnick et al.* (1998); *Workman and Hart* (2005); *McDonough and Sun* (1995); and S: *Brimblecombe* (2013); *Rudnick and Gao* (2014); *Lorand et al.* (2003); *McDonough and Sun* (1995); *Hirose et al.* (2013)

²Oxygen is counted here as oxygen required to move the system to the reference redox state (e.g., following *Evans* (2006)); when oxygen removal is required this is counted as a positive number (as the system contains oxygen compared to the reference state) and oxygen addition being counted as a negative number (as the system is lacking oxygen compared to the reference state). For the atmosphere the reference state is defined as an oxygen-free atmosphere; for the biosphere the reference state is oxygen-free organic matter; for the hydrosphere this is dioxygen-free seawater (i.e., counting the small amount of dissolved oxygen in seawater) and neutral sulfur (counting the large amount of oxygen in sulfate); for the silicate portions of the planet (crust, lithosphere, convecting mantle, and core), we focus on the oxidation state of Fe, as the dominant multi-valent element. The reference state we choose is Fe²⁺O, with reservoirs either being more oxidised if they contain Fe³⁺, or reduced if they contain Fe-metal (Fe⁰). The core’s negative oxygen abundance occurs because the reducing power of its metallic iron overwhelms the small amount of oxygen it may contain.

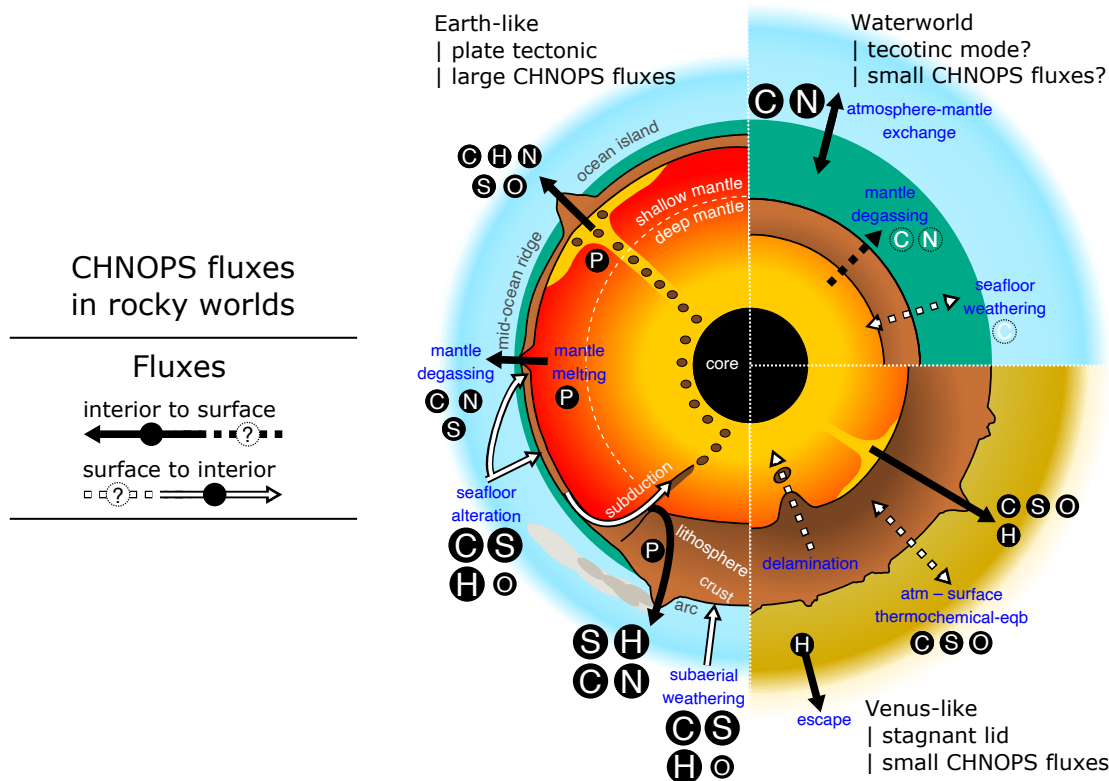


Fig. 1.—: Abiotic CHNOPS fluxes on mature rocky worlds. Left, fluxes on an Earth-like planet, with plate tectonics, a hydrosphere, and a low-mass atmosphere. Top right, fluxes on a water world planet. Bottom right, fluxes on Venus-like planets, with high surface temperatures, dry atmospheres, and stagnant lid tectonics. Black arrows indicate fluxes from the interior to surface, white arrows indicate fluxes from the surface to the interior, black symbols with element names indicate the elements involved in the process, with larger circles indicative of larger fluxes. Dotted arrows and hollow symbols indicate uncertain fluxes (e.g., for many of the CHNOPS fluxes on water worlds).

ets, of which modern Venus is likely an example, the thick lithosphere (the non-convecting ‘lid’ of the planet) can only exchange with the interior by blobbing off at the bottom (‘delamination’), whilst volcanic degassing from the interior is suppressed. Limited volcanic degassing on Venus is evidenced by the planet’s atmospheric argon (Ar) inventory. Argon can trace the time integrated degassing of planetary mantles because ^{40}Ar is produced *in rocks* by ^{40}K decay: as K is a lithophile element present in a planet’s rocks, the ^{40}Ar decay product is also trapped there unless the rocks melt and that melt is transported to the surface. Therefore, the degree to which the ^{40}Ar in a planet has been able to escape to the atmosphere constrains the efficiency of melting of the planet’s interior. Venus’s atmosphere is observed to contain less radiogenic ^{40}Ar than Earth’s atmosphere, which given an inferred K abundance in the planet suggests it has experienced less volcanic input to its atmosphere than Earth (Kaula 1999).

Combined, lower rates of volcanism and inefficient recycling of surface material to the planet’s interior may limit the efficiency of long-term chemical cycling on stagnant lid planets. Although modelling has suggested stagnant lid planets may be able to sustain habitability for Gyr

timescales (e.g., Tosi *et al.* 2017; Foley and Smye 2018), the effectiveness of the processes involved in this remain highly uncertain. Further study of Venus, and new constraints on its early history, offer a prime opportunity for solar system sciences to inform exoplanet habitability (Kane *et al.* 2021).

Whilst the above suggests that plate tectonics is important for chemical habitability (i.e., CHNOPS), Venus also exemplifies how CHNOPS may be important for plate tectonics. A central aspect of plate tectonic theory is that the deformation associated with the creation and destruction of the plates is localised. The epitome of localised deformation is the fault, those fractures in the Earth’s crust responsible for seismicity that allow two blocks of crust to slide past each other. In the absence of water, faults would have to move at their dry frictional strength of over 700 MPa (Amiguet *et al.* 2012). This stress is so large that plate tectonics could be entirely suppressed, resulting in a single unbroken plate (a stagnant lid). However, the presence of water is able to decrease fault strength, both forming low-friction hydrous mineral phases and hydraulically opening the fault (Amiguet *et al.* 2012; Sleep and Blanpied 1992). Hence, plate tectonics has a role in sustaining surface water inventories, and is itself sustained by the presence of water.

This connection between water and tectonics reaches all the way to Earth's core and the creation of the magnetic field, which on Earth-mass planets is likely enabled by plate tectonics's effective extraction of heat from the planet's interior (Nimmo 2002) — with the magnetic field helping preserve a planet's surface liquid water inventory by offering enhanced protection against solar wind-driven water loss (e.g., Lundin et al. 2007).

Carbon cycle: Earth is the only rocky planet in the solar system with a functioning carbon cycle (sketched in Fig. 1). On Venus, carbon released from the planet's interior is on a one way journey to its atmosphere, where it has so far accumulated ~ 90 bar of CO_2 , whilst on Mars, the tenuous atmosphere is so cold CO_2 condenses and is unable to support temperate conditions. Although Earth's carbon cycle is heavily influenced by biology, and may have been so for billions of years, carbon is likely central to achieving environmental homeostasis even on abiotic worlds (Kasting et al. 1993). A key insight exoplanets can provide is how effective this abiotic carbon cycle is (Lehmer et al. 2020), whether it is indeed effective in the absence of biology, and how robust it is to changing planetary regimes, e.g., the water-worlds, which may be common outcomes of planet formation (Fig. 1; Kite and Ford 2018; Foley and Smye 2018; Lichtenberg et al. 2019).

However, the carbon cycle is not just reliant on a planet's inventory of C. The geochemical cycle removing carbon from the atmosphere requires abundant liquid water to enable the silicate weathering reaction, in which 2 moles of CO_2 dissolve to produce carbonic acid, which reacts with rocks, and ultimately sequesters one mole of that CO_2 in mineral form as carbonate (Urey 1952). The sensitivity of this reaction to temperature, via kinetics and rainfall (Walker et al. 1981; Maher and Chamberlain 2014), creates homeostatic feedback whereby increasing temperatures driven by CO_2 greenhouse forcing increases the rate of reactions that remove CO_2 from the atmosphere. Though CO_2 - H_2O are at the centre of climate regulation on the modern Earth, it is also important to note the direct climate role of other CHON species (but likely not P or S). Early in its history Earth was faced with a 'faint young sun' problem, in that the $\sim 70\%$ weaker light from the young sun would have been insufficient, given Earth's present atmosphere, to maintain liquid water at its surface Sagan and Mullen (1972). The abundance of CHON gas species in Earth's early atmosphere is central to solving this problem and reconciling the geological record of liquid water with climate models. High CH_4 and CO_2 concentrations and/or a combination of N_2 - H_2 warming may have sustained habitable conditions on the early (possibly pre-biotic) Earth (Calling and Zahnle 2020; Wordsworth and Pierrehumbert 2013).

2.1.2. Earth's CHNOPS through space and time

To understand what is required for chemical habitability it is essential to know the distribution of CHNOPS on the modern Earth. The budgets of major planetary reservoirs

are listed in Tables 1 & 2, and below we discuss the key factors governing their distribution and redistribution.

Carbon: Most of Earth's carbon is likely in its core, which results from carbon acting as a siderophile element at the high pressures at which metal-silicate segregation took place on Earth (Dasgupta 2013): i.e., carbon has a strong affinity for metallic phases rather than silicate oxide phases in the extreme conditions of planetary interiors. However, this carbon is inaccessible during subsequent planetary evolution, so the core's key role occurs early by setting the proportion of the total planetary C inventory available for subsequent distribution and cycling among terrestrial reservoirs. In 'accessible', i.e., silicate Earth, the overwhelming majority of carbon is stored in the mantle as carbonate (shallow mantle), metal-sulfur alloys (Zhang et al. 2019), and diamond (deep mantle; Dasgupta 2013). The amount present in the deep mantle has large uncertainties (Miller et al. 2019; Marty et al. 2020). Mantle carbon is supplied to the atmosphere when melting occurs; carbon has a strong affinity for silicate liquids over minerals (Rosenthal et al. 2015), meaning it enters magmas and the magma migrates to the surface where carbon's volatile nature drives it into the gas phase and thereby the ocean-atmosphere system. The efficacy of silicate weathering in removing this volcanic carbon from Earth's atmosphere is evidenced by the very small amount of Earth's carbon inventory that the atmosphere contains and the large crustal carbon pool it overlies: 10^5 times the present atmospheric inventory, an amount that if put back into the atmosphere would give Earth a Venus-like ~ 100 bar CO_2 atmosphere (Table 1).

Hydrogen: Unlike for carbon, the surface environment is a major reservoir of hydrogen on Earth, where it is present in oxide form as water. Earth has been able to retain surface water over its history, unlike Venus, because of the stratospheric cold trap that prevents water molecules reaching a height in the atmosphere where photodissociation can produce H atoms that are light enough to escape to space. Water interacts with the crust and produces hydrous mineral phases with structurally bound hydrogen, which have formed a significant reservoir of Earth's surface water ($\sim 15\%$) being locked in the crust (Lécuyer et al. 1998). It has been proposed that such reactions could provide a major (and terminal) sink for water on some planets (Wade et al. 2017), but on Earth the restoration of water occurs by degassing at volcanoes and during metamorphism (high temperature/pressure transformation of rocks; Fig. 1). Earth's lithospheric and mantle reservoirs combined contain between 1 and 2 Earth oceans of hydrogen (Hirschmann and Kohlstedt 2012), primarily stored as defects in the crystal lattice. A very significant fraction of Earth's hydrogen could also be present in the core (Wu et al. 2018; Tagawa et al. 2021), although significant uncertainty remains in estimating its core abundance.

As with carbon, hydrogen has an affinity for silicate liquids over silicate minerals (e.g., Peslier et al. 2017), meaning mantle melting transports water from the planet's interior to the surface. Unlike carbon, however, there are

strong feedbacks between water storage in the mantle and the vigour of mantle convection, as hydrogen defects in minerals have a profound impact on the viscosity of ‘dry’ rocks. Numerical simulations have shown how in principle these feedbacks can regulate the surface inventory of water on Earth, with increased mantle water lowering mantle viscosity, increasing the vigour of convection, which drives more mantle melting and thereby drives water back out of the mantle (McGovern and Schubert 1989). These strong feedbacks between water storage in the mantle and the processes that cycle it between Earth’s interior and surface may explain the observation that Earth’s oceans have maintained an approximately constant volume through time (e.g., Windley 1977).

Nitrogen: Has major reservoirs in the atmosphere, crust, mantle and core (Johnson and Goldblatt 2015). The presence of so much nitrogen in the planet’s interior is at first surprising, because nitrogen’s chemical similarity to the noble gases might suggest it should have primarily entered Earth’s atmosphere during the magma ocean epoch and have had little route back into the interior thereafter. However, nitrogen’s solubility in silicate melts has been shown to be strongly dependent on oxygen fugacity (a measure of how oxidising a system is), allowing for a reducing early atmosphere to have driven nitrogen into Earth’s magma ocean (Fig. 2; Libourel et al. 2003; Wordsworth 2016). Crucially, this model predicts that the distribution of nitrogen on a planet is tied closely to how oxidised the magma ocean atmosphere is, which will depend on the abundance and rate of oxidising power created in the atmosphere by water dissociation and hydrogen loss to space (Wordsworth 2016) — a prediction that may eventually be testable from exoplanet observations. An important additional sink for N during the planet formation stage is the core, which may host a majority of Earth’s N incorporated into interstices in the Fe-metal alloy (Li et al. (2016); Table 1). As with atmosphere-magma ocean partitioning, experimental work has shown that metal-silicate nitrogen partitioning is sensitive to how oxidising the system is at the time of equilibration, with more oxidised conditions promoting nitrogen storage in the core (Grewal et al. 2019). There are therefore two important events in a planet’s life, during core formation and during magma ocean-atmosphere equilibration, where the fate of its nitrogen may be decided by how oxidising its surface and/or interior is.

As nitrogen is the major constituent of Earth’s atmosphere, archives of paleo-atmospheric pressure indirectly probe its accumulation in the surface environment. Various attempts have been made to infer past atmospheric pressure using fossilised raindrops (Som et al. 2012), the size of bubbles frozen in magmas (Som et al. 2016), the oxidation state of micrometeorites (Rimmer et al. 2019), and the noble gas composition of trapped bubbles of gas (e.g., Avice et al. 2018). Combined, these proxies suggest paleo-atmospheric pressures in the Earth’s Archean (>2.5 Ga) less than or equal to the present day. If anything then, nitrogen may have been added to Earth’s atmosphere over time, which

has significant implications for mechanisms of early climate warming, which cannot then rely on N₂-based collisionally-induced absorption (Wordsworth and Pierrehumbert 2013).

Oxygen: Is unique amongst the CHNOPS elements in not being a minor element in the bulk Earth, rather it is the most abundant element in the planet (e.g., Palme and O’Neill 2014). However, free oxygen (as dioxygen) is vanishingly rare in a planetary context, with most oxygen bound as metal oxides, and even slight variations in its chemical availability driving significant changes in, for example, atmospheric chemistry, the composition of volcanic gasses, and the physical properties of the Earth’s mantle. In Table 2, oxygen accounting is done by crudely considering ‘available’ oxygen, that which is present in excess of a reference state (apart from in the atmosphere, where just O₂ is considered). In most of the silicate Earth we simply consider Fe²⁺O as this reference oxide, and therefore account for available oxygen as that present in Fe³⁺O_{1.5}. In the core, conversely, iron metal (Fe⁰) provides a potential oxygen sink (for both atmospheric and mantle oxygen), and contributes ‘negative’ oxygen to our budgeting. Apparent from Table 2 is that the core’s reducing power overwhelms all the available oxygen in all terrestrial reservoirs combined — the bulk Earth is very reduced (e.g., Zhang 2017). However, Earth’s shallower reservoirs are saved from being tied to the reducing conditions of the core, as at least since the time of magma ocean crystallisation the core has been effectively chemically isolated from the silicate Earth. Whilst Table 2 shows that there is in principle many times the atmospheric inventory of ‘available’ oxygen in the mantle, the mantle itself is much more reducing than Earth’s modern atmosphere, which with 21% O₂ is extremely oxidising. Therefore, chemical interaction between the mantle and atmosphere would lead to oxygen transfer from the atmosphere into rocks; this is indeed the process that happens on Earth to form the long term oxygen cycle (Lécuyer and Ricard 1999; Shorttle et al. 2015). In this context, the fragility of Earth’s 21% atmospheric oxygen is evident, as it sits atop a vast and vastly more reducing reservoir of rock and iron. This unstable state is only sustained by oxygenic photosynthesis, with dioxygen’s rapid loss from the atmosphere inevitable were the biosphere to collapse (Lécuyer and Ricard 1999; Ozaki and Reinhard 2021).

It is important to note that for chemical habitability free oxygen is likely to be highly problematic: all life on Earth exploits reduced forms of carbon that are destroyed in the presence of oxygen, and the chemistry to start life would be even more vulnerable to oxidative destruction (Sasselov et al. 2020). Therefore, by agnostic (less anthropocentric) standards of habitability, the modern Earth is a profoundly hostile environment. Fortunately, Earth’s surface has not always been like this, and before the Great Oxidation Event at ~ 2.3 Ga ago the atmosphere was almost completely free of O₂ (Holland 2002; Catling and Zahnle 2020). There has been significant debate over whether the timing of the great oxidation event was due to an evolution in the oxidising properties of mantle-derived magmas and gases (e.g.,

Holland 2002), versus having been triggered by the biological innovation of oxygenic photosynthesis (e.g., Fischer et al. 2016). From a planetary perspective, it is interesting to note that while Earth’s mantle rocks are reduced compared to its atmosphere, it has the most oxidised mantle in the solar system (with there being a lack of constraint on Venus’s mantle; Wadhwa 2008), and has a low iron content that diminishes its absolute buffering capacity. Whilst these facts must have contributed to allowing biological O₂ production to overwhelm reducing sinks of oxygen ~2.3 Ga (Lécuyer and Ricard 1999; Sleep 2005), there is little evidence presently for long-term changes in how reducing Earth’s mantle has been (e.g., Trail et al. 2011).

Phosphorus: Likely constitutes the limiting nutrient for life on Earth (e.g., Tyrrell 1999). The throttling of the biosphere by phosphorus availability results from its absence as a stable gas phase in the atmosphere (unlike CHNO), meaning life must access its required P in aqueous form. Aqueous environments obtain their supply of P from rock weathering, however, the low solubility of phosphate (PO₃²⁻) in water means P released from rocks rapidly re-enters mineral form (Ruttenberg 2003). Life therefore goes to remarkable efforts to recycle the pool of P it has available to it, with the result that in some environments almost all P is contained in biomass (Ruttenberg 2003). Huge reservoirs of P exist in the silicate Earth, either as a P-bearing phase such as apatite (Ca₁₀(PO₄)₆(OH, Cl, F)₂, as in the crust), or as a trace component in nominally P-free mineral phases (as is the case in the mantle). However, in all these reservoirs, whether the crust, mantle, or mantle-derived magmas, the P concentration in rocks is typically low, at ~0.1 wt%. As observed for C and N, P is also moderately siderophile (e.g., Righter et al. 2018), meaning significant loss occurred to Earth’s core (Table 2).

The major mineral reservoir that life relies on for its P supply may have changed significantly over Earth’s history. On the modern Earth most crustal P is bound in the P-mineral apatite. However, the presence of apatite in rocks depends on their composition, and the less silica-rich nature of early crustal rocks may have limited its presence (e.g., Lipp et al. 2021). Instead, the early P cycle may have had to rely on trace P liberated from basalts (Walton et al. In press). Stepping back further in time, meteoritic P sources may have been essential in supplying reactive P for pre-biotic chemistry, in the form of schreibersite ((Fe, Ni)₃P, Walton et al. In press).

Sulfur: Is degassed from the mantle at volcanoes, primarily as SO₂ and H₂S (e.g., Symonds and Reed 1993). However, these species are unstable in Earth’s atmosphere, lasting just days–weeks before they are deposited out or converted to sulfuric acid. For this reason the modern oceans host huge reserves of sulfur as sulfate, ultimately sourced from oxidation of the reduced volcanic sulfur species (Brimblecombe 2013). This oceanic sulfur reservoir cycles back to the mantle via subduction of sulfide minerals, produced in part by biological sulfate reduction, and sulfate minerals, precipitated during hydrothermal cir-

ulation at mid-ocean ridges and in evaporite deposits. In the mantle, sulfur is stored as sulfide minerals/melts with distinct physical properties compared to the silicate minerals. This difference potentially came into play most dramatically during Earth’s magma ocean solidification when saturation of the crystallising magma in sulfide drove segregation of a separate sulfide liquid (the ‘Hadean matte’), which due to its high density sank to the core (Fig. 2; O’Neill 1991). This episode has enormous implications not only for the remaining budget of S on Earth, but also of other sulfide-loving (‘chalcophile’) elements (e.g., silver; Righter et al. 2019). Sulfide matte formation is sensitive to the chemical conditions that affect sulfide solubility in magma, its pressure, temperature, and composition. Notably, the loss of chalcophile elements to a sulfide matte is not thought to have occurred on Mars (Righter et al. 2019), and sulfur on the planet is inferred to be correspondingly more abundant and more important in surface geochemical cycles than on Earth (e.g., King and McLennan 2010). As well as being lost at a late stage by sulfide matte formation, sulfur is siderophile, partitioning into the core during metal segregation (2). Together, these processes explain the prediction that Earth’s core hosts a majority of the planet’s sulfur (Table 2).

The major transition in sulfur behaviour at Earth’s surface occurred in response to the Great Oxidation Event. Before this time, sulfur was stable at Earth’s surface as sulfide minerals, and sulfate concentrations in the oceans were extremely low. After the rise of atmospheric oxygen at ~2.3 Ga, sulfide minerals were no longer stable, being oxidised to sulfate on exposure to the atmosphere and hence ushering in significant sulfate concentrations in Earth’s oceans (e.g., Brimblecombe 2013).

2.2. The Accretion of Earth

Bulk Earth’s chemical and isotopic composition was determined by both *how* it grew and the materials from which it grew. The Earth has important contributions of materials from potentially widely separated reservoirs. We review briefly key constraints pertaining to the the timing of accretion, composition and dynamical origin of the Earth’s building blocks.

2.2.1. Timing Earth’s Accretion

When discussing timing, we equate $t = 0$ to the time of CAI formation (calcium aluminum inclusions, the oldest nebular condensates with an age of 4.567 Gyr, Connelly et al. 2008, 2012). The gaseous solar nebula dispersed about 4–5 Myr after the formation of CAIs (Wang et al. 2017). By this time, Mars was pretty much fully formed (Dauphas and Pourmand 2011), and both Venus and Earth were large enough ($\gtrsim 0.5M_{\oplus}$) to bind a primordial atmosphere H/He (Marty 2012; Williams and Mukhopadhyay 2019), but small enough ($\lesssim 0.8M_{\oplus}$) to lose it after the nebula dispersed (Owen and Mohanty 2016; Lammer et al. 2018). Another timing constraint is provided by the Moon-

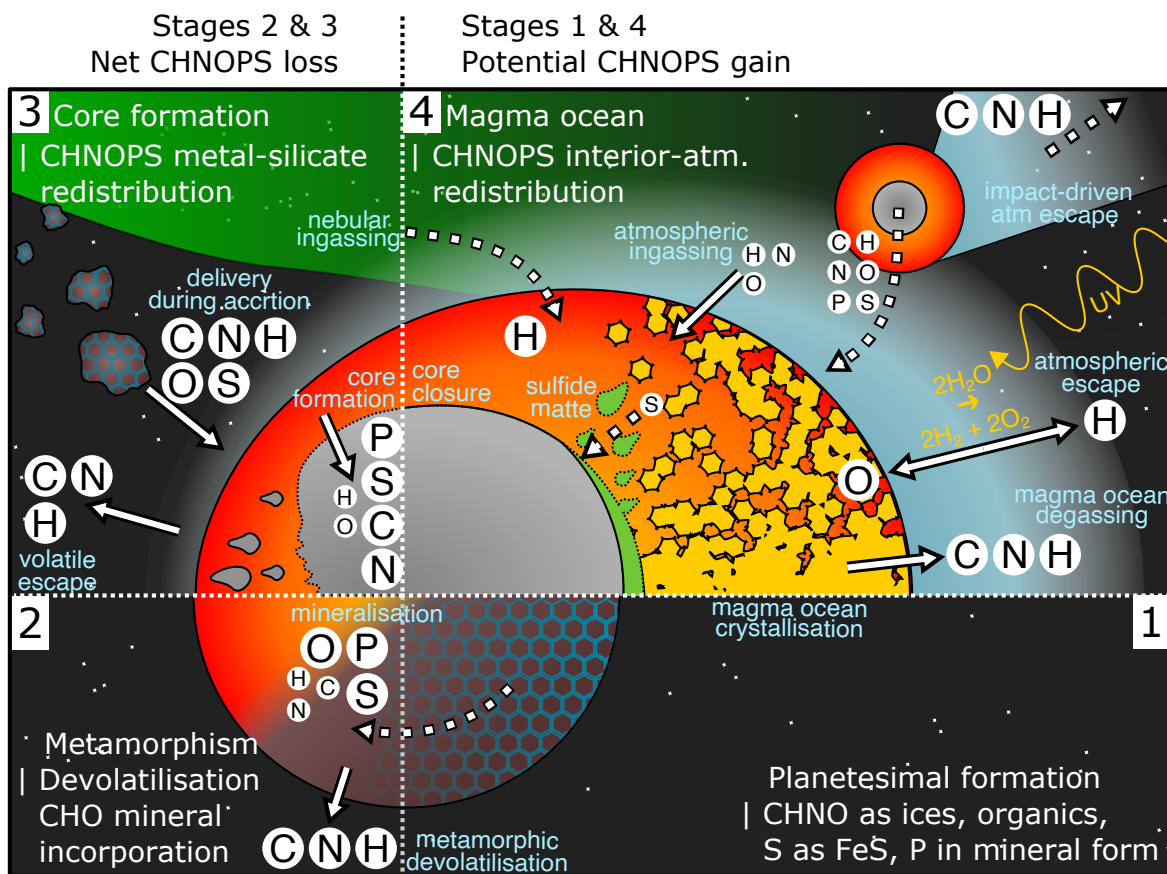


Fig. 2.— CHNOPS fluxes during planetary assembly. CHNOPS are tracked through the planetesimal assembly stage (1), planetesimal heating by short lived radionuclide decay driving metamorphic volatile processing and loss (2), eventual planetesimal melting and growth (3), and magma ocean crystallisation on Earth-sized objects (4). Stages (2) and (3) represent periods of potentially significant CHNOPS loss, either to space or the object’s growing metallic core. Whilst in stage (4) the planet is massive enough to retain C-N-O-P-S against atmospheric escape (H is likely still lost at this stage), further loss of siderophile elements to the core is prevented as it becomes isolated from the silicate portion of the planet, C-N-H are being expelled from the crystallising magma ocean into the nascent atmosphere, and S may be substantially lost to the lower mantle and outer core during sulfide matte segregation.

forming impact, arguably the most dramatic event in the history of the Earth (and the Moon), which occurred some 50-150 Myr after the formation of the solar system, long after the solar nebula had dispersed (e.g., *Kleine et al.* 2009; *Jacobson et al.* 2014; *Avicé and Marty* 2014; *Zahnle and Carlson* 2020).

2.2.2. Up to the Moon-forming impact

The Earth is considered to be largely built from material that was isotopically similar (but not identical, see e.g., *Fitoussi and Bourdon* 2012) to Enstatite chondrite (EC) meteorites, which are typically linked to asteroids found on the innermost edge of the asteroid belt (*Dauphas* 2017). Chemically, however, there are several differences. Earth’s upper mantle does not match Enstatite’s Mg/Si, and the bulk silicate Earth’s (BSE’s) C/N, C/H, and C/S ratios differ from ECs as well (*Dasgupta and Grewal* 2019). Finally, Enstatite chondrites are generally considered overwhelmingly dry, with some being even drier than Earth (*Zahnle and Carl-*

son 2020), although *Piani et al.* (2020) recently inferred water contents of between 0.08–0.5 wt% for a collection of EC meteorites suggesting their parent bodies may have been much wetter than previously thought. Contributions of C and N are generally more similar to carbonaceous chondrite (CC) meteorites that predominate further out in the asteroid belt (*Marty* 2012). In total, comets are responsible for at most 1% of Earth’s water, and at most a few percent the nitrogen, but may have delivered significant amounts of noble gases and organic material (*Marty et al.* 2016, 2017; *Altwegg et al.* 2019). The origins of Earth’s water are discussed in more detail in *Meech and Raymond* (2019).

Dynamically, the accretion from these two reservoirs (EC-like and CC-like) is often tied to the formation and behavior of Jupiter. First, isotope properties of iron meteorites (*Budde et al.* 2016; *Kruijer et al.* 2017) and an isotopic bimodality, particularly in titanium and chromium, amongst a wide class of meteorites (*Warren* 2011) point strongly to different reservoirs of carbonaceous type materials and non-

carbonaceous type materials with limited inter-mixing during much of the gas disk lifetime (see also chapter by Nomura et al.). This barrier is frequently attributed to the rapid formation of Jupiter (*Morbidelli et al.* 2016; *Kruijer et al.* 2017), although non-planetary origins for this dichotomy have also been proposed (e.g. *Brasser and Mojzsis* 2020). Recent models of planetesimal formation have found that the isotopic dichotomy may potentially correspond to distinct episodes of planetesimal formation that are separated in space or time (e.g. *Lichtenberg et al.* 2021; *Morbidelli et al.* 2022). Separated from the rest of the nebula, Earth, Mars, and Venus grew from materials with similar isotopic fingerprints (*Burkhardt et al.* 2021), while chemical differences arose from disk and planetary processes (see Sect. 6).

The rapid accretion of gas by Jupiter perturbed nearby planetesimal orbits strongly and scattered many inward (*Raymond and Izidoro* 2017). The gas disk can damp their orbits and provide a capture mechanism, thus providing a generic pathway for outer solar system planetesimals to find their way to the Main Asteroid Belt and also to accrete on to the still growing terrestrial planets. Indeed, the diverse structure of the Main Asteroid Belt (*DeMeo and Carry* 2014) demands significant input of material from the outer Solar System to the inner Solar System in the form of planetesimal-sized objects (30–300 km).

Jupiter's orbital migration may have had a similar effect on the distribution of planetesimals of different compositions, scattering a large enough mass in carbonaceous type planetesimals to account for the mass observed in the asteroid belt and total masses accretion of water on Earth (*Walsh et al.* 2011). While distinguishing these models from each other and any future models for explaining the composition of the asteroid belt is a worthy exercise, fundamentally the asteroid belt serves as a strong indicator of planetesimal transport that likely occurred during the gas disk phase of the Solar System (see review by *Raymond and Nesvorný* 2020).

2.2.3. Moon-forming impact and late veneer

Following the dissipation of the gas disk, various dynamical mechanisms are still capable of mixing material, with the Earth-Moon impact (*Canup and Asphaug* 2001) and the diverse structure of the Main Asteroid belt as indications of this process (*DeMeo and Carry* 2014; *Raymond and Nesvorný* 2020). In fact, the asteroid belt is rich not only with low-albedo C-type asteroids typically linked with carbonaceous chondrite meteorites, but it also has a smattering of D- and P-type interlopers closely linked with the Jupiter Trojans and the Kuiper Belt (*Levison et al.* 2009; *DeMeo et al.* 2014). These interlopers are successfully modeled as being captured during the giant planet instability after the solar nebula dispersed (*Levison et al.* 2009). Capture probabilities are quite low (*Nesvorný et al.* 2013) suggesting that the total transport of primitive and ice-rich Kuiper Belt-like material was orders of magnitude lower than what would

have been expected during the transport and implantation of the C-type asteroids into the Main Belt.

Nearly every model for terrestrial planet formation in our Solar System ends with the giant impact phase of growth where tens of Moon to Mars sized planetary embryos violently come together to form a system of planets (see *Morbidelli et al.* 2012; *Raymond et al.* 2018b, for reviews). Outside of possible growth entirely by pebble accretion (see *Schiller et al.* 2018; *Johansen et al.* 2021), there must be a final step for piece-wise accretion of planetary building blocks. The late-stage giant impacts present an opportunity for material mixing across larger distances than often afforded from localized accretion by planetesimals, as long as planetary embryos and planetesimals formed in a broad disk.

The isotopic similarities between the Earth and Moon (e.g., *Wiechert et al.* 2001; *Zhang et al.* 2012; *Dauphas et al.* 2014), have spurred numerous works investigating the likelihood that Theia (the Earth-Moon impactor) originated from near enough the Earth to account for their similar compositions. However, large suites of terrestrial planet formation find that this particularly stochastic phase of growth leads to overlapping feeding zones for Venus, Earth and Mars – which has a slightly different oxygen isotopic composition (*Franchi et al.* 1999) – and relatively low probabilities that Theia was formed close enough to the Earth to account for the Earth-Moon isotopic similarities (see *Kaib and Cowan* 2015; *Mastrobuono-Battisti et al.* 2015).

The abundance of highly-siderophile elements in Earth's mantle – elements that should presumably have sunk to the core during any energetic impact – indicate that Earth collided with a small population of leftover planetesimals after its final giant impact, generally considered to be the Moon-forming impact (*Day et al.* 2007; *Walker* 2009). The amount of material accreted in this late veneer makes up $\approx 0.5\%$ of the Earth's mass (*Morbidelli and Wood* 2015; *Jacobson et al.* 2014; *Dauphas* 2017), and the isotopic composition of (based on molybdenum and ruthenium) implies inner solar system (e.g. Enstatite chondrite-like) material dominated also this component (*Fischer-Gödde and Kleine* 2017). For various assumptions about the tail end of planetary accretion, the final sweep up and accretion of material by the Earth can be used to date the Earth-Moon impact, where only about $\approx 0.5\%$ of an Earth mass is typically accreted after ~ 95 Myr, which would then be the nominal time for the Earth-Moon impact (albeit with large error bars; *Jacobson et al.* 2014). *Sakuraba et al.* (2021) show how, for a relatively oxidized magma ocean, numerous (small) chondritic impactors can explain the BSE's C/N/H depletions.

Based on experimental results finding that C may become less siderophile in some scenarios while N is unaffected, *Grewal et al.* (2019) propose instead that the C/N ratio in bulk silicate Earth may be explained with a single Mars-sized impactor, and rely on far less contribution from carbonaceous chondrite materials. In this scenario, a singular giant impact – presumably the Earth-Moon forming

impact – is responsible for the delivery of carbon, nitrogen, and sulfur to the BSE. Compared to the late veneer model this alternative pathway would then require a near-absence of available planetesimals, which would otherwise still be accreted.

2.3. Origins in the Solar Nebula

The asteroids, comets, and other planetary building blocks have their origins in the solar nebula, the protoplanetary disk of our sun. Here we summarize key observations/inferences regarding the CHNOPS budgets contained within these building blocks. Motivated by the previous section, we discuss for each element the dominant reservoirs in the inner solar system (as traced by Enstatite chondrites), the outer asteroid belt (Carbonaceous Chondrites), and the outer solar nebula (drawing in particular upon new insights from studies of dwarf planet Ceres, the comet 67P/Churyumov-Gerasimenko, Pluto, and the Kuiper Belt Object Arrokoth). The discussion of CHNOPS in the outer expanses of the Solar system is particularly important for the connection to protostellar and protoplanetary systems (Sect. 5).

For some time, an important focus has been placed on the origin and delivery of water to terrestrial worlds and the formation of the Earth inside the water iceline (*van Dishoeck et al. 2014; Meech and Raymond 2019*). However, over the past decade there has been substantial work on the origin and supply of other important volatile elements including carbon/nitrogen (*Alexander et al. 2012; Marty et al. 2013; Bergin et al. 2015; Alexander et al. 2017; Marty et al. 2020; Johansen et al. 2021*) and sulfur (*Kama et al. 2019*). These works highlight very important trends within the solar system that go beyond the traditional picture of a water iceline and hint at substantial gradients in the volatile element inventory in primitive materials supplied to terrestrial worlds - i.e. the inner solar system solids were ultimately carbon-, nitrogen- and water-poor.

2.3.1. Two nebular paradigms: reset vs. inheritance

The thermal *reset* model is commonly used when discussing the inner solar system and meteoritic constraints. In this model, all solids are initially sublimated to their elemental form due to viscous heating in the rapidly accreting disk. As the nebula cools, the volatile content of solids is determined by an equilibrium condensation sequence of successive mineral formation based on the half-mass condensation temperature at a given pressure. In this context, deviations from solar abundances observed in e.g., primitive CI chondrites and Earth itself can be linked to the temperature at which they (or their building blocks) condensed. For example, for a gas of solar composition at a pressure of 10^{-4} bar, the rock-forming elements Mg, Fe, and Si condensation temperatures are around 1350 K (condensing as e.g. forsterite and enstatite, taking roughly 20% of the oxygen with them), P & S condense around 1230 and 650 K (as Fe_3P and FeS), while H, C, N, and the leftover

O freeze out as ices (e.g., H_2O , CH_4 , NH_3) at temperatures below a few 100 K (*Lodders 2003*). Indeed, elements with low condensation temperatures show the largest deviations when comparing solar nebula abundances with primitive CI chondrites, or even Earth itself (e.g., *Grossman 1972; Lewis 1972; McDonough and Sun 1995; Fegley et al. 2020*).

The *inheritance* model is motivated by the presence of pristine (never heated) ices in outer solar system bodies, such as comets with abundances that correlate with ices observed in the interstellar medium tracing stages prior to planetary birth (*Bockelée-Morvan et al. 2000; Altwegg et al. 2019; Drozdovskaya et al. 2019*, discussed in more detail in Sect. 5). Further, chondritic meteorites contain pre-solar grains, highlighting even inner solar system materials escaped a complete reset (e.g., *Nittler and Ciesla 2016*).

The interplay of radial in- and outward transport of solids between the reset and pristine reservoirs is an integral process in our picture of the early solar system, and it is in this context that we discuss each CHNOPS element individually, grouping H & O together to highlight water.

2.3.2. Evolving CHNOPS reservoirs

Carbon: To provide some perspective, Fig. 3 provides a linked view of the bulk carbon content of solar system bodies and the carbon carried by interstellar dust grains which represent a likely source term for the carbon of inner solar system solids.

The total abundance of carbon in the young sun was $\text{C/H} = 2.88 \times 10^{-4}$ (*Lodders 2003*) and interstellar carbon grains carry about 50% of this carbon. Within the solar nebula, accounting from comets Halley, 67P, and others suggests that this carbon was in refractory form (*Geiss 1987; Fomenkova 1999; Bergin et al. 2015; Rubin et al. 2019a; Woodward et al. 2021*) in abundances close that seen in interstellar carbon grains. The best accounting is from comet 67P (*Rubin et al. 2019a*) and shows that a $\gtrsim 5$ -to-1 majority of elemental carbon in such objects is carried by refractories and not volatile ices. Refractory carbon is found in meteoritic material, tracing the asteroid belt, but in amounts lower than that in comets by a factor of $\gtrsim 10$, depending on the meteoritic class (*Alexander et al. 2013; Bergin et al. 2015*). In contrast, primitive meteorites are uniformly carbon-depleted as is the Earth and, likely, Venus. The Earth's surface has significantly less carbon (see § 2.1), with the possibility of significant carbon reservoirs in the core. Estimates of the Bulk Earth carbon content provide stringent upper limits that confirm Earth's carbon depletion at least to levels seen in meteoritic material (*Li et al. 2021*). Thus some aspects of reset (or loss) appear to be present in the solid state inventory.

In terms of refractory carriers, the dominant form for comets is believed to be similar to the macromolecular materials comprised of C, H, O, N in meteorites (*Alexander et al. 2007; Fomenkova et al. 1994*), along with lower abundances of aliphatic and aromatic compounds. Meteoritic organics also have significant deuterium enrichments

(Alexander et al. 2010). It is this material that has the most relevance for terrestrial planets as its sublimation temperature is estimated to be of order 500 K for nebular pressures (Li et al. 2021).

The most volatile material, carried only by the coldest bodies in the solar system, is CO and CO₂ ices Gail and Trieloff (2017). The evidence from Arrokoth (Grundy et al. 2020) and other KBOs, and from the CO-dominated comet C/2016 R2 (Wierzbach and Womack 2018; McKay et al. 2019), further establishes that both CO and CH₄ were significant volatile carbon reservoirs in the outer solar nebula. All three species sublime at temperatures below ~70 K and should have been present in the gas in the inner disk. However, as discussed above the refractory inventory of the inner solar system also suggests that substantial refractory carbon must have been released to the gas at some stage, perhaps alongside the more volatile ices.

Nitrogen: The story of nitrogen, to some extent, mirrors that of carbon as all inner solar system bodies (Earth, meteorites) are even more severely depleted in nitrogen when compared to carbon (Bergin et al. 2015; Marty et al. 2020). However, fascinating new results have emerged since PPVI. The total protosolar nitrogen abundance was $N/H = 7.94 \times 10^{-5}$ (Lodders 2003). An absorption feature at 3.2 μm in Rosetta spectroscopy of comet 67P has been attributed to ammonium salts, $\text{NH}_4^+ \text{X}^-$ (Quirico et al. 2016; Poch et al. 2019). These may constitute ≤ 40 wt% of the cometary surface material which contributes to the NIR spectrum (Poch et al. 2020). A more conservative estimate of 5 wt% ammonium formate implies a cometary elemental nitrogen budget where ~1 % is in volatiles (HCN, NH₃, etc.), ~47 % in ammonium salts, and ~52 % in refractory organics (Poch et al. 2020). The Dawn mission detected ammoniated phyllosilicates on dwarf planet Ceres (de Sanctis et al. 2015). Recent laboratory results support the feasibility of forming these phyllosilicates from NH₃ accreted at Ceres' formation (Singh et al. 2021). Forming these salts in the cometary ice required the presence of NH₃, which would need to be inherited from the protostellar core stage (see also Section 5.1) or be produced from N₂ dissociation (Schwarz and Bergin 2014).

Nitrogen in the comae of Oort cloud comets is generally mostly in NH₃ and not N₂. The hypervolatile-rich comet C/2016 R2 (PANSTARRS) was the first comet ever observed to have a high N₂ abundance (Wierzbach and Womack 2017, 2018; Biver et al. 2018a; McKay et al. 2019). The relative role of N₂ in the spectroscopically observed elemental nitrogen budget was >500 times larger than that of NH₃ (McKay et al. 2019), likely indicating inheritance of N₂ as a dominant primordial nitrogen carrier in a relatively cold, shielded region of the outer protosolar nebula (Wierzbach and Womack 2018).

If N₂ carried $\gtrsim 99$ % of all volatile N in natal solar system material, the observation that it was largely processed into NH₃ seems to imply a relatively high cosmic-ray like ionizing particle flux in the comet-forming region. However, nitrogen is present in refractory organics within mete-

oric material and, at present, the relation between organic carriers and the nitrogen carried by salts is not clear.

Grewal et al. (2021) found evidence for distinct ¹⁵N/¹⁴N ratios in NC vs. CC meteorites, implying a relatively refractory carrier of nitrogen (e.g., N-bearing complex organics or dust) was present already very early on in the solar system. The ¹⁵N/¹⁴N ratio of the BSE falls between the NC and CC values, suggesting Earth's current nitrogen reservoir was accreted from both inner and outer solar system materials. The contribution of CC-like materials was found to fall between 30-60% depending on the assumed total nitrogen budget of NC vs. CC bodies.

Hydrogen, oxygen, and water: We treat the H, D, and O nuclei together because water is a volatile molecule whose presence is likely a crucial condition for habitability, while the D/H isotope ratio in water and other compounds is a useful diagnostic of the physico-chemical history of a given solar system sample. Our story of the deuterium-to-hydrogen ratio begins at the creation of time itself, with the baseline D/H ratio for solar system materials being set at the Big Bang (Cooke et al. 2018) and remaining essentially unaltered as $D/H = (2.0 \pm 0.1) \times 10^{-5}$ in the local ISM (Prodanović et al. 2010). Low-temperature chemistry can, however, lead to a highly significant elevation of D/H along certain chemical routes, such that HDO or D₂O abundances become comparable to that of H₂O at the 1 % or even closer level. D/H ratios in various carriers (comets, meteorites) show modest (factors of a few variation) diversity but in comparison to the elemental inventory are relatively flat (Hartogh et al. 2011; Cleeves et al. 2014; Altwegg et al. 2015a) while gradients the oxygen isotopic composition are uncertain (Altwegg et al. 2015a).

The oxygen abundance in our sun at formation was $O/H = 5.75 \times 10^{-4}$ (Lodders 2003). In a solar composition gas, equilibrium condensation calculations place ≈ 23 % of oxygen atoms into refractory minerals, while volatile compounds such as H₂O carry the remaining ≈ 77 % (Lodders 2003). Chemical kinetics, transport, and growth processes complicate attempts to directly link this to the refractory-to-volatile ratio in solar system bodies, however. From the empirical side, the actual ratio of refractories to volatiles in small icy bodies is difficult to pin down.

The Jupiter-family comet 67P/Churyumov-Gerasimenko (67P) is thought to come from the scattered Kuiper Belt. During each passage close to the sun, it loses a significant surface layer, revealing pristine inner material. Determination of the dust-to-gas ratio in 67P vary from $\lesssim 1$ to $\gtrsim 6$ (Choukroun et al. 2020) with a best estimate of $2.3^{+0.20}_{-0.16}$ based on the total mass loss (O'Rourke et al. 2020). Volatile oxygen in 67P was almost entirely in H₂O ice. The other major oxygen carriers had a low relative abundance: CO₂/H₂O = $(4.7 \pm 1.4)\%$, CO/H₂O = $(3.1 \pm 0.9)\%$, and O₂/H₂O = $(3.1 \pm 0.9)\%$ (Bieler et al. 2015; Rubin et al. 2019b). The presence of free O₂ even at this level was unexpected and evidence points to its inclusion in the comet during assembly (Bieler et al. 2015). Chemical models also point to a pre-solar cloud origin for

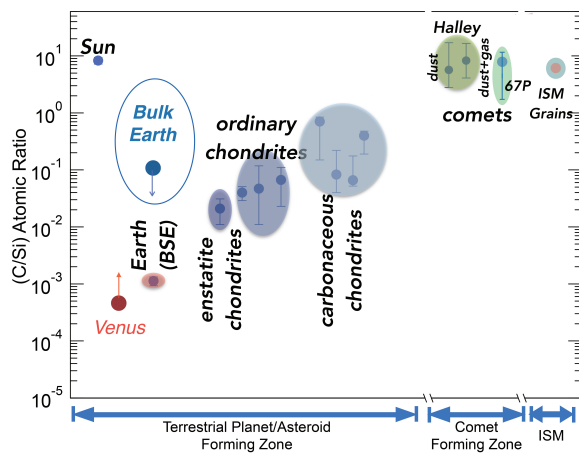


Fig. 3.— Atomic ratios of carbon to silicon in various solar system bodies including the Sun, Earth, Venus, chondrites, comets, and interstellar grains. Two values are shown for the Earth: the Bulk Silicate Earth (BSE - mantle and fluid envelopes minus the core) and the Bulk Earth (including the stringent upper limit on the amount of carbon in the core). For chondrites the error range reflects the intrinsic range within the meteoritic classes, while the errors for cometary composition are estimated uncertainties including measurement error. For Venus the estimate is from *Halliday* (2013) and is lower limit as the abundance of carbon in the rocky planetary interior is unknown. The carbon content of 67P is taken from *Rubin et al.* (2019a). Figure adapted from *Bergin et al.* (2015) and *Li et al.* (2021).

the O_2 molecules (*Taquet et al.* 2016a; *Heritier et al.* 2018), consistent with a thermally unprocessed volatile reservoir in the comet-forming zone. An origin of O_2 in clathrates in a cooling protosolar disk (i.e., post-reset) has also been put forward (*Mousis et al.* 2016).

The high deuteration fraction of water in comet 67P (*Altwegg et al.* 2015b) is likely primordial, based on results from protoplanetary disk ionization and chemistry models that show high D/H ratios can only be inherited from the cold, protostellar cloud (*Cleeves et al.* 2014). In contrast to comet 67P, the cold classical Kuiper-belt object (KBO) 486958 Arrokoth has remained in the icy outer solar system at 45 au, its primordial surface being rich in CH_3OH and (surprisingly) poor in H_2O (*Stern et al.* 2019; *Grundy et al.* 2020). While the former can be formed through hydrogenation of CO ice, the simultaneous depletion of H_2O also suggests radiolysis of water and CH_4 as the formation channel (*Grundy et al.* 2020).

A central perspective is that oxygen can be carried to inner solar system bodies via silicates. However, given the generic abundance of water ice in outer solar system bodies, it is clear that the Earth and most meteoritic pre-cursors formed inside the nebular ice line and are hydrogen, i.e. water, poor (*Morbidelli et al.* 2000).

Sulfur: The sulfur abundance in the young sun was $S/H = 1.89 \times 10^{-5}$ (*Lodders* 2003). Based on meteoritic

and cometary data, there is evidence for a dominant role for volatile sulfur (e.g., H_2S) in pristine inherited material, while sulfur in the thermally reset inner solar system reservoir is almost entirely in refractory carriers (e.g., FeS).

The simultaneous presence of a high abundance of volatile and refractory sulfur in comets testifies to a remarkable efficiency of transporting sublimated, re-condensed (or re-frozen) material into the comet-forming zone prior to comet formation. Earlier laboratory work on FeS formation demonstrated the feasibility of converting H_2S to FeS through interaction with exposed solid Fe surfaces at temperatures relevant to the early solar nebula (*Lauretta et al.* 1996). The *Stardust* mission later found a high abundance of FeS in dust from 81P/Wild 2 (*Westphal et al.* 2009). Radial mixing (the mechanism of which is as-yet unclear) may have transported this processed material outward to mix with pristine material in the comet-forming zone (*Westphal et al.* 2009).

Two recent measurements strengthen the case for sulfur having been volatile in inherited material at solar system formation. Firstly, *Rosetta* measurements of volatiles in comet 67P/C-G reveal H_2S as the dominant outer solar system sulfur reservoir, at $H_2S/H_2O = 1.1\%$ (*Calmonte et al.* 2016; *Rubin et al.* 2019b). Atomic S was second at $\approx 42\%$ of H_2S , followed by SO_2 , SO , OCS , and CH_3SH at ratios $\leq 4\%$. The evidence supports only a relative trace abundance of sulfur chains (S_n ; $n \in [2, 8]$) in comets. Secondly, a previously unidentified absorption feature at $1.8 \mu m$ in the spectrum of the KBO 486958 Arrokoth was found to be consistent with a sulfur-rich tholin-like organic residue which could have formed through photochemistry in H_2S -rich ice (*Mahjoub et al.* 2021).

Phosphorus: The young sun had a total phosphorus abundance of $P/H = 3.47 \times 10^{-7}$ (*Lodders* 2003). The fractional abundance in dust from comet Halley was $P/H = 2.92 \times 10^{-7}$ (scaled from P/Mg using proto-solar Mg/H ; *Schulze et al.* 1997). This leaves little for volatiles, consistent with the low abundance of volatile P identified in the coma of comet 67P. Volatile phosphorus carried by PO was found in comet 67P at a total abundance $P/O \approx 10^{-4}$ (*Rubin et al.* 2019b). Given a solar $P/O = 5 \times 10^{-4}$, the above results are consistent with most elemental phosphorus being contained in cometary dust. In CC meteorites, phosphorus is carried primarily in the oxidized mineral apatite. In enstatite chondrites, however, phosphorus is found mainly as the reduced mineral schreibersite. Of particular note, CI chondrites carry near solar abundance of phosphorous (*Wasson and Kallemeyn* 1988) within the aforementioned refractory minerals.

2.4. Summary

In summary, the Earth's CHNOPS budget (Sect. 2.1) is the result of a complex and drawn out accretion of a variety of building blocks (Sect. 2.2), the ingredients of which have their origins in the solar nebula and beyond (Sect. 2.3). Recognizing that the Solar System is just one possible out-

come of the long and windy star & planet formation process, we now set out to summarize important and recent observations of CHNOPS in diverse astronomical settings, interpreting these data in the context of the formation of (exo)planetary systems. The aim is to highlight diversity and variation, emerging trends, and gaps in our understanding of how CHNOPS elements arrive in terrestrial worlds.

3. CHNOPS IN THE COSMOS

The CHNOPS elements have different nucleosynthetic origins in stars and thus vary in relative abundances and proportions as generations of stars are born and die and move throughout the Galaxy; this process has traditionally been known as Galactic chemical evolution (GCE), although more recently it has expanded to include a more complete picture of Galactic “chemo-dynamical” evolution.

3.1. Variations in stellar CHNOPS

While measuring the compositions of planets outside the solar system is a nascent field, studying the detailed compositions of stellar photospheres is a well-established cornerstone of astrophysics. Just like we used the Sun as a proxy for the Solar Nebula (Sect. 2.3), stellar abundances can serve as a proxy method for measuring the chemical composition and variation in star and planet forming regions throughout the Galaxy.

The Milky Way stars are often subdivided into components based on their kinematics and chemistry – (1) the inner bulge, which has the highest density of stars, many with large inclinations relative to the disk plane (2) the diffuse halo, which contains only old metal-poor stars that have been suggested to subdivide into “high-alpha” and “low-alpha” abundance populations¹ (e.g. *Nissen and Schuster* 2010; *Bensby et al.* 2014), and (3) the disk, which is often divided into thin (higher metallicity) and thick (lower metallicity), where there is continuing star formation and a wide range of metallicities and ages of stars (e.g., *Haywood et al.* 2013). Here “metallicity” can be broadly understood as the abundance of elements heavier than H, but it is often parameterized by the iron abundance, which increases with time as Type Ia supernovae (arising from long-lived white dwarfs accreting enough mass from a binary companion to trigger carbon fusion and runaway thermonuclear explosion) start to contribute more to the ISM.

Hydrogen (along with helium) is the starting material from which the earliest stars were born, and originated not in stellar nucleosynthesis (as in the other CHNOPS elements) but soon after the birth of the universe; ~380,000 years after the Big Bang the universe had cooled enough for neutral atoms to form. Hydrogen fusion is the main source of energy in the centers of stars on the main sequence, mainly through the proton-proton chain reaction

(dominant in lower-mass/cooler core stars) and/or the CNO cycle (dominant in higher mass/hotter core stars). Given its overwhelming abundance relative to other elements (~74% of baryonic matter), other elemental abundances are often quoted as relative to hydrogen, with the solar abundance measured/set at 10^{12} H atoms (see discussion in *Lodders* 2019).

Carbon is produced via the triple- α process during the end stages of low- to intermediate-mass stars’ evolution, and ejected into the interstellar medium (ISM) through either stellar winds (lower mass stars) or Type II (core-collapse) supernova explosions (more massive stars). $[C/Fe]^2$ is between ~-0.15 and 0 dex for most thin disk stars, and rises from ~0 dex to a plateau of ~0.3 dex for thick disk and high-alpha halo stars; low-alpha halo stars (with $[Fe/H] \lesssim -0.8$ dex) show a range of $[C/Fe]$ values between roughly -0.3 and 0.1 dex (e.g., *Nissen et al.* 2014).

Oxygen is produced in hydrostatic burning in massive stars that then explode as Type II supernovae and inject oxygen into the ISM. The abundances of $[O/Fe]$ show a tighter trend with $[Fe/H]$ in thin disk stars, increasing from $[O/Fe] \sim -0.2$ dex around $[Fe/H]$ of 0.3 dex to 0.2 dex around $[Fe/H]$ of -0.4 dex, when thick disk and high-alpha halo stars take over to continue the upward trend to $[O/Fe] \sim 0.8$ dex. The low-alpha halo stars follow a similar trend in $[O/Fe]$ vs. $[Fe/H]$ as the high-alpha halo stars, but offset to slightly lower $[O/Fe]$ values. $[C/Fe]$ and $[O/Fe]$ are actually correlated and well-fit with a line of slope one, and thus the C/O ratio shows a tight, increasing trend from about 0.4 to about 0.8 dex as a function of $[Fe/H]$, although importantly C/O does not actually appear to exceed 0.8 (see below) even at the highest $[Fe/H]$ values (*Nissen* 2013; *Teske et al.* 2014; *Brewer and Fischer* 2016).

Nitrogen is produced in the CNO-cycle, which catalyzes H-burning in stars, with C and O decreasing as N increases. The abundances of nitrogen are harder to measure than C and O (which are already challenging) due to the lines being very weak, and thus less reliable. A handful of studies suggest that $[N/Fe]$ is ~constant across a wide $[Fe/H]$ range (~-1.0 to 0.1 dex) (*Clegg et al.* 1981; *Laird* 1985; *Carbon et al.* 1987; *Chiappini et al.* 1999; *Shi et al.* 2002), although precisely what that constant is is not clear due to systematic errors causing scatter. A roughly constant $[N/Fe]$ suggests a late source of N (such as low and intermediate mass stars; *Prantzos* 2003; *Chiappini et al.* 2003) is also needed to match the late source of Fe.

Sulfur, similar to oxygen, is an alpha-element produced in massive stars and injected into the ISM through Type II supernovae explosions. Around solar $[Fe/H]$, $[S/Fe]$ is slightly sub-solar, and at higher metallicities it appears to increase above solar by ~0.2 dex. $[S/Fe]$ then increases

¹“Alpha” refers here to elements whose most stable isotopes form via the α -capture process in massive stars prior to Type II SNe explosions, e.g., Mg, Si, Ca, and Ti. O and S are often also considered alpha elements; see *Nissen and Schuster* (2014) for a discussion of C.

²This notation refers to the relative number density of carbon atoms in a star’s photosphere relative to the amount of iron atoms, normalized to these values in the Sun, in log units: $[C/Fe] = [C/H] - [Fe/H]$, where $[X/H] = \log(N_X/N_H) - \log(N_X/N_H)_{\text{solar}}$. Thus the solar value in this notation is equal to zero.

with decreasing $[\text{Fe}/\text{H}]$ in both thin and thick disk stars to a plateau at a $[\text{S}/\text{Fe}] \sim 0.3$ dex between $-3.5 \leq [\text{Fe}/\text{H}] \leq -0.1$ dex, although with a scatter of about ± 0.2 dex (Chen et al. 2002; Nissen et al. 2007; Spite et al. 2011; Matrozis et al. 2013; Duffau et al. 2017).

Phosphorous is produced via neutron capture on silicon, a process thought to occur in the hydrostatic neon-burning shells of massive stars prior Type II supernovae explosions, and also during the explosion itself in carbon- and neon-burning layers (Koo et al. 2013). Similar to other alpha-elements, $[\text{P}/\text{Fe}]$ increases as $[\text{Fe}/\text{H}]$ decreases down to $[\text{Fe}/\text{H}] \sim -0.5$ dex, at which $[\text{P}/\text{Fe}]$ plateaus around 0.3 dex; $[\text{P}/\text{Fe}]$ is close to zero for solar metallicity, and perhaps increases with $[\text{Fe}/\text{H}]$ above solar (e.g., Caffau et al. 2007; Meléndez et al. 2009; Caffau et al. 2011; Roederer et al. 2014).

3.2. Radionuclides

In addition to the CHNOPS elements of focus, the chemical habitability of a planet will be influenced by the system's inventory of long-lived radionuclides (half lives $\gtrsim 700$ Myr, e.g., ^{235}U , ^{238}U , ^{232}Th , ^{40}K), key to a planet's heat budget (Lichtenberg et al., in this volume) and short-lived ones (half lives $\lesssim 100$ Myr, e.g., ^{26}Al and ^{60}Fe), which, if in sufficient abundance, can lead to differentiation and dehydration/devolatilization of planetesimals (Sect. ??).

Uranium and thorium are produced via r -process nucleosynthesis, likely in neutron star merges (e.g., Pian et al. 2017; Kasen et al. 2017), while ^{40}K is produced via oxygen-burning and the s -process in massive stars. ^{26}Al can be injected into the ISM from core-collapse supernovae or from stellar winds emitted during post-Main-Sequence evolution of massive stars (Gaidos et al. 2009; Gounelle and Meynet 2012; Young 2014). Much of our knowledge about ^{26}Al actually comes from observations of the 1809 keV gamma rays produced when it decays (Reiter 2020), which support the idea that ^{26}Al is produced by high-mass stars, with up to 50% coming from pre-supernova mass loss, especially from Wolf-Rayet stars (Crowther 2007). Iron-60 is likely produced in the helium- and/or carbon-burning shells of massive stars via neutron capture on preexisting stable iron isotopes (see Wang et al. 2020 for further details).

The levels of short-lived radionuclides (particularly ^{26}Al and ^{60}Fe) found in meteorites are greater than that expected from steady-state production in the Galaxy (although see Tang and Dauphas 2012), indicating there was likely a local source of enhancement within ~ 1 Myr and ~ 0.2 pc of the birth of the Solar System (Harper 1996; Wasserburg et al. 1996; Meyer and Clayton 2000; Adams 2010). The enhanced short-lived radionuclides could have come from (1) a supernova explosion or mass loss from a "super"-asymptotic giant branch star near the Sun's protoplanetary disk (Chevalier 2000; Ouellette et al. 2007; Lugaro et al. 2012), although based on simulations of stellar cluster evolution this seems unlikely (Parker et al. 2014), (2) a trig-

gered cloud collapse with accompanying direct injection of the radionuclides from a single supernova (Cameron and Truran 1977; Foster and Boss 1997; Boss and Keiser 2015), or (3) a more sequential process in which the Sun formed in an inter-generational giant molecular cloud enriched first in ^{60}Fe and then ^{26}Al , the latter perhaps from winds from Wolf-Rayet stars (Arnould et al. 2006; Gaidos et al. 2009; Young 2014; Dwarkadas et al. 2017). Whether ^{60}Fe is mildly or strongly under-produced vs. ^{26}Al , and thus how decoupled the sources of ^{26}Al and ^{60}Fe were in the early Solar System, is still a topic of active study (e.g., Nittler and Ciesla 2016). See Desch et al. (in this volume) for a more comprehensive review of short-lived radionuclides in the context of the early Solar System.

All of these radioactive elements are expected to be mixed in the ISM from shear forces in the differentially-rotating Milky Way disk, on the order of 250 Myr (Frank et al. 2014), meaning the short-lived nuclides could experience inhomogenous dispersal within their half-lives (and indeed may be differently distributed, see Wang et al. 2020), but longer lived nuclides are likely more homogeneously dispersed at a given Galactic radius (Huss et al. 2009). Reiter (2020) concluded that the ISM is regularly replenished with high levels of ^{26}Al that can be sustained for millions of years, and if $\sim 50\%$ of stars are born in high-mass star forming regions (e.g. Dukes and Krumholz 2012), then as many as $\sim 25\%$ of systems may be enriched in ^{26}Al at a level similar to the early Solar System. However, it is important to note that the large-scale emission observed from ^{26}Al is irregular (Wang et al. 2009), indicative of a nonuniform distribution of massive stars, and even if a giant molecular cloud is in the vicinity of a massive star association, it does not guarantee ^{26}Al will find its way into the cold clumps of star formation (see Lugaro et al. 2018 for an extended discussion). Lichtenberg et al. (2016) modeled this process with N -body simulations of large (10^3 - 10^4) clusters of stars with a range of initial conditions, and found a wide range of resulting short-lived radionuclide enrichment factors, with ~ 10 – 30% of systems enriched commonly at Solar System levels, but also many systems with negligible or zero short-lived radionuclide abundances.

4. LESSONS FROM EXO-PLANETS AND THEIR HOST STARS

Before continuing our journey of CHNOPS from their cosmic origins to molecular clouds and protoplanetary systems (Sect. 5), we take a moment to highlight important lessons from studies of exoplanets and their host stars. While measuring detailed CHNOPS budgets on/in individual extra-solar terrestrial worlds is currently out of reach, it has become possible to study emerging trends between the occurrence rates of different planet types and host star properties. We choose here to highlight two selected host star characteristics: metallicity ($[\text{Fe}/\text{H}]$) and CHNOPS budget. For more in-depth assessments of the lessons from *Kepler* and emerging trends in exoplanetary architectures, we point

the interested reader to Lissauer et al., and Weiss et al., (this volume).

4.1. Host star metallicity

Giant planets (at least in relatively short orbital periods) are observed more frequently around metal-rich stars (e.g., Santos et al. 2004; Fischer and Valenti 2005; Johnson et al. 2010; Mortier et al. 2013), while smaller planets appear to form around stars with a wider variety of metallicity (e.g., Gonzalez 1997; Sousa et al. 2011; Buchhave et al. 2012, 2014; Wang and Fischer 2015; Petigura et al. 2018). The predicted fraction of stars with giant planets is often parameterized as a function of metallicity using a power law, $f([\text{Fe}/\text{H}]) \propto 10^{\beta[\text{Fe}/\text{H}]}$, and previous studies have found β for hot ($P < 10$ day period) Jupiters to range from $0.71^{+0.56}_{-0.34}$ (Osborn and Bayliss 2020, although note this study was not sensitive to the absolute occurrence rate) to $3.4^{+0.9}_{-0.8}$ (Petigura et al. 2018). The index β then decreases for smaller planets, e.g., Petigura et al. found 1.6 ± 0.3 for hot sub-Neptune planets and 0.6 ± 0.2 for hot super-Earths in the *Kepler* sample of FGK dwarf stars between $[\text{Fe}/\text{H}] = -0.4$ and 0.4 dex. Interestingly, the metallicity dependence measured by Petigura et al. appears to weaken or flatten out for longer period planets of all sizes (consistent with e.g., Mulders et al. 2016; Buchhave et al. 2018). However, how metallicity impacts the formation and resulting compositions of different planets is still somewhat qualitative and deserves continued study as more detailed exoplanet data are measured and larger spectroscopic surveys of stars are conducted. For example, it is curious that Teske et al. (2019) did not find a clear correlation between stellar metallicity and planet residual metallicity (the relative amount of metal versus that expected from the planet mass alone) in a sample of non-inflated giant exoplanets, which conflicts with common predictions from formation models that a feeding zone of a forming giant planet with twice as much metal should produce a giant planet with \sim twice as much metals.

Several RV searches for planets around metal-poor ($-2.0 \leq [\text{Fe}/\text{H}] \leq -0.6$ dex) stars resulted in a prediction for the average frequency of giant planets (hot Jupiters with periods < 10 days) $\lesssim 2\%$, versus their frequency at higher metallicities of $\sim 3\text{-}8\%$ (Sozzetti et al. 2009; Mortier et al. 2012). The recent work of Boley et al. (2021) made use of the boon of TESS observations of halo stars to search for transiting hot Jupiters in the same metal-poor regime, resulting in an mean $1\text{-}\sigma$ upper limit of 0.18% for $0.8\text{-}2 R_J$ planets orbiting with periods between $0.5\text{-}10$ days. But due to the technical challenges of detecting smaller planets around metal-poor stars, which have fewer absorption lines and are generally farther away and thus fainter, there is currently no strong observational constraints on, “How low can you go?” for small planet host star metallicity. The lowest-metallicity stars known to host a planet with $M_p \leq 10 M_\oplus$ or $R_p \leq 4 R_\oplus$ have $[\text{Fe}/\text{H}] = -0.89$ dex (Kapteyn’s star; Anglada-Escudé et al. 2014) and $[\text{Fe}/\text{H}] = -0.65 \pm 0.10$ dex

(K2-180, Korth et al. 2019), respectively. Interestingly, observations of iron-poor planet-hosting stars (mostly larger planets) show that the host stars exhibit preferential enhancement in alpha-element abundances, indicating that perhaps other heavy elements may compensate for solid planetary building blocks when iron is lacking (Brugamyer et al. 2011; Adibekyan et al. 2012a,b, 2015).

4.2. Host star CHNOPS abundances

With increasing interest in distinguishing populations of exoplanets and their potential to host life, the ratio of carbon to oxygen (C/O) in exoplanet host stars has also been the focus of detailed study. The ratio of carbon to oxygen (along with that of magnesium to silicon) significantly influences the bulk mineralogy planets, such that a C/O ratio > 0.8 will produce carbon-rich planets dominated by graphite, silicon carbide, and titanium carbide (e.g., Gaidos 2000; Kuchner and Seager 2005) and likely geodynamically inactive (Unterborn et al. 2014).

As noted above, despite significant variations in $[\text{C}/\text{Fe}]$ and $[\text{O}/\text{Fe}]$ with $[\text{Fe}/\text{H}]$, these trends do not depart from each other very much and thus the C/O ratio spans only about 0.4 to 0.7 (between -0.4 and 0.5 dex in $[\text{Fe}/\text{H}]$) in high-precision chemical abundance studies, with no difference between stars known and not known to host planets (Teske et al. 2014; Nissen et al. 2014). The larger sample study (849 Sunlike RV planet search stars) of Brewer and Fischer (2016) showed a slightly wider distribution of C/O across roughly the same $[\text{Fe}/\text{H}]$ (see their Figure 1), with a median C/O of 0.47 and only four stars even approaching C/O=0.8 (the maximum stellar C/O in their sample is 0.66 ± 0.068); indeed, they suggest the Sun at C/O=0.55 is slightly carbon-rich. Other studies have found similar C/O spreads and the lack of a difference between the C/O ratio in stars known vs. not known to host planets (e.g., Suárez-Andrés et al. 2017, 2018; Clark et al. 2021), but it is important to note that these previous studies of C/O in planet host stars were dominated by stars hosting planets that are somewhat or much larger than what we would consider terrestrial. While Brewer and Fischer (2018) derived $[\text{C}/\text{H}]$ and $[\text{O}/\text{H}]$ ratios for ~ 1000 *Kepler* stars, many of which are known to host smaller planets, they do not report on differences between the distribution of C/O in different sub-populations of host stars.

There have been fewer studies of the variation in abundances of N, P, and S in planet host stars. Ecuivillon et al. (2004) presented a spectroscopic analysis of nitrogen in 66/25 stars with/without known planets, combining abundances derived from both the near-UV NH band and the near-IR N I line, and found no significant difference in the behavior of $[\text{N}/\text{Fe}]$ vs. $[\text{Fe}/\text{H}]$ in planet hosts. More recent studies have confirmed these results (da Silva et al. 2015; Suárez-Andrés et al. 2016). Due to the challenges in measuring P abundances in general (see above), there are only \sim a dozen exoplanet host stars with P measured along with another element (Hypatia Catalog, Hinkel et al. 2014), so it

is not possible to draw conclusions about the behavior of P in stars known to vs. not known to host planets, other than there is not obviously larger or smaller scatter between the two populations in most ratios (P/Si appears to show some high outliers that are planet hosting stars). For sulfur, the recent study of *Costa Silva et al.* (2020) found no distinctive trends or differences between the behavior of [S/Fe] vs. [Fe/H] in planet host stars (110 Jovian-type planets, 24 Neptune- or super-Earth type planets) versus stars not known to host planets (585), although below [Fe/H] of -0.3 dex their sample suffers from a small-number statistics for the planet host stars.

5. MOLECULAR CLOUDS AND THE FORMATION OF PROTOPLANETARY DISKS

The interstellar medium consists of phases which cover multiple orders of magnitude in density, temperature, and radiation field intensity. The CHNOPS elements aside from hydrogen are made in stars (Section 3), released into the diffuse ISM where they are mostly in atomic form, and may later get incorporated in molecular clouds.

Dense regions of molecular clouds can become gravitationally bound pre-stellar cores, which can collapse in the protostellar core stage, forming a central protostar with an accretion disk (re-)supplied by the collapsing envelope. Up to the sublimation temperature, heating of ices can lead to increasing chemical complexity, including complex organics which sublime at higher temperatures (*Öberg et al.* 2009; *Boogert et al.* 2015). Most of the new star's mass is built up within 0.5 Myr (*Machida and Matsumoto* 2011; *Hartmann et al.* 2016). The disk starts out small and hot, but quickly grows and is thought to reach its largest angular extent and highest mass in the still warm Class 0/I stage (*Hueso and Guillot* 2005). ALMA observations confirm that Class 0 disks are warm (*van't Hoff et al.* 2020). "Time zero", corresponding to CAI condensation in the innermost solar system, is thought to happen somewhere in the Class 0/I stage. After this the disk loses angular momentum and mass due to viscous evolution and winds in the Class II stage. Viscous heating loses its importance and stellar irradiation largely dictates the temperature for most of the disk's lifetime.

Millimeter grains in most Class 0 disks remain confined to ≈ 60 au (*Maury et al.* 2019) and some have centimeter grains extending out to 12 au (*Segura-Cox et al.* 2018). Class II disks are both larger and more diverse in size (*Najita and Bergin* 2018a). Dust growth starts very early, with growing grains increasingly settling on the midplane and drifting inwards due to gas drag. The surface-to-midplane vertical separation of irradiation heating and dust cooling result in a shielded midplane containing most of the mass, sandwiched between warmer molecule-rich layers a few scale heights from the midplane and a third, PDR-like layer which envelops the whole disk (e.g., *Aikawa et al.* 2002; *Henning and Semenov* 2013). Moving outwards along the midplane, the decreasing temperature gives rise to a se-

quence of snow- or ice-lines which may play a key role in deciding the CHNOPS content of any planets that form (*Öberg et al.* 2011). In the youngest, hottest disks, H₂O is only frozen out at radii ≈ 10 –100 au (*van't Hoff et al.* 2021) and CO is entirely in the gas. As these disks cool and radially spread, the snowlines of all ice and organic species move closer towards the star and CO can freeze out in the outer disk for the first time (e.g. Class I, *van't Hoff et al.* 2020). Eventually an N₂ snowline develops as well, as implied by gas-phase nitrogen depletion in mature disks (e.g. TW Hya, *van't Hoff et al.* 2017; *Hily-Blant et al.* 2019; *McClure et al.* 2020).

Infrared observations of protostars reveal pure CO₂ ice (*Pontoppidan et al.* 2008), requiring the complete sublimation of CO ice in most of the protostellar envelope which may in turn point to episodic accretion luminosity bursts (*Kim et al.* 2012; *Visser et al.* 2015; *Hartmann et al.* 2016). Such bursts would also impact other CHNOPS ice species, pushing snowlines outwards by tens of au (e.g., *Taquet et al.* 2016b). Spectra showing crystalline CO₂ signatures in some protostellar cores furthermore suggest repeated sublimation/condensation events of ices up to 70 K (*Poteet et al.* 2013). "Relic snowlines" consistent with past outbursts have also been seen for H₂O (*van't Hoff et al.* 2018). Some ices such as H₂O may survive these events in large parts of the envelope, contributing a relatively pristine material reservoir for disks (*Visser et al.* 2009). The D/H ratio of Earth's water is also consistent with a significant inherited H₂O ice reservoir (*Cleeves et al.* 2014; *Furuya et al.* 2017). An example of a system currently in outburst is V883 Ori, with an apparent H₂O snowline at 42 au based on dust emission (*Banzatti et al.* 2015; *Cieza et al.* 2016) or even ≈ 100 au based on HCO⁺ (*Leemker et al.* 2021). Such objects are excellent laboratories for gas-phase spectroscopy of evaporated ices, which for V883 Ori show a comet-like COM inventory (*Lee et al.* 2019).

The small angular size of disks in combination with the high optical depths and efficient freeze-out of volatiles in the outer disk make observing molecules challenging, and only about two dozen of the >200 molecules identified in the ISM and protostars have been found in protoplanetary disks (*McGuire* 2018). At IR wavelengths, vibrational transitions of gas-phase H₂O and CO₂ are seen in emission, allowing for an accounting of CNO-bearing molecules in the surface layers of the inner few au (*Carr and Najita* 2008; *Najita et al.* 2013; *Pontoppidan et al.* 2014). In rare cases, ro-vibrational absorption features allow an accounting of otherwise nearly invisible species such as CH₄ (*Gibb and Horne* 2013). Molecules with a permanent dipole moment (e.g., CO, HCN, or CH₃OH) often have rotational transitions at (sub)millimeter wavelengths that can be seen with (sub-)millimeter telescopes such as ALMA (*Öberg et al.* 2015; *Walsh et al.* 2016; *Booth et al.* 2021b). Figure 6 illustrates the spatial scales probed by IR and mm-wavelength observations for the disk of AS 209. Finally, in disks with favourable near-edge-on inclinations, ice species may be seen in absorption, allowing for the characterisation of their

abundances as well as ice properties along selected sight-lines (*Pontoppidan et al. 2005; Terada et al. 2007; Ballering et al. 2021*).

5.1. Elemental Accounting from the ISM to Protoplanetary Disks

We next review the budget of each element on its journey from the ISM through to late-stage protoplanetary disks, forming a backdrop for a closer look at planet formation which follows in Section 6.

Oxygen: The depletion of oxygen in the diffuse atomic ISM is consistent with its depletion into silicate minerals. However, with increasing ISM density, oxygen depletes from the gas more rapidly than its partner elements in silicates, suggesting the existence of an additional significant (solid?) oxygen reservoir of unclear nature (*Jenkins 2009*). Refractory organics are a likely candidate (*Whittet 2010*). Based on the elemental budget, viable outcomes O and CO accretion, and spectroscopic constraints, it has been suggested that the missing oxygen reservoir is an organic carbonate, which would also tie up ~ 12 to 19% of all elemental carbon (*Jones and Ysard 2019*), but the latest oxygen budget reviews do not favour a significant refractory organic component for O (*van Dishoeck et al. 2021*). Focussing purely on the ices in dense clouds and molecular clouds (*Boogert et al. 2015*), oxygen appears first as amorphous H_2O ice. With the formation of CO ice, CH_3OH ice also forms. The ice budget in protostellar cores, where disk formation is thought to start, accounts for ≈ 26 to 60% of total elemental O as H_2O , CO, and CO_2 . In the outermost regions of the late-stage protoplanetary disk HD 142527, around 80% of elemental O is present as crystalline H_2O (*Min et al. 2016*).

Carbon: The disposition of elemental carbon in interstellar space is such that roughly 50% is thought to be in the form of refractory carbonaceous grains formed in asymptotic giant branch stars and 50% in the gas, primarily as CO in diffuse and dense clouds (*Cardelli et al. 1996; Jenkins 2009; Parvathi et al. 2012; Mishra and Li 2015*). New results suggest that polycyclic aromatic hydrocarbons can form in cold ($T \sim 10$ K), dense filaments (*McGuire et al. 2021*). Thus there is the potential for large molecule/small carbon grain formation as part of the star formation process, though the abundance of the precursors is very low (*McGuire 2018*). In protostellar cores, spectroscopically identified ices account for 14 to 27% of C (*Boogert et al. 2015*). This does not include PAHs.

Nitrogen: In the diffuse ISM, nitrogen is present as an atomic gas which, unlike carbon, shows no statistically significant depletion with increasing extinction (*Jenkins 2009*). The 20% level of depletion observed at 1σ significance may be related to N incorporated in carbonaceous nanoparticles (*Jones 2016*), a form of CHON material. In star-forming molecular clouds, observational estimates of the molecular nitrogen to ammonia ratio yield $\text{N}_2/\text{NH}_3 = (170 \pm 100)$ (*Womack et al. 1992*). This appears broadly consistent with

the value of $\gtrsim 500$ estimated for the coma of the hyper-volatile rich comet C/2016 R2, perhaps suggesting a dominant role for N_2 at the time of protostellar core formation. In such cores, ices carry ≈ 11 to 30% of total elemental N as NH_3 , NH_4^+ , and OCN^- , while the role of N_2 is empirically poorly constrained (*Boogert et al. 2015*). If N is released from N_2 by He^+ , both gas-phase interactions (with H_2) or grain surface processes (H) can convert it into NH_3 (e.g., *Fedoseev et al. 2015*). The possible presence of a significant fraction of total N as ammonia and ammonium salts is consistent with the solar system findings described in Section 2.3. In the IM Lup protoplanetary disk, *Cleeves et al. (2018)* found no evidence of gas-phase nitrogen depletion, consistent with the directly identified high fractional abundance $\text{NH}_3/\text{H}_2\text{O} = 7$ to 84% in TW Hya (*Salinas et al. 2016*). Finally, inside ≈ 10 au in three disks, *Pontoppidan et al. (2019)* found little NH_3 which may signify an efficient conversion back into N_2 .

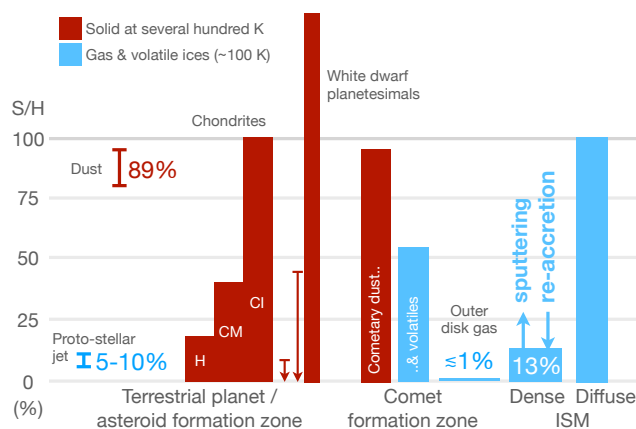


Fig. 4.— The fraction of total sulfur locked in volatile (blue, $T_{\text{sub}} \lesssim 100$ K) or refractory (red) carriers in the inner and outer disk, and in their natal ISM material. Values are normalised to solar, capped arrows are upper limits. Figure adapted from *Kama et al. (2019)*.

Sulfur: Sulfur is released by AGB stars and Type II supernovae in the form of volatile species such as SO (*Matsuura et al. 2017; Danilovich et al. 2016, 2017, 2018*) and as refractory minerals such as MgS (*Hony et al. 2002; Lombaert et al. 2012*), though the significance of the solid-state spectral feature underlying the MgS identification is disputed (e.g., *Volk et al. 2020*) and equilibrium condensation calculations suggest FeS is the dominant refractory form. In the diffuse atomic ISM, sulfur is entirely “reset” into an atomic gas (*Jenkins 2009*). This is likely due to sputtering of sulfide minerals by high-energy particles (*Keller et al. 2010*), though there is evidence that at least some FeS grains survived their interstellar journey, to be incorporated in meteorites as prestellar grains (*Haenecour et al. 2016*). With increasing column density, sulfur depletes from interstellar gas into a solid form of unclear nature. In protostellar cores, only 5% of total elemental S has so far been recovered in ices (H_2S , OCS, and SO_2) (*Boogert*

et al. 2015). In protoplanetary disks, $\approx 89\%$ of total S is accounted for by a fairly refractory species, likely FeS (Kama et al. 2019), while gas-phase volatiles (H_2S , CS, SO) carry $\lesssim 1\%$ (Dutrey et al. 1997; Fuente et al. 2010; Dutrey et al. 2011; Pacheco-Vázquez et al. 2016; Semenov et al. 2018; Booth et al. 2018). The sulfur budget for planet formation is summarised in Fig. 4.

Phosphorus: All elemental phosphorus is in atomic gas form in the diffuse ISM and it depletes rapidly towards higher densities (Jenkins 2009). Very little is known empirically about the reservoirs phosphorus depletes into as it enters molecular clouds. Gas-phase PO and PN have been found to carry only 0.05 to 0.5% of elemental P in star-forming regions (e.g., Ziurys 1987; Bergner et al. 2019), while P-bearing ices themselves remain entirely undetected. Desorbed ices and sputtered refractory P are both potential sources for the gas-phase PN and PO (Mininni et al. 2018). It seems likely that nearly all P is locked in refractories, as it is in the solar system (Section 2.3).

5.2. Disks: the context for planet formation

As a snapshot of the current observational perspective in Fig. 6 which presents molecular emission images with ~ 15 au resolution towards the AS 209 protoplanetary disk from the ALMA large program Molecules At Planet-forming Scales or MAPS (Oberg et al. 2021; Czekala et al. 2021; Law et al. 2021). The dust emission image (top left) exhibits significant sub-structure (gaps and rings) which are associated with one or more hidden planets (Zhang et al. 2018). In contrast, the molecular emission, exhibits evident sub-structure, but seemingly not concurrent with the dust (Law et al. 2021). This complex structure hints at a chemistry that is linked to the dust evolution but is also influenced by other factors such as the enhanced UV penetration as a result of dust growth and settling and elevated C/O ratios present on the disk surface (Alarcón et al. 2021; Bosman et al. 2021b; Guzmán et al. 2021; Ilee et al. 2021). ALMA images of molecular emission generally resolve into tens of au and do not readily probe the terrestrial planet forming zone (0.1–3 au). Molecular spectra at mid-infrared wavelengths can access this gas (and dust). In AS209 the Spitzer spectrum exhibits emission lines of water, CO_2 , HCN, and C_2H_2 . With the launch of JWST, and its anticipated science return there is a bright future to try to link the composition seen in ALMA images tracing the giant-planet forming zone (in our solar system) with that probed by JWST tracing gas coincident with the birth place of terrestrial planets.

Illuminating the temperature structure and cooling sequence in both young and old disks is of critical importance to planet formation, as evidence from the Solar System suggests that planetesimal formation started within 0.25 Myr after CAI formation and continued through ~ 4 Myr (Nittler and Ciesla 2016). One might then expect planetesimals formed in the early, warm disk phase to be poorer in CHNOPS than planetesimals formed at the colder, later stages. However, the exact CHNOPS composition of plan-

etesimals also depends on various formation and disk dynamical processes, as we discuss next.

6. CHNOPS DURING PLANET FORMATION

6.1. Early stages of planet formation

6.1.1. Chemical processing and mixing

Variations in gas density, temperature, and the radiation field found in protoplanetary disks give rise to a rich combination of grain-surface and gas-phase chemistry on a variety of time-scales (van Dishoeck and Bergin 2020; Öberg and Bergin 2021, and references there-in). Moreover, advection and diffusion of molecules and (small) dust grains complicates the chemistry, as timescales for mixing can be comparable to those for chemical processing of materials (Semenov and Wiebe 2011). Small grains, when mixed up to the surface, can be exposed to high temperatures and intense UV radiation, resulting in processing or loss of their ice mantles (Ciesla and Sandford 2012; Bergner and Ciesla 2021), or, in the inner regions, even oxidation and photolysis of more refractory carbon carriers (Lee et al. 2010; Anderson et al. 2017; Klarmann et al. 2018; Bosman et al. 2021a). Condensates from the inner nebula can also be transported outward, through viscous spreading (Dullemond et al. 2006; Najita and Bergin 2018a), meridional flows (Ciesla 2007; Desch et al. 2018), or by being picked up and flung out by disk winds (Shu et al. 1996; Giacalone et al. 2019), though winds may not be very effective at reinserting swept-up grains into the outer disk (Booth and Clarke 2021). In the Solar System evidence for (early) outward transport can be found in comets and CC meteorites (Nittler and Ciesla 2016, and references therein). Signatures of a similar movement of solids in protoplanetary disks come from observations of crystalline silicate grains (van Boekel et al. 2004; Apai et al. 2005). However, as grains coagulate and grow larger, their dynamics change considerably and instead, in the absence of pressure bumps (see Sect. 6.2.4), inward radial drift along the midplane is expected to dominate (Weidenschilling 1977; Misener et al. 2019).

6.1.2. CHNOPS and the meter-size barrier

Locally, microscopic dust particles collide and stick in collisions to form larger dust aggregates. This pairwise growth stops when aggregates reach the bouncing or fragmentation barrier (when collisions no longer result in sticking), or when radial drift removes aggregates on timescales that are shorter than their coagulation timescales (e.g., Birnstiel et al. 2016). Collectively, these bottlenecks are often referred to as the "meter-size barrier" (see Fig. 5). CHNOPS elements and their partitioning between gas, ice, and solid phases influence this picture in several ways.

First, the condensation of major ices (water, CO, CO_2) increases the local mass surface density of solids, speeding up dust coagulation shifting the radial drift barrier. Typical (initial) values of the total ice/rock ratio in solar neb-

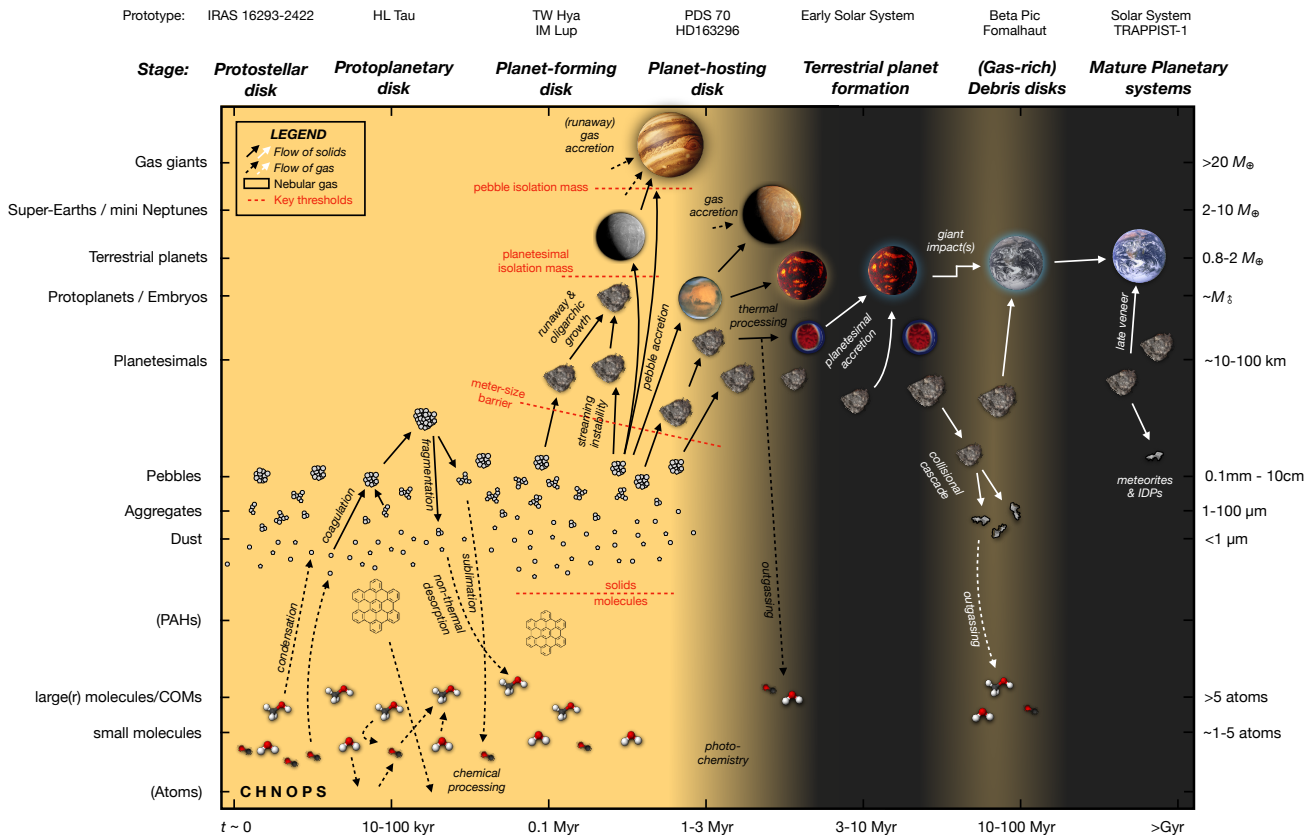


Fig. 5.— Modern planet formation theory provides an unbroken chain of processes connecting nebular dust and gas (bottom left quadrant), through pebbles and planetesimals, all the way to giant planets, terrestrial planets, and everything in between. The picture is highly dynamic, with large-scale/disk-wide mixing and transport processes (not shown here) pervasive (and sometimes essential) at every mass/size scale. With this roadmap in hand, we can attempt to follow life-essential CHNOPS elements from the inter-stellar medium to mature and diverse worlds.

ula analogs vary between 2 (Lodders 2003) and 4 (Dodson-Robinson et al. 2009), but may be increased by an order of magnitude or more near major icelines (see e.g. Cuzzi and Zahnle 2004, and below). Second, the presence of icy or organic coatings on the surfaces of refractory grains can change the dominant collisional outcomes. Traditionally, the presence of a water ice mantle was expected to raise the sticking threshold velocity of aggregates by a factor of ≈ 10 (e.g. Dominik and Tielens 1997; Wada et al. 2013; Gundlach and Blum 2015), although more recently this canonical image of non-sticky refractory vs. sticky water ice grains has been called into question (Kimura et al. 2015; Steinpilz et al. 2019). Collision-induced phase-transitions leading to fusion/annealing can increase the stickiness even further (Wettlaufer 2010). The expected jump in particle properties³ across the water iceline then plays an important role in planetesimal formation models (see Sect. 6.1.4) and may be used to locate the snowline indirectly using dust continuum emission (Banzatti et al. 2015; Cieza et al. 2016). Organic coatings have also been suggested to increase particle

stickiness at temperatures between 200 and 400 K (Kouchi et al. 2002; Homma et al. 2019), although recent experiments are not conclusive (Bischoff et al. 2020). Conversely, laboratory experiments have demonstrated that cold water ice ($T < 200$ K) behaves similar to bare silicates (Musiolik and Wurm 2019, and see Kimura et al. 2020). In addition, mixing in other, more volatiles ice species like CO_2 was also found to decrease the (effective) surface energy (Musiolik et al. 2016), suggesting the disk region where water ice enhances sticking is limited (e.g. Pinilla et al. 2017).

Finally, even minor molecular species may play an important role through the process of sintering (essentially the fusing of grains at temperatures just below the sublimation point of one of their constituents). Operating near the snowlines of species with a range of abundances this process can turn aggregates more brittle and thus more susceptible to fragmentation (Sirono 2011; Sirono and Ueno 2017), near the snowlines of species with even relatively minor abundances. Modeling by Okuzumi et al. (2016) has shown that the presence of sintered aggregates near snowlines in HL Tau can explain the radial structure observed in the dust continuum (ALMA Partnership et al. 2015; Zhang et al. 2015). More work is needed to understand the mechanical

³A factor 10 increase in the sticking threshold translated to an increase in the maximum particle size that of a factor 10^2 in turbulence-driven growth (Birnstiel et al. 2012).

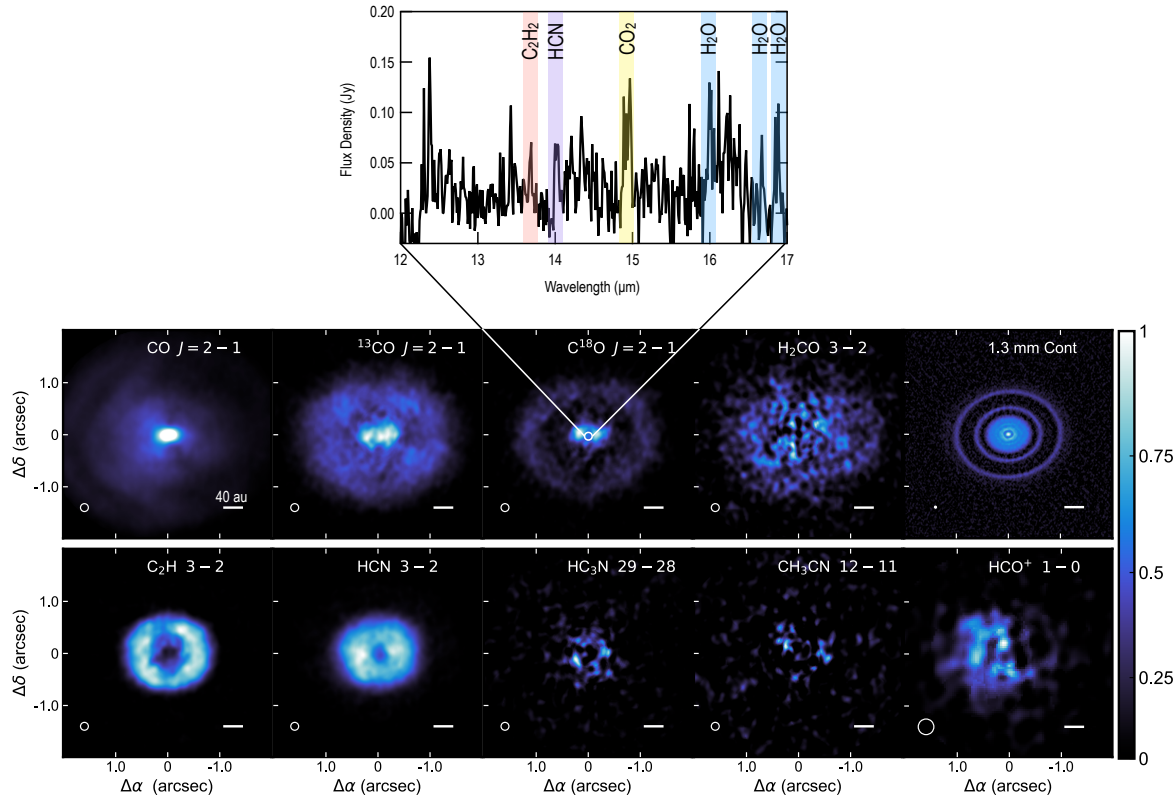


Fig. 6.—: Images of the AS209 obtained as part of the Molecules at Planet-forming Scales (MAPS) ALMA large program (Oberg et al. 2021). Molecular emission images are from Czekala et al. (2021) and Law et al. (2021). Dust emission image is from the ALMA large program The Disk Substructures at High Angular Resolution Project or DSHARP (Andrews et al. 2018; Huang et al. 2018a). All emission images are normalized to the peak with ^{12}CO having a different normalization in order to enhance the weak extended emission. Spitzer spectrum of AS209 is shown on top with particular features identified. This emission arises from the inner few au of the disk as illustrated. Spitzer spectrum kindly provided by C. Salyk.

behavior of realistic, complex aggregates that are mixtures of different refractory and ice phases.

6.1.3. Pebble dynamics and CHNOPS redistribution

The formation and evolution of pebbles can have a profound effect on CHNOPS abundances and elemental ratios in a variety of disk reservoirs.

First, the removal of small dust as a source of opacity from the outer disk and disk surface layers changes the disk temperature structure and radiation field, altering the freeze-out/condensation balance of (highly) volatile species (e.g., Cleeves 2016). Second, efficient vertical settling can lead to sequestration of volatile species in the midplane, and thus their removal from the surface, through the “vertical cold finger” effect (Meijerink et al. 2009; Krijt et al. 2016b; Xu et al. 2017; Van Clepper et al. 2022). Observational support for this comes from low abundances of C and O carrying species (Kama et al. 2016; Du et al. 2017; Zhang et al. 2019, 2020b). In IM Lup, contrary to C and O, N does not appear to be depleted, suggesting a highly volatile carrier (N_2) that cannot readily be sequestered in this disk’s midplane (Cleeves et al. 2018).

Arguably more important for planet formation is that pervasive radial drift will profoundly alter elemental and molecular abundances in the disk midplane, often concentrating material around snowlines (e.g. Cuzzi and Zahnle 2004; Öberg and Bergin 2016; Booth et al. 2017; Stammer et al. 2017; Krijt et al. 2018; Booth and Ilee 2019; Krijt et al. 2020). Radially resolved CO depletion profiles inferred by Zhang et al. (2019) resemble model results when pebble settling and drift is included (Krijt et al. 2018, 2020), and Zhang et al. (2020a) use this framework to estimate the pebble flux across the CO snowline as $\approx 15\text{--}60 M_{\oplus}/\text{Myr}$ in HD163296.

An unresolved question concerns the fate of ice-rich pebbles as they drift through major snowlines and begin to sublimate. For compact pebbles with a core/mantle structure, the drift timescale is shorter than the thermal desorption timescales for pebbles with sizes $\gtrsim 1$ cm, meaning ice-coated particles may drift considerable distances before fully sublimating, effectively dragging snowlines in by as much 40-60% (Piso et al. 2015). For porous, more loosely bound aggregates, however, sublimation of major phases may lead to aggregate disintegration (Aumatell and Wurm

2011), possibly leading to an enhancement of small grains near e.g., the water snowlines (*Schoonenberg and Ormel* 2017). Recent laboratory experiments indicate aggregates may escape disruption if their ice content is below $\approx 15\%$ or if they contain significant small dust grains (*Spadaccia et al.* 2022), although it is not clear how robust the surviving structures are against fragmentation in future collisions.

While the inner disk midplane is hidden from view, there are tantalizing signs of a link between the details of CNO chemistry in the inner disk and the behavior pebbles further out, with higher ratios of HCN/H₂O fluxes being found (on average) for systems with a more massive (*Najita et al.* 2013; *Najita and Bergin* 2018b) and/or more radially extended (*Banzatti et al.* 2020) pebble disk. These results suggest that disks in which significant inward migration of pebbles has occurred contain more water vapor (or, lower C/O) in their terrestrial planet formation regions. It is interesting to note that while IR line fluxes of e.g. HCN and C₂H₂ look very different around cooler M5-M9 stars (*Pascucci et al.* 2009), ALMA observations of CO, HCN, and C₂H indicate the (observable) chemistry around 10-100 au is similar in cool (M4-M5) stars compared to Sun-like stars – although hydrocarbons may be more abundant around the cooler objects (*Pegues et al.* 2021).

Despite the lack of a clear correlation between the locations of molecular rings and rings and gaps in seen in dust continuum (*Jiang et al.* 2022), evidence is mounting that sub-structure in the gas and dust (Sect. 6.2.4) plays a role in shaping the observable chemistry in complex ways. For example, *Facchini et al.* (2021) present a resolved observations of e.g., CO, CS, HCN, and small hydrocarbons in the ringed and planet-hosting disk of PDS70, highlighting how emission of different molecules peaks at different locations relative to the dust continuum. Overall, the observed chemistry (e.g., the lack of SO) however points to a C/O > 1. In contrast, *Booth et al.* (2021a) present detections of SO and SO₂ (but not CS) in Oph-IRS 48, suggesting C/O values below unity in this disk that contains an azimuthally asymmetric distribution of pebbles (*Booth et al.* 2021a). For a larger sample of 26 protoplanetary disks, *van der Marel et al.* (2021) find a tentative correlation between the C/O ratio (as traced by C₂H emission) and the location of the outermost pressure bump relative to the CO snowline location.

Finally, the effects of radial drift may be mitigated by so-called ‘dust traps’ in disks: radial locations where there are local pressure maxima that cause the drifting pebbles to pile up (*Pinilla et al.* 2012b). Dust traps are thought to cause the rings in millimeter-sized dust grains that form at the edges of disk gaps (*Pinilla et al.* 2012a), and they may also exhibit asymmetric pebble clustering (e.g. Oph-IRS 48 *van der Marel et al.* 2013). The presence of traps should produce a volatile depletion in the gas interior to the trap’s location, in contrast with the volatile enhancement expected from radial drift. Such a trap-induced depletion in C-rich gas has been inferred from measurements in the inner disks of young Taurus stars, some of which are compact disks

for which millimeter grain substructure has yet to be seen (*McClure* 2019). This ability of inner disk gas depletion to probe traps in known millimeter substructure was confirmed for TW Hya (*Bosman et al.* 2019). If silicon gas is also measured, then the bulk solid composition of dust in the traps can be calculated and compared with Solar System bodies. For TW Hya, the dust has a C, N, O composition indicative of both CI chondrites and comets *McClure et al.* (2020).

6.1.4. Planetesimal Formation: Where & When

In modern planet formation theory, planetesimals form via a two-step process: pebbles are accumulated in dense clumps (or clouds) via the streaming instability (SI), and these clouds gravitationally collapse to directly form macroscopic planetesimals (*Youdin and Goodman* 2005; *Johansen et al.* 2014, *Drążkowska et al.*, this volume). The initial mass function of planetesimals formed in this way peaks between 50 and a few 100 km (*Simon et al.* 2016), largely independent of pebble properties (*Simon et al.* 2017). This characteristic size of 100 km is supported by more recent theoretical considerations (*Klahr and Schreiber* 2020), simulations (*Klahr and Schreiber* 2021), and roughly matches observed kinks in the size distributions of asteroids (*Bottke et al.* 2005; *Morbidelli et al.* 2009). The gravitational collapse of a pebble clump is rapid but gentle (e.g., *Visser et al.* 2021), and it is customary to assume the primordial planetesimal essentially inherits the composition of the pebbles and ices present in that particular part of the disk. Observational support for planetesimal formation via pebble clump collapse comes from studying the orientation of Kuiper Belt binaries (*Nesvorný et al.* 2019) and the structure of individual Kuiper Belt Objects like Arrokoth that have been visited upclose (*McKinnon et al.* 2020).

Roughly since *Protostars & Planets VI*, perhaps inspired by *Johansen et al.* (2014), hybrid models have become popular that connect disk-wide dust coagulation and drift to planetesimal formation via the streaming instability (e.g., *Krijt et al.* 2016a; *Drążkowska et al.* 2016; *Drążkowska and Alibert* 2017; *Carrera et al.* 2017; *Schoonenberg and Ormel* 2017; *Schoonenberg et al.* 2018; *Lenz et al.* 2019). In many such studies of the conditions needed to trigger SI, the required increase in dust-to-gas ratio (by a factor of ≈ 2 , when starting from a solar metallicity; *Carrera et al.* 2015) was found to be too restrictive, and additional ways of “pre-concentrating” solids in specific disk locations (e.g., at a snowline) appeared to be necessary⁴.

Depending on the method of pre-concentration, as well as specifics in the dust properties (e.g. sticking threshold and variation therein, porosity) and disk properties (initial surface density, turbulence), such hybrid models yield very

⁴*Li and Youdin* (2021) recently revised the metallicity threshold for SI down to below 0.01 (for selected pebble sizes), suggesting easier planetesimal formation across a range of disk locations, although the impact on disk-wide dust evolution & planetesimal formation models has not yet been assessed.

TABLE 3
 COMPILATION OF CHNOPS CARRIERS IN THE ISM AND PROTOPLANETARY DISKS

Carrier	T_{cond} (K) "Reset"	T_{sub} (K) "Inheritance"	Approximate midplane snowline location ¹ (au)	
			Class 0 disk	Class II disk
Graphite		2400	≤ 0.05	≤ 0.05
Silicates	1350	1350	0.11	0.50
(Fe,Ni) ₃ P	1000	1000	0.65	0.15
FeS	655	655	1.0	0.23
CHON(S)		400	1.8	0.40
NH ₄ ⁺ X ⁻		$\approx 200-500$	3.9	0.88
H ₂ O	100–150	100–150	7.5	1.7
NH ₃	109	109	7.6	1.7
CH ₃ OH		99	8.5	1.9
PH ₃	88	88	9.7	2.2
H ₂ S	54	54	17	3.8
CO ₂		53	17	3.8
CH ₄	26	26	38	20
PO	24	24	41	18
CO	23	23	43	27
N ₂	20	20	49	36

¹Locations based on the midplane temperature of an irradiated, viscously evolving *Chambers* (2009) disk model around a young solar-mass star evaluated at $t = 40$ kyr (Class 0) and 2 Myr (Class II).

different outcomes. For example, some models favour short bursts of planetesimal formation around the water snowline (*Schoonenberg and Ormel* 2017), others form planetesimals late and at large heliocentric distances (*Carrera et al.* 2017), and others still predict planetesimal formation over extended periods and essentially throughout the entire disk (*Lenz et al.* 2019). Recent studies also highlight the possibility of efficient planetesimal formation in existing pressure bumps (*Stammler et al.* 2017; *Carrera et al.* 2021). It is worth noting that many of these models rely on volatiles (usually H₂O) and the radial drift of pebbles to locally increase dust-to-gas ratios via either: (1) retro-diffusion across the snowline followed by rapid freeze-out, and/or (2) a dramatic change the sticking behavior of grains near the snowline (see Sect. 6.1). In disks with different temperature structures (for example those around M stars) these models would predict the main planetesimal formation zone to lie closer to the star (*Ormel* 2017).

The locations where planetesimals and planets form can be probed implicitly through the radial positions of dust traps. Oph-IRS 48 is the best example of this, as the dust is both radially and azimuthally confined (*van der Marel et al.* 2013). However, for disks without resolved substructure, *McClure et al.* (2020) have proposed that it is possible to locate planet-forming zones relative to different volatile snowlines using the relative depletion of different volatiles from inner disk gas. Specifically, any significant depletion of elements such as N, C, O, or Si suggests dust traps, but a low N/C or C/O abundance ratio implies traps beyond the N₂ or CO₂ snowlines, respectively. High O/Si abundance ratios are sensitive to traps outside versus inside the H₂O snowline. Future observations of inner disk gas with CRIRES+ and JWST will help to establish this technique.

An indirect way of timing widespread planetesimal formation in nearby protoplanetary disks is to compare their

solid mass budget to the masses of mature planetary system (*Najita and Kenyon* 2014; *Manara et al.* 2018; *Tychoniec et al.* 2020; *Mulders et al.* 2021; *Lovell et al.* 2021). While there are many uncertainties associated with converting continuum fluxes to dust masses (e.g. *Zhu et al.* 2019) these studies suggest planetesimal formation may begin early. Similarly, comparing spatial scales of observed pebble disks to planetary system demographics reveal dramatic inward mass transport must take place at some stage of planet formation, either in the form of early pebble migration, or later planet migration (*Mulders et al.* 2021). It is worth noting that while gas disks (as revealed by excess IR emission) live longer around cool stars (*Carpenter et al.* 2006; *Luhman and Mamajek* 2012, and Sect. 6.2.5), the total mass contained in pebbles (as estimated from submillimeter continuum emission) decreases faster (*Pascucci et al.* 2016), suggesting radial drift operates faster/differently (*Pinilla et al.* 2020) and/or a faster conversion of pebbles into planetesimals.

6.2. Planetesimal Evolution & Protoplanet Accretion

6.2.1. Local planetesimal accretion

Rapid runaway growth amongst small planetesimals results in the formation of bodies up to 100-km sizes on timescales of 10^{4-5} yr around 1 au (*Wetherill and Stewart* 1989; *Kokubo and Ida* 1996; *Weidenschilling et al.* 1997). There is a transition from runaway to oligarchic growth once the largest planetesimals dynamically excite smaller bodies in their feeding zones, which shuts down focusing (*Wetherill and Stewart* 1989; *Kokubo and Ida* 1996; *Weidenschilling et al.* 1997); this transition occurs roughly at a few 100 km in inner disk and $\sim 10^3$ km in the outer parts (*Ormel et al.* 2010). Oligarchs continue to slowly but steadily gain mass by accreting smaller planetesimals

(Kokubo and Ida 1998; Rafikov 2003). After $\sim 10^6$ yrs, the result is then a handful of Moon to Mars-sized planetary embryos, separated by 5-10 Hill radii and surrounded by a swarm of smaller planetesimals (Kokubo and Ida 1998). Planetesimal accretion (in the absence of perturbing planets) can be thought as a fairly localized process, with feeding zones of growing bodies of the order of roughly 10 Hill radii (Tanaka and Ida 1999), which, for an $\sim 0.1 M_{\oplus}$ at 1 au correspond to roughly 0.03 au.

Moreover, planetesimal-planetesimal collisions during the runaway and oligarchic growth phases are not expected to lead to the loss of volatiles in hydrated minerals (Daly and Schultz 2018) or even ices (Schwartz et al. 2018), suggesting that compositional gradients in the planetesimal population (as shaped by formation and thermal evolution, see below) will be largely preserved during runaway and oligarchic growth. However, large numbers of successive embryo-planetesimal and embryo-embryo impacts may still lead to significant water loss, with simulations assuming perfect merging possibly overestimating the final water mass fraction by up to 10-20% (Haghighipour and Maindl 2022).

6.2.2. Planetesimal Thermal Evolution and ^{26}Al

While planetesimal-planetesimal impacts contribute little to heating, the presence of short-lived radionuclides (SLR) can significantly alter the physical/chemical structure and CHNOPS budgets of planetesimals that form relatively early and/or large. In particular, ^{26}Al 's half-life of 0.7 Myr makes it a potent source of internal heating.

Depending on how much a planetesimal's temperature rises, outgassing of highly-volatile ices (if present), followed by melting of water ice (if present), and finally partial and complete differentiation (i.e., the formation of a metal core and separation of lithophile and siderophile elements) can occur following melting of metal-sulfides and later silicates (Elkins-Tanton 2012; Fu and Elkins-Tanton 2014; Fu 2017). When heating is efficient (i.e., when planetesimals form early, are born larger, or the system just happens to have a high SLR abundance), silicate melting can lead to dramatic water loss at the planetesimal stage – even if the planetesimal formation mechanism itself may have preferentially formed water-rich bodies (e.g. Grimm and McSween 1993; Lichtenberg et al. 2019, 2021). Similarly, volatiles like CO and CO₂ (Lichtenberg and Krijt 2021), and more refractory carbon carriers can be lost, greatly reducing the bulk C/S ratio (Hirschmann et al. 2021).

The importance of formation age on parent body internal evolution is evidenced by the nature of the oldest meteorites in our collections: the iron meteorites, which were produced by metal-silicate segregation on a molten parent body following its accretion within just < 300 kyr (less than one half life of ^{26}Al) of CAI formation (Kruijer et al. 2014). In contrast, the high porosities (i.e., low densities) of small ($\lesssim 100$ km) Kuiper Belt Objects suggests limited SLR heating, and hence planetesimal formation times of

>4 Myr after CAI's in the outermost regions of the Solar System (Bierson and Nimmo 2019).

6.2.3. Pebble accretion and gas-driven migration

As embryos continue to grow, the orderly picture painted above is complicated by orbital migration (the change in a planet's semi-major axis) and pebble accretion.

The speed and even direction (i.e. inward vs. outward) of gas-driven Type I migration depends sensitively not just on planet mass (Ward 1997; Tanaka et al. 2002) but a slew of (local) disk properties including temperature and pressure profiles but also viscosity and details of heating/cooling/radiative transfer (see Paardekooper et al., this volume, for a review). In addition, convergent zones (where net torques on planets of certain masses vanish) can act as planet traps (e.g., Masset et al. 2006; Lyra et al. 2010; Dittkrist et al. 2014). Heat transitions, major snowlines, and dead zones can all act as planet traps (Hasegawa and Pudritz 2011; Bitsch et al. 2015b), and their locations are expected to move as disks evolve. In addition, excitation of orbital eccentricities from planet-planet interactions affects the planets' torque balance and drastically reduces the effectiveness of convergence zones (Cossou et al. 2013; Izidoro et al. 2017). While outward migration may dominate for low-mass cores in disks with low viscosity (Speedie et al. 2022), inward migration is still expected for planets with masses $\lesssim M_{\oplus}$ around Sun-like stars (Bitsch et al. 2015a).

Pebble accretion plays a major role in modern theories of planet formation (Ormel et al. 2010; Lambrechts et al. 2014). For our Solar System, there appears to be consensus on pebble accretion playing a role in the rapid growth of the giant planets (Lambrechts and Johansen 2012; Levison et al. 2015; Johansen and Lambrechts 2017; Alibert et al. 2018). The formation of the terrestrial planets does not appear to require pebble accretion per se (see also Chambers 2016; Nimmo et al. 2018; Izidoro et al. 2021c), perhaps because pebble accretion was less efficient inside the water snowline due to the smaller pebble sizes (Morbidelli et al. 2015), or because Jupiter blocked the influx of pebbles altogether as early as ≈ 1 Myr (Sect. 2.2). Nonetheless, some recent studies argue pebbles played an important role in the formation of Venus, Earth and Mars (Johansen et al. 2021).

For extra-solar systems, many studies have focused on modeling the formation of Super-Earths and Mini-Neptunes, highlighting the interplay between pebble accretion and planet migration (including Bitsch et al. 2019; Coleman et al. 2019; Schoonenberg et al. 2019; Izidoro et al. 2021a). Within this framework, emerging planetary architectures in the terrestrial planet region depend sensitively on the (evolution of the) pebble mass flux (Lambrechts et al. 2019; Drżkowska et al. 2021). The formation of systems like TRAPPIST-1 around low-mass stars may be explained via a combination of planetesimal formation near the water iceline, efficient pebble accretion until the pebble isolation mass is reached, followed by Type I migration and

the formation of resonant chains (Ormel 2017; Coleman et al. 2019; Schoonenberg et al. 2019).

6.2.4. Role of Giant Planets & Disks Substructure

The sizes of pebbles are roughly similar to the operating wavelengths of interferometers like ALMA, which means their spatial distributions in nearby protoplanetary disks can be studied down to spatial scales of $\lesssim 5 - 10$ au, revealing the pervasive and dramatic presence of so-called substructure (e.g., Andrews 2020; Bae et al., Manara et al., this volume), even in very young protoplanetary disks (ALMA Partnership et al. 2015; Segura-Cox et al. 2018). Although other origins are not easily ruled out, the deeper gaps in the radial distribution of pebbles are usually attributed to the presence of forming giant planets (Huang et al. 2018b; Zhang et al. 2018). The direct detection of PDS70b offers convincing evidence of this happening in at least one system (Keppler et al. 2018; Benisty et al. 2021).

Given the importance of the pebble flux on the growth of the inner planets (Lambrechts et al. 2019), it is reasonable to assume the (early) formation of giant planets on wide orbits has a profound influence on slowing down the growth of the inner planets by starving them of pebbles. And indeed, the stellar mass dependent occurrence rates of giant planets, super Earths, and extended (i.e. structured) vs. compact disks seem to support such a picture (van der Marel and Mulders 2021). Speedie et al. (2022) propose that this observed split between compact and large, structured disks is caused by diverging giant planet migration pathways in high vs. low viscosity disks. The efficiency with which giant planets can block the flow of solids depends sensitively on planet mass, disk viscosity, and the dust/pebble size distribution (e.g., Bae et al. 2019). In the fragmentation-limited region of the disk (Sect. 6.1), solids will frequently change size and thus aerodynamic behavior (e.g., Misener et al. 2019), suggesting fragments can still carry mass and solids CHNOPS through the gap.

There are several other mechanisms that become important in the presence of giant planets. First, by blocking the inward flux of solids and therefore ices, the appearance of giant planets on the scene effectively freezes in the current snowline location, creating what is known as a *fossilized* snowline (Morbidelli et al. 2016). The idea here is that the barrier thrown up by a giant planet (outside the snowline) results in the gas arriving in the inner disk through advection being depleted in water vapor.

Second, giant planets themselves are not static but migrate inward via Type II migration at a velocity roughly equal to the viscous speed of the disk (Lin and Papaloizou 1986). Thus, the planet population inferred from e.g. the DSHARP sample may look quite different once these planetary systems mature (Lodato et al. 2019). If giants planets form early, and the disk sticks around for long enough (see next Section), one or more giant planets can migrate through the terrestrial planet-forming region, which can disrupt the growth of rocky planets and drastically widen their

feeding zones (Raymond et al. 2006b; Mandell et al. 2007).

In this context, it is interesting to highlight uncertainties in the early growth of Jupiter’s core; with some studies favouring the water snowline as the formation region (Morbidelli et al. 2012), and others favouring core formation outside N_2 iceline followed by inward migration to explain the enhancements of C, N, S, P, Ar, Kr and Xe in Jupiter’s atmosphere (Öberg and Wordsworth 2019; Bosman et al. 2019). Irrespective of its role in separating reservoirs of material, the need to form Jupiter before the dissipation of the gas disk strongly supports the role of pebble accretion in the outer solar system, as approaches relying on accretion by planetesimals alone largely failed to work rapidly enough (e.g., Levison et al. 2010, 2015; Johansen and Lambrechts 2017; Alibert et al. 2018).

6.2.5. Gas Disk Dispersal & Primordial Atmospheres

Eventually the outer disk gas either accretes or dissipates (Pascucci et al. this volume). The inevitable exit of the primordial gas disk does not signal the end of terrestrial planet formation (next Section) but does bring a halt to important processes like pebble accretion and Type I and Type II migration. Average dispersal timescales are around 2–4 Myr (Lada et al. 2006; Mamajek 2009), with gas disks around low-mass stars sticking around longer (Carpenter et al. 2006; Luhman and Mamajek 2012), while disks around stars with $>2M_\odot$ evolve faster (Ribas et al. 2015). The short lifetimes however may be attributed to a bias towards dense star forming environments, with Pfalzner et al. (2014) finding higher disk fractions in co-moving groups, and arguing that 30% of all field stars can host disks for more than 10 Myr. Recently, Michel et al. (2021) argued lifetimes of closer to 8 Myr may be more representative for disks with considerable substructure. In this context then the Solar nebula, with a lifetime of ≈ 4 Myr (Wang et al. 2017 and Sect. 2.2) does not appear to be unusual, although a considerable spread in ages – possibly influenced by the evolution of substructure and environment – is found.

If planetary embryos manage to grow large enough before the disk dissipates, they may be able to hold on to a (primordial) hydrogen and helium dominated atmosphere. These atmospheres can play a role in shaping CHNOPS budgets by processing any incoming pebbles (Johansen et al. 2021). Lee and Chiang (2015) estimate that embryos with masses $\sim 0.5 - 0.8M_\oplus$ are capable of binding atmospheres of $\sim 10^{-4} - 10^{-2}M_\oplus$ (see also Sect. 2.2). In systems where icy pebbles enriched the inner disk gas in volatiles, these primordial atmospheres may have had molecular and elemental abundances (and abundance ratios) very unlike the primordial nebula (Booth and Ilee 2019; Banzatti et al. 2020 and Sect. 6.1.3). For example, Bitsch et al. (2021) show how wet mini-Neptunes can form wholly inside the water snowline just from the accretion of inner disk gas enriched in water.

6.3. Endgame: Final assembly of terrestrial planets

6.3.1. Dynamical (In)stability

It has been argued that the two key dynamical processes shaping the orbital architectures of planetary systems are migration and dynamical instability. Starting from a universal set of planetary precursors, just those two ingredients – migration and instability – can broadly explain the diversity of planetary systems, from the Solar System to giant exoplanets and systems of close-in ‘super-Earths’ (see extensive discussion in *Raymond et al.* 2018b).

Analysis of systems containing multiple close-in low-mass planets discovered by the *Kepler* mission has found that such systems on average tend to be spaced, in units of Hill radii, more widely than expected (*Fang and Margot* 2012; *Pu and Wu* 2015). This is interpreted as the signature of a late phase of giant impacts, as decades of simulations of late-stage accretion of the terrestrial planets have shown that spacing by Hill radii is the characteristic outcome of a late collisional phase (see reviews by *Morbidelli et al.* 2012; *Raymond et al.* 2014). Systems of giant exoplanets also show clear signs of dynamical instability. Their broad eccentricity distribution is naturally matched if 75-95% of all giant exoplanet systems are the survivors of planet-planet scattering, triggered by dynamical instability in the high escape-speed regime (*Ford and Rasio* 2008; *Jurić and Tremaine* 2008; *Chatterjee et al.* 2008). This model is well-accepted as it is extremely robust, deceptively simple, and able to explain several other aspects of the dynamical configurations of giant exoplanet systems (*Raymond et al.* 2010). Likewise, to match the period ratio distribution of close-in small planets, 95% or more must be the survivors of a late phase of collisions (*Izidoro et al.* 2017, 2021a). Such instabilities among giant planets, at least within a few au, would have a devastating effect on the growth of rocky planets in the same systems (*Veras and Armitage* 2006; *Raymond et al.* 2011, 2012) and in some cases close-in super-Earths (*Mustill et al.* 2017).

There is a plausible narrative that can explain why late instability are likely common, built on the processes of orbital migration and dynamical instability (for more detail see *Raymond et al.* 2018b). The narrative goes as follows. Planetary embryos and giant planet cores cannot avoid orbital migration as long as they grow sufficiently massive early enough in the gaseous disk phase (*Kley and Nelson* 2012; *Baruteau et al.* 2014). Many generations of hydrodynamical simulations of migrating protoplanets show that they are naturally organized into chains of mean motion resonances, in which neighboring planets’ orbital periods form the ratio of small integers such as 2:1, 3:2, 4:3 and so on (*Cresswell et al.* 2007; *Pierens et al.* 2013). Many resonant chains likely migrate all the way to the inner edge of the gaseous disk, where a strong positive torque acts as a migration barrier (*Masset et al.* 2006; *Romanova and Lovelace* 2006). This is thought to be the case for low-mass planets such as the progenitors of ‘super-Earths’ and ‘sub-Neptunes’ (*Terquem and Papaloizou* 2007; *Ogihara and Ida*

2009; *Cossou et al.* 2014). Other migration halting mechanisms may exist to trap resonant chains of planets at larger orbital radii; for instance, the HR8799 system consists of four mega-Jupiters in a chain of resonances extending from ~ 18 au to ~ 70 au (*Marois et al.* 2008, 2010; *Fabrycky and Murray-Clay* 2010).

6.3.2. Giant impacts & Late Accretion

The late phases of the growth of terrestrial planets are thought to have been characterized by a series of giant impacts between roughly Mars-mass or larger planetary embryos (*Morbidelli et al.* 2012; *Raymond et al.* 2014). These giant impacts had the potential to alter the planets’ bulk compositions by preferentially stripping the outer layers, leading to erosion of a growing planet’s atmosphere, oceans, or even mantle (*Genda and Abe* 2005; *Asphaug et al.* 2006). Yet there is a broad spectrum of outcomes of such impacts (*Genda et al.* 2012; *Leinhardt and Stewart* 2012), and certain configurations may lead to the formation of a large satellite such as the Moon (*Benz et al.* 1989; *Canup and Asphaug* 2001). The stochastic nature of this phase effectively erases much of the previous phases of planetary growth such that the nature of the Moon-forming impact cannot be used to trace back our system’s earlier history.

Late planetesimal impacts can have a strong erosive effect on a planet’s atmosphere and water budget (*Schlichting et al.* 2015; *Schlichting and Mukhopadhyay* 2018), with habitable zone planets around M stars being more susceptible to impact stripping (*Wyatt* 2020). While the Earth’s late veneer likely had a local origin (Sect. 2.2), a substantial amount of volatile rich material from the outer system may be directed towards terrestrial planet formation regions in systems with different planetary architectures (*Marino et al.* 2018). Finally, terrestrial planets in relatively old gas-rich debris disk systems may be able to accrete some of the secondary C and O rich gas directly (*Kral et al.* 2020). As discussed earlier, P was likely delivered to rocky planets in the solar system as schreibersite, $(\text{Fe,Ni})_3\text{P}$. The P from schreibersite can be made available for life by hydration or by lightning-induced chemistry (*Hess et al.* 2021).

7. BRANCHING POINTS FOR MAKING CHEMICALLY HABITABLE WORLDS

We now speculate about what we consider to be major branching points in the formation of chemically habitable planets, using Fig. 7 to illustrate diverging pathways.

7.1. A note on stellar environment

While planet formation is often discussed in the context of isolated protoplanetary disks, we recognize that the stellar *environment* can play an important if indirect role at several key stages during the planet formation process. *Parker* (2020) reviews three key stellar density thresholds: First, above $\sim 10 M_{\odot} \text{pc}^{-3}$, FUV and EUV radiation from nearby massive stars can affect protoplanetary disks. At

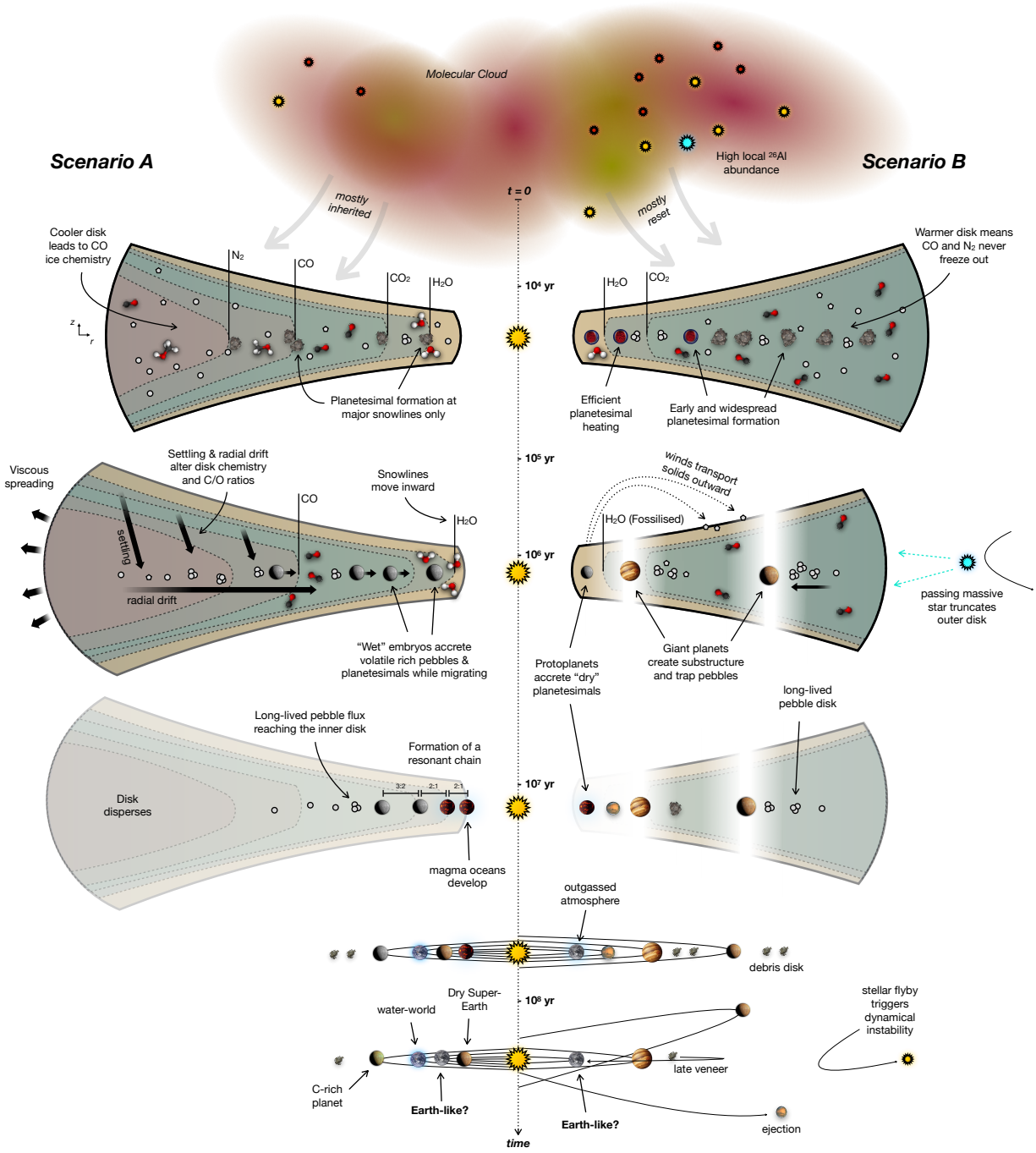


Fig. 7.— Illustration of two hypothetical scenarios leading to the formation of diverse planetary systems and planets with varying degrees of chemical habitability. Individual processes and key branching points are discussed in more detail in Sects. 6 and 7. In Scenario A, a cold disk forms in a relatively quiet part of a star forming region, and planetesimal formation occurs exclusively at major snowline locations. Planetary embryos accrete volatile-rich planetesimals (this particular system formed without much ²⁶Al) and pebbles, while themselves migrating inward to form a resonant chain. This system does not become dynamically unstable, but variations in distance to the star and ongoing geophysical processes (e.g., the duration of the magma ocean phase, and ability of the core to sequester volatiles) leads to variations in the types of planets that form. In Scenario B, the disk forms with a higher metallicity and SLR abundance, and planetesimals are able to form throughout. The formation of giant planets causes substructure, fossilizes the water snowline, and shuts off the radial pebble flux early on. Terrestrial planets form from dry, de-volatilized planetesimals, but may still acquire CHNOPS later on during externally triggered instability and late veneer-like event.

stellar densities $>100 M_{\odot} \text{ pc}^{-3}$ planetary orbits (i.e., eccentricity, inclination, and semi-major axis) can be altered, and in the densest regions with $>1000 M_{\odot} \text{ pc}^{-3}$ protoplanetary disks themselves can be truncated by close stellar encounters. Proximity to nearby high mass stars increases the density threshold required to form ices in dense molecular clouds, with less strong ice absorption towards Ophiuchus, which is exposed to the irradiation from A-stars in upper Scorpius, than towards the less-exposed Taurus molecular cloud (see discussion on p.89 of *McClure et al.* 2010; *Williams et al.* 1992). Moreover, proximity to short-lived massive stars can play a major role in setting the SLR abundance, greatly affecting volatile losses during the planetesimal stage.

Within the vicinity of the Sun (500 pc), the Orion Nebula Cluster is likely the only star forming region that may have met or exceeded the third density threshold. *Winter et al.* (2020), by identifying old co-moving groups in Gaia data, find planetary system architecture (in this case the median semi-major axis and orbital period) differ in stellar clusters versus field stars, with, e.g., Hot Jupiters existing primarily in stellar phase space overdensities. (However, see also the independent analysis of the Winter et al. data by *Adibekyan et al.* (2021), which comes to different conclusions when considering a smaller but less biased sample.). And yet, planets are predicted to survive (*Fujii and Hori* 2019) and have been observed in open clusters (e.g., *Quinn et al.* 2012; *Meibom et al.* 2013; *Livingston et al.* 2018; *Curtis et al.* 2018).

7.2. Stellar metallicity and CHNOPS abundances

At the most fundamental level, the metallicity and relative elemental abundances protostellar system control the amount of solids and CHNOPS available for planet formation.

Metallicity clearly plays an important role in planet formation. On the one hand, an environment with a metallicity that is too low may prohibit any planet formation altogether. Protoplanetary disks with low metallicities have shorter lifetimes (due to increased efficiency photoevaporation) (*Kornet et al.* 2005; *Yasui et al.* 2010; *Ercolano and Clarke* 2010), decreasing the chances for planet formation to occur, and theoretical models of planet formation in circumstellar disks predict that Earth-mass planets would only start to appear around host star metallicities of -1.0 dex (*Johnson and Li* 2012; *Mordasini et al.* 2012).

On the other hand, an environment with a metallicity that is high is more likely to form giant planets. These have been suggested as detrimental to small planet formation (or at least chemically habitable planet formation) due to the influence of the giant planet’s eccentricity and/or migration on the terrestrial planet’s long-term dynamical stability (e.g., *Dressing et al.* 2010; *Kita et al.* 2010), or even prohibitive of the formation of a terrestrial planet in the first place (e.g., *Raymond et al.* 2011; *Lambrechts et al.* 2014; *Izidoro et al.* 2015; *Owen and Murray-Clay* 2018).

Owen and Murray-Clay (2018) observe that super-Earths (\sim terrestrial planets) with long periods are more common around lower metallicity stars (which host fewer giant planets), consistent with fewer solids resulting in cores not massive enough to accrete large H/He envelopes and/or formation after the disk dispersed. And *Booth and Owen* (2020) flipped the script on the “solar twin”–small planet connection first proposed by *Meléndez et al.* (2009), instead suggesting that the 10% refractory element depletion seen in \sim 10-20% of solar twin stars is due to trapping of dust exterior to the orbit of a forming giant planet, preventing refractory-rich material from accreting onto the star. However, there is evidence from both the *Kepler* sample and the combination of direct imaging and long-term radial velocity (RV) monitoring that longer period giant planets are *highly likely* to be accompanied by an inner small ($\lesssim 4R_{\oplus}$) planet (*Zhu and Wu* 2018; *Bryan et al.* 2019), although this evidence is complicated by the recent survey of giant planet hosting-systems by *Barbato et al.* (2018) that found no inner super-Earth companions.

Thus far, however, few obvious differences have been observed in the detailed compositions stars known to host (mostly large) planets versus those not known to host planets, beyond that first observed in [Fe/H] and an enhancement in alpha elements when [Fe/H] is low (Sect. 4). With the advent of both space-based all-sky surveys for planets (e.g., TESS, PLATO) and ground-based all-sky stellar spectroscopic surveys (e.g., APOGEE, LAMOST, GALAH, WEAVE, 4MOST, MOONS), larger-scale and/or more precise comparisons between the compositions of stars hosting different types of planets, particularly potentially-terrestrial ones, will be of great interest to the context of chemical habitability. If the the interior or surface compositions of rocky planets depend on their host star abundances, this may also be observationally constrained via their atmospheric abundances, although this is a relatively new area of research (*Herbort et al.* 2020; *Bitsch and Battistini* 2020).

7.3. Planetesimal Formation & Evolution

Despite the success of the streaming instability model of planetesimal formation to overcome the meter-size barrier, uncertainties in the timing and location of planetesimal creation constitute a major obstacle in our understanding of how, where, and what types of planets emerge inside protoplanetary disks. Snowlines and their evolution in time play an important role by (1) influencing the volatile budget of dust and pebbles and (2) being prime sites of efficient planetesimal formation. Indeed, it is possible that, rather than a continuous disk, two or three spatially-separated rings of planetesimals formed, associated with the condensation fronts of silicates, water and CO (*Morbidelli et al.* 2022; *Izidoro et al.* 2021b). If planetesimal formation indeed follows snowline locations, we may expect similar intra-system compositional variability to emerge in different sys-

tems⁵. While highlighting the role of snowlines, it is interesting to note that their locations (during the protoplanetary disk phase) relative to the location of the classical habitable zone (for mature systems) are strongly stellar mass dependent. For low-mass stars, for example, the habitable zone is located considerably further inside the water snowline (e.g., *Mulders et al.* 2015; *Desch et al.* 2020), suggesting the building blocks forming near what would become the habitable zone were originally much drier.

Another major source of inter-system variability can come from variation in SLR abundances⁶. In systems with considerable amounts of SLR, heating followed by the loss of volatiles from planetesimals that form early and/or are born big can be very dramatic. In these systems we expect planetesimals to be water, C, and N poor, while losses of P and S may be less severe as they exhibit more siderophile/chalcophile behavior during planetesimal differentiation.

There exist few direct constraints on planetesimal CHNOPS compositions in extra-solar systems. Possible avenues are studying second-generation gas originating in planetesimal belts in debris disks (e.g., *Marino et al.* 2016; *Matrà et al.* 2017; *Wyatt* 2020), or constraining the composition of material raining down on polluted white dwarfs (e.g., *Jura and Young* 2014; *Xu et al.* 2014, 2017; *Doyle et al.* 2019). So far, these constraints paint a picture of planetesimal compositions reminiscent of the asteroid and Kuiper Belt populations in our solar system. In the near future, JWST, especially in combination with ALMA, will be instrumental in further constraining inner disk chemistry and elucidating its link to the large-scale redistribution of pebbles. Further detailed spectroscopic investigations of the ~500,000 new white dwarf candidates from Gaia DR2 (*Gentile Fusillo et al.* 2019; *Melis et al.* 2018; *Kaiser et al.* 2021) will likely greatly increase the sample of polluted white dwarfs and thus constraints on the diversity of extra-solar planetesimal CHNOPS budgets.

7.4. Pebble vs. Planetesimal Accretion

In terms of emerging planetary CHNOPS budgets, planetesimal and pebble accretion pathways involve very different feeding zones and loss mechanisms for CHNOPS elements: Planetesimals are mostly accreted locally and can devolatilize following internal heating and differentiation. Following the dissipation of the gas-disk, mixing and transport of material is still possible, albeit by less efficient dynamical mechanisms (Sect. 6.3). Conversely, while peb-

ble accretion is quite fast it is not particularly efficient and would require potentially hundreds of Earth masses of pebbles to build for example the Solar System's terrestrial planets. Such mass is not expected to be available exclusively within the inner regions of protoplanetary disks, and therefore a large influx of material from more distant regions of the disk would be required, potentially flooding the terrestrial planet formation region with water and other volatiles.

The radial pebble flux reaching inner protoplanetary disks can be decreased or completely shut down by changing pressure gradients in the disk (*Haghighipour and Boss* 2003), where possible mechanisms to stop the flow from the outer disk to inner disk include the growth a giant planet core (*Kruijer et al.* 2017), or pressure bumps preceding giant planet growth (*Brasser and Mojzsis* 2020), so it is possible to have pebble accretion in one place (or at a certain time), but a lack of pebbles elsewhere.

Simulations of rocky planet formation accounting for planetesimal accretion offer different predictions about the role giant planets in terrestrial planet composition, for example: the scattering of planetesimals following Type II Jovian planet migration results in terrestrial planets with high water fractions (*Raymond et al.* 2006a; *Carter-Bond et al.* 2012); higher eccentricities of Jovian planets reduce water delivery to terrestrial planets (*Raymond et al.* 2009); and inner super-Earths with outer giant companions will be volatile-poor and have higher densities (*Schlecker et al.* 2021).

There has been less work investigating emerging rocky planet compositions in pebble accretion-dominated scenarios. Even though pebbles will originate from the outer disk regions, and their journey inward will have them traverse multiple snowlines (e.g. Table 3), the standard assumption is that their relatively small size will not allow them to hold on to most volatile species for very long (*Piso et al.* 2015). Thus, while they may alter the gas-phase abundances in the inner disk (see Sect. 6.1.3), the pebbles themselves will be fairly "dry" once they reach the inner disk. Nonetheless, in the absence of a barrier in the outer disk, the terrestrial planet formation region may be flooded with material rich in water ice (*Bitsch et al.* 2021) and refractory/organic carbon, erasing any (prior) carbon loss that occurred via oxidation or photolysis (*Klarmann et al.* 2018). Still, the H₂/He envelopes of early Earth and Mars analogues (see also Sect. 6.2.5) may be hot and dense enough for organic molecules to undergo pyrolysis and sublimation during pebble accretion, allowing the carbon and oxygen to diffuse back to the protoplanetary disk and resulting in relatively dry and carbon-poor planets (*Johansen et al.* 2021).

With the increase in exoplanet detection and characterization capabilities, these predictions are now becoming testable via detailed, careful comparisons of small planets with and without known giant planet companions.

⁵Interstellar interloper 2I/Borisov was observed to be very CO rich (*Cordiner et al.* 2020; *Bodewits et al.* 2020), prompting comparisons to the unusual comet C/2016 R2 (*Biver et al.* 2018b) and theories about an origin near the CO iceline (*Mousis et al.* 2021; *Price et al.* 2021).

⁶There could also be more spatial variation in the ²⁶Al distribution in the same disk: Recent work by *Adams* (2021) suggests that it may be common for planet-forming material close to the the magnetic truncation radius of star/disk systems (~0.1 AU) to have ²⁶Al abundances enhanced over early Solar System values by factors of ~10-20 due to spallation reactions from stellar cosmic rays.

7.5. Migration & Instabilities

Two major lessons learned in the last few decades are that planets do not necessarily form where we find them today and that potentially violent dynamic instabilities are likely the norm rather than exception (Sect. 6.3.1). Even with perfect knowledge of a system’s initial conditions (which elements primarily in what form in which regions of the disk) and detailed knowledge of the primary modes of accretion, planets can thus move great distances and then combine with each other in chaotic fashion in a way that can frustrate reverse engineering the provenance of each. Close-in super-Earths are a good example of this phenomenon, as models for their starting location span from the innermost parts of the disk (*Chatterjee and Tan 2014*) to far beyond the snow line (*Terquem and Papaloizou 2007; Izidoro et al. 2021a*).

A number of lines of evidence – from the giant planets’ orbits and small body populations – suggest that our Solar System also underwent a dynamical instability (*Nesvorný 2018*). Our current understanding of the instability indicates that the giant planets likely scattered off of each other, perhaps even ejecting a primordial additional ice giant. However, the Solar System’s instability was gentle in comparison with that experienced by most giant exoplanet systems, as Jupiter and Saturn never underwent a close encounter; if they had, our Earth would not have survived (see *Raymond et al. 2011*).

Planetary migration during the gas-rich protoplanetary disk phase, especially when crossing (major) snowline locations, can lead to planetary compositions that may be unexpected purely from the planet’s final location. For example, if planetary cores form near or outside the water ice-line, planets ending up well within the snowline location may hold large reservoirs of water, with water mass fractions of up to ~ 10 wt% (e.g. *Raymond et al. 2008; Ogihara and Ida 2009; Bitsch et al. 2019*), although migration can also create a diversity of super-Earth compositions including purely rocky planets (*Raymond et al. 2018a; Izidoro et al. 2021a*). *Bitsch and Johansen (2016)* showed that decreasing the water-to-silicate ratio of dust grains in the disk from 1:1 (as in the pebble accretion model of *Bitsch et al. 2015a*) to 1:3 resulted in more migration of icy cores to sub-AU orbits, as lower water content decreases the temperature gradient near the ice line thereby reducing the chances of outward migration; this implies that some short period super-Earths, perhaps those around oxygen-poor stars, should contain larger fraction of water accreted from beyond the ice line (see also *Bitsch et al. 2021*). For compact systems around M dwarfs, the formation scenario outlined above predicts very wet planets with water contents $\sim 10\%$ (*Unterborn et al. 2018; Schoonenberg et al. 2019*). For TRAPPIST-1, density constraints for the outer 4 planets (e-h) allow up to $\approx 5\%$ water if they sport an Earth-like core and mantle, but other solutions that allow higher water contents cannot be ruled out (*Agol et al. 2021*).

While the radius-period distribution of short period

super-Earth/mini-Neptune planets is consistent with planet formation models that result in predominantly “rocky” versus icy compositions (e.g., *Owen and Wu 2013, 2017; Jin and Mordasini 2018; Rogers and Owen 2021*), in some contexts rocky planets may have up to 20% water content by mass (*Gupta and Schlichting 2019*). The true diversity of super-Earth/mini-Neptune compositions is an important issue that will be informed by additional precise mass measurements, atmospheric composition constraints, and better constraints on the occurrence rate of small planets beyond ~ 30 days (*Lee et al. 2022*).

Resonant chains are generally stable during the gaseous disk phase. In some cases they may break – for instance, leading to a collision between neighboring low-mass planets close to their star – but if the gas disk is still present the resonant chains can simply re-form. After the dissipation of the gaseous disk, a large fraction of resonant chains become dynamically unstable. The instability trigger may be chaotic overlap of orbital resonances (*Batygin and Morbidelli 2013*), interactions with a remnant disk of planetesimals (*Levison et al. 2011*), or even the dispersal mechanism of the disk itself (*Liu et al. 2022*). There are hints that external triggers for instability may play a role, for instance from stellar flybys (*Malmberg et al. 2011*) or from long-term perturbations from wide binary stars (*Kaib et al. 2013*). An interesting opportunity is then presented by systems in which resonant chains of multiple planets have been able to survive. For example, *Raymond et al. (2022)* used the current resonant architecture of the TRAPPIST-1 system to show that each planet accreted at most $10^{-4} - 10^{-2} M_{\oplus}$ after the disk dissipated, implying that any large reservoirs of e.g., water must have been incorporated already during the early formation (see above).

7.6. CHNOPS in the Core, Mantle, and Atmosphere

Moving beyond bulk abundances, the partitioning of CHNOPS elements between the core, mantle, surface and atmosphere is controlled by geophysical processes associated with the later stages of planet formation. The main avenues for removing CHNOPS from the (near) surface are loss to space (through outgassing or through impacts) and sequestration in to the core. Replenishment can occur via planetesimal impacts after core formation and magma ocean solidification (see below). The role these processes played in shaping the Earth is discussed in Sect. 2.

Large amounts of volatile elements can be sequestered in the metallic core during core formation (e.g. Tables 1 & 2 and Fig. 2), potentially leaving the mantle highly depleted in siderophile and chalcophile elements while lithophile species largely stay behind. The process of core formation therefore plays an important role in shaping the mantle’s composition and oxidation state, influencing for example the composition of secondary outgassed atmospheres. Generally, more reducing conditions increase the amount of H and C entering the core, while N and S become increasingly lithophile (e.g. *Grewal et al. 2019; Desch et al. 2020*). The

detailed partitioning of elements during core formation depends sensitively on pressure and temperature, but also on composition – e.g. oxygen fugacity.

Planetary-scale magma oceans may develop already during the protoplanetary disk phase, or following giant impacts like the Moon-forming event, and can take between ~ 1 –100 Myr to fully crystallize depending on its composition and distance from the star (e.g., *Hamano et al.* 2013). The specifics of the crystallisation process the nature of the primordial/secondary atmosphere will determine the partitioning of available CHNOPS elements between the atmosphere, upper/lower mantle and core. If still embedded in the primordial protoplanetary disk, significant amounts of hydrogen may be ingassed, while atmospheric escape can become important later on⁷. These processes are punctuated by small and large impacts (see previous sub-section), complicating things further. Solubilities of CHNOPS elements depend on the composition and oxygen fugacity of the melt. Generally, C solubility is lower than water's, and N is less soluble than both of those. S instead is very soluble in silicate melts, although the behavior is a complex function of temperature, pressure, etc. For reduced mantles, C and N (and S) stay in the mantle. For oxidized mantles, C outgasses as CO₂ (before water does), N outgasses as N₂, and S stays in the mantle (e.g., *Grewal et al.* 2019; *Unterborn et al.* 2020; *Desch et al.* 2020). A detailed discussion of the geophysical evolution of planetary-scale bodies is presented in Lichtenberg et al. (this volume).

The variation in outcomes during these potentially crucial stages of terrestrial planet construction is difficult to predict accurately because of uncertainties in the behavior of CHNOPS carriers across large variations of temperatures, pressures, redox states, etc. However, the outcome of such processes is influenced greatly by the CHNOPS budgets as set during early stages, e.g., those leading up to and following planetesimal formation.

7.7. Consequences of Compositional Variability

CHNOPS are essential for life and many of the climatic and geodynamic characteristics of the modern Earth (Sect. 2). Yet, these elements are often present at trace quantities in the environment and early in a planet's life have many possibilities for loss to space or terminal sequestration into its interior (Fig. 2). Given this, it is tempting to focus on how fortunate Earth is to have acquired enough of these vivifying elements. Whilst this view is important, it is also the case that larger quantities of CHNOPS could cause severe problems for the chemical habitability of a planet, and the origin of life. Given that alternative routes of planet formation can lead to significantly increased CHNOPS contents, we here briefly comment on the outcome for chemical habitability when CHNOPS are much more abundant than on Earth.

Carbon and oxygen: Carbon alone has a clear role in setting planetary climate. However, silicate weathering offers the potential to remove vast quantities of carbon present as CO₂ in the atmosphere into mineral form and longterm storage, provided the surface hosts liquid water. A more subtle interaction between carbon and oxygen, and the reason for considering them together, is in setting planetary redox. Carbon's impact on climate is very much dependent on how it is speciated in the atmosphere and in a planet's mantle, both of which depend on how oxidising those respective planetary reservoirs are. In the mantle, carbon will be present dissolved in nominally carbon-free minerals, and as a separate carbon-bearing phase, carbonate in oxidising mantles and graphite/diamond in reducing mantles. Changing the mineral form of carbon has a dramatic impact on its release to the environment during magmatism, with reduced forms retaining carbon in the interior more effectively than oxidised forms (e.g., *Ortenzi et al.* 2020).

Carbon is not just passively responding to planetary redox, as an abundant multi-valent element it itself sets how oxidising planetary reservoirs are. Therefore, the C/O ratio of planetary building blocks is a key variable in deciding the eventual mineralogy, geodynamics, climates, and habitability of planets (e.g., *Kuchner and Seager* 2005). The emerging planets can look qualitative different if a significant component of building blocks condense in disk regions where C/O > 0.8, in which case SiC, graphite, and TiC become dominant phases (*Bond et al.* 2010). While stellar abundances indicate such ratios are unlikely in systems as a whole (Sect. 3), disks may develop regions with high C/O ratios as the result of pebble drift (Sect. 6.1.3). The dominant form of C in carbon-rich planets can vary from graphite and diamond to carbonate rocks when more oxygen is available. The high viscosity and thermal conductivity of diamond in particular (compared to silicates) results in very slow interior convection (*Unterborn et al.* 2014). Whilst high C/O planets would have reducing interiors, and more reducing volcanic gasses and surface environments than Earth at any point in its known geological history (*Catling and Zahnle* 2020), in some respects they may provide more favourable environments for the origin of life. In oxidising environments prebiotic chemistry has to compete with oxygen, which will readily react with the reduced compounds life is built out of (*Sasselov et al.* 2020). High C/O planets (planets with carbon inventories) will be an exciting target for future habitability studies and observation.

Hydrogen: Too much water can pose myriad problems for habitability. High surface pressure from thick water oceans may reduce a planet's ability to have magmatism, replenish the surface, and drive stabilising feedback cycles. For example, *Kite et al.* (2009) showed that, for an Earth-mass planet with a stagnant-lid tectonics mode, only 0.4 wt% water (about 30 Earth oceans) is enough to increase the pressure at the water-rock boundary to prevent decompression melting. This mass fraction decreases with increasing planet mass (to 0.2% for a 2.5M_⊕ planet). Such a lack of melting can shut down deep carbon or water cycles, limiting

⁷For planets orbiting M stars in particular, water loss from the surface during the magma ocean or runaway greenhouse phase on HZ-like orbits around M dwarfs may be significant (e.g., *Luger and Barnes* 2015).

the planet's ability to regulate its climate.

Even if a planet is able to regulate its climate with large surface water inventories, and in a sense preserve its habitability, that is not to say it retains the potential for abiogenesis. Whilst water is a key solvent in prebiotic chemistry, it is critical at stages in reaction pathways to exclude water from the system: for example, phosphorylation reactions require dry-down steps (e.g., *Patel et al.* 2015), and it is unclear how these would be achieved in the context of a deep global ocean. More fundamentally, the emergence of life represents (and likely required) the creation of closed environments in which chemistry could occur isolated from the dilute environment. The closed basins of sub-aerial land provide an ideal niche for prebiotic chemistry to have occurred on Earth, without the problem of infinite dilution that doing chemistry in a global ocean would entail.

Nitrogen: Nitrogen is highly insoluble in magmas, so the likely consequence of increased inventories of N for planets is more massive N₂-dominated atmospheres. As *Wordsworth and Pierrehumbert* (2013) described, increased nitrogen partial pressure can produce greenhouse warming, and, as with thick water oceans, high pressures of nitrogen would suppress volcanic degassing. Prebiotic chemistry is reliant on a surficial inventory of nitrogen, which can be incorporated into organic molecules, such as amino acids and nucleotides. Not only is N a structural component in the key biomolecules of life, but prebiotic chemistry experiments have also identified the N-bearing gas HCN as a key feedstock molecule to initiate prebiotic synthesis: from the earliest spark experiments of Miller-Urey (*Miller* 1957) to the more recent photoredox cyanosulfidic chemistry of *Patel et al.* (2015), HCN, and therefore nitrogen is central to building more complex molecules on the way to life.

Sulfur & phosphorus: It is less clear what the consequences of large inventories of sulfur and phosphorus would be for chemical habitability. Phosphorus is a limiting nutrient for life, and perhaps more so for prebiotic chemistry, where it is typically desired in high concentrations. Simply increasing the abundance of phosphorus would be advantageous in both cases. Sulfur exists in multiple forms in planets, as gas species in the atmosphere, in dissolved form in oceans, in mineral form in the crust, and as sulfide melts at higher temperature in the mantle. There are therefore a number of potential reservoirs for sulfur in a planet, where sulfur could be sequestered without impacting habitability. The study of Venus-like exoplanets may provide a key insight into the behaviour of sulfur in planets, and whether sulfur-dominated atmospheres are a common occurrence (e.g., *Jordan et al.* 2021).

8. SUMMARY

In conclusion, planet formation is a story of accretion, of elements and compounds with sometimes very different origins coming together and ending up in the same planetary body. But it is also a story of pathways di-

verging, with tremendous diversity both between planetary systems, and between different worlds orbiting the same star. We have attempted here to provide an overview of the behavior of CHNOPS en route to and during planet formation, highlighting in places the active role CHNOPS-bearing molecules play in these processes. Loss processes and dynamics (i.e., spatial mixing within the protoplanetary disk or in the young planetary system) play a role at virtually every size scale, with pebble drift, planet migration, and dynamical instabilities in particular featuring prominently in modern planet formation theory. Key open questions relevant for understanding a planet's chemical habitability concern e.g., the detailed chemical composition of inner protoplanetary disk midplanes, the timing and location(s) of planetesimal formation, and the thermal evolution of planetary building blocks. During the later stages of planet formation, the continued accretion of pebbles and planetesimals, as shaped by the system's architecture, will have to be considered in concert with the planet's ongoing geophysical evolution. Given the observed variation in pre-stellar, protoplanetary, and mature exo-planetary systems, it seems likely then that small rocky worlds ending up near the habitable zone can form with a range of CHNOPS budgets that exceeds the variation observed in the inner solar system.

Acknowledgments. S. N. R. is grateful to the CNRS's PNP programming for funding, and to the *Virtual Planetary Laboratory* lead team of NASA's Astrobiology Institute. E. A. B. acknowledges support from NASA's Emerging Worlds Program, grant 80NSSC20K0333, and Exoplanets Research Program, grant 80NSSC20K0259, along with Grant #1907653 from NSF AAG. M. K. M. acknowledges support from the NWO Veni Talent scheme, under the CORVETTE project.

REFERENCES

- Adams F. C., 2010 *ARA&A*, 48, 47.
 Adams F. C., 2021 *arXiv e-prints*, arXiv:2107.03329.
 Adibekyan V. et al., 2015 *A&A*, 581, L2.
 Adibekyan V. et al., 2021 *A&A*, 649, A111.
 Adibekyan V. Z. et al., 2012a *A&A*, 547, A36.
 Adibekyan V. Z. et al., 2012b *A&A*, 543, A89.
 Agol E. et al., 2021 *The Planetary Science Journal*, 2, 1, 1.
 Aikawa Y. et al., 2002 *A&A*, 386, 622.
 Alarcón F. et al., 2021 *ApJS*, 257, 1, 8.
 Alexander C. M. O. et al., 2012 *Science*, 337, 6095, 721.
 Alexander C. M. O. D. et al., 2007 *GeoCoA*, 71, 17, 4380.
 Alexander C. M. O. D. et al., 2010 *GeoCoA*, 74, 15, 4417.
 Alexander C. M. O. D. et al., 2013 *GeoCoA*, 123, 244.
 Alexander C. M. O. D. et al., 2017 *Chemie der Erde / Geochemistry*, 77, 2, 227.
 Alibert Y. et al., 2018 *Nature Astronomy*, 2, 873.
 ALMA Partnership et al., 2015 *ApJL*, 808, 1, L3.
 Altwegg K. et al., 2015a *Science*, 347, 6220, 1261952.
 Altwegg K. et al., 2015b *Science*, 347, 6220, 1261952.
 Altwegg K. et al., 2019 *ARA&A*, 57, 113.

- Amiguet E. et al., 2012 *Earth and Planetary Science Letters*, 345, 142.
- Anderson D. E. et al., 2017 *ApJ*, 845, 1, 13.
- Andrews S. M., 2020 *ARA&A*, 58, 483.
- Andrews S. M. et al., 2018 *ApJL*, 869, 2, L41.
- Anglada-Escude G. et al., 2014 *MNRAS*, 443, L89.
- Apai D. et al., 2005 *Science*, 310, 5749, 834.
- Arnould M. et al., 2006 *A&A*, 453, 2, 653.
- Asphaug E. et al., 2006 *Nature*, 439, 7073, 155.
- Aumatell G. and Wurm G., 2011 *MNRAS*, 418, 1, L1.
- Avice G. and Marty B., 2014 *Philosophical Transactions of the Royal Society of London Series A*, 372, 2024, 20130260.
- Avice G. et al., 2018 *Geochimica et Cosmochimica Acta*, 232, 82.
- Bae J. et al., 2019 *ApJL*, 884, 2, L41.
- Ballering N. P. et al., 2021 *arXiv e-prints*, arXiv:2105.12169.
- Banzatti A. et al., 2015 *ApJL*, 815, 1, L15.
- Banzatti A. et al., 2020 *ApJ*, 903, 2, 124.
- Bar-On Y. M. et al., 2018 *Proceedings of the National Academy of Sciences*, 115, 25, 6506.
- Barbato D. et al., 2018 *A&A*, 615, A175.
- Baross J. A. et al., 2020 *The Environmental Roots of the Origin of Life*.
- Barstow J. K., 2021 *Astronomy and Geophysics*, 62, 1, 1.36.
- Baruteau C. et al., 2014 *Protostars and Planets VI* (H. Beuther, R. S. Klessen, C. P. Dullemond, and T. Henning), p. 667.
- Batygin K. and Morbidelli A., 2013 *AJ*, 145, 1, 1.
- Bell E. A. et al., 2015 *Proceedings of the National Academy of Sciences*, 112, 47, 14518.
- Benisty M. et al., 2021 *ApJL*, 916, 1, L2.
- Bensby T. et al., 2014 *A&A*, 562, A71.
- Benz W. et al., 1989 *Icarus*, 81, 1, 113.
- Bergin E. A. et al., 2015 *Proceedings of the National Academy of Science*, 112, 29, 8965.
- Bergner J. and Ciesla F., 2021 *arXiv e-prints*, arXiv:2107.03350.
- Bergner J. B. et al., 2019 *ApJL*, 884, 2, L36.
- Betts H. C. et al., 2018 *Nature ecology & evolution*, 2, 10, 1556.
- Bieler A. et al., 2015 *Nature*, 526, 7575, 678.
- Bierson C. J. and Nimmo F., 2019 *Icarus*, 326, 10.
- Birnstiel T. et al., 2012 *A&A*, 539, A148.
- Birnstiel T. et al., 2016 *SSRv*, 205, 1-4, 41.
- Bischoff D. et al., 2020 *MNRAS*, 497, 3, 2517.
- Bitsch B. and Battistini C., 2020 *A&A*, 633, A10.
- Bitsch B. and Johansen A., 2016 *A&A*, 590, A101.
- Bitsch B. et al., 2015a *A&A*, 582, A112.
- Bitsch B. et al., 2015b *A&A*, 575, A28.
- Bitsch B. et al., 2019 *A&A*, 624, A109.
- Bitsch B. et al., 2021 *A&A*, 649, L5.
- Biver N. et al., 2018a *A&A*, 619, A127.
- Biver N. et al., 2018b *A&A*, 619, A127.
- Bockelée-Morvan D. et al., 2000 *A&A*, 353, 1101.
- Bodewits D. et al., 2020 *Nature Astronomy*, 4, 867.
- Boley K. M. et al., 2021 *AJ*, 162, 3, 85.
- Bond J. C. et al., 2010 *ApJ*, 715, 2, 1050.
- Boogert A. C. A. et al., 2015 *ARA&A*, 53, 541.
- Booth A. S. et al., 2018 *A&A*, 611, A16.
- Booth A. S. et al., 2021a *A&A*, 651, L6.
- Booth A. S. et al., 2021b *Nature Astronomy*, 5, 684.
- Booth R. A. and Clarke C. J., 2021 *MNRAS*, 502, 2, 1569.
- Booth R. A. and Ilee J. D., 2019 *MNRAS*, 487, 3, 3998.
- Booth R. A. and Owen J. E., 2020 *MNRAS*, 493, 4, 5079.
- Booth R. A. et al., 2017 *MNRAS*, 469, 4, 3994.
- Bosman A. D. et al., 2019 *A&A*, 632, L11.
- Bosman A. D. et al., 2021a *ApJ*, 910, 1, 3.
- Bosman A. D. et al., 2021b *ApJS*, 257, 1, 7.
- Boss A. P. and Keiser S. A., 2015 *ApJ*, 809, 1, 103.
- Bottke W. F. et al., 2005 *Icarus*, 175, 1, 111.
- Brasser R. and Mojzsis S. J., 2020 *Nature Astronomy*, 4, 492.
- Brewer J. M. and Fischer D. A., 2016 *ApJ*, 831, 1, 20.
- Brewer J. M. and Fischer D. A., 2018 *ApJS*, 237, 2, 38.
- Brimblecombe P., 2013 *Treatise on Geochemistry: Second Edition*, pp. 559–591, Elsevier Inc.
- Brugamyer E. et al., 2011 *ApJ*, 738, 1, 97.
- Bryan M. L. et al., 2019 *AJ*, 157, 2, 52.
- Bryson S. et al., 2020 *The Astronomical Journal*, 159, 6, 279.
- Buchhave L. A. et al., 2012 *Nature*, 486, 7403, 375.
- Buchhave L. A. et al., 2014 *Nature*, 509, 7502, 593.
- Buchhave L. A. et al., 2018 *ApJ*, 856, 1, 37.
- Budde G. et al., 2016 *Earth and Planetary Science Letters*, 454, 293.
- Burkhardt C. et al., 2021 *Science Advances*, 7, 52, eabj7601.
- Caffau E. et al., 2007 *A&A*, 473, 2, L9.
- Caffau E. et al., 2011 *A&A*, 532, A98.
- Calmonte U. et al., 2016 *MNRAS*, 462, S253.
- Cameron A. G. W. and Truran J. W., 1977 *Icarus*, 30, 3, 447.
- Canup R. M. and Asphaug E., 2001 *Nature*, 412, 6848, 708.
- Carbon D. F. et al., 1987 *PASP*, 99, 335.
- Cardelli J. A. et al., 1996 *ApJ*, 467, 334.
- Carpenter J. M. et al., 2006 *ApJL*, 651, 1, L49.
- Carr J. S. and Najita J. R., 2008 *Science*, 319, 5869, 1504.
- Carrera D. et al., 2015 *A&A*, 579, A43.
- Carrera D. et al., 2017 *ApJ*, 839, 1, 16.
- Carrera D. et al., 2021 *AJ*, 161, 2, 96.
- Carter-Bond J. C. et al., 2012 *ApJ*, 760, 1, 44.
- Catling D. C. and Zahnle K. J., 2020 *Science Advances*, 6, 9, eaax1420.
- Cegla H., 2019 *Geosciences*, 9, 3, 114.
- Chambers J. E., 2009 *ApJ*, 705, 2, 1206.
- Chambers J. E., 2016 *ApJ*, 825, 1, 63.
- Chatterjee S. and Tan J. C., 2014 *ApJ*, 780, 1, 53.
- Chatterjee S. et al., 2008 *ApJ*, 686, 1, 580.
- Chen Y. Q. et al., 2002 *A&A*, 390, 225.
- Chevalier R. A., 2000 *ApJL*, 538, 2, L151.
- Chiappini C. et al., 1999 *ApJ*, 515, 1, 226.
- Chiappini C. et al., 2003 *MNRAS*, 339, 1, 63.
- Choukroun M. et al., 2020 *SSRv*, 216, 3, 44.
- Ciesla F. J., 2007 *Science*, 318, 5850, 613.
- Ciesla F. J. and Sandford S. A., 2012 *Science*, 336, 6080, 452.
- Cieza L. A. et al., 2016 *Nature*, 535, 7611, 258.
- Cieza L. A. et al., 2021 *MNRAS*, 501, 2, 2934.
- Clark J. T. et al., 2021 *MNRAS*, 504, 4, 4968.
- Cleeves L. I., 2016 *ApJL*, 816, 2, L21.
- Cleeves L. I. et al., 2014 *Science*, 345, 6204, 1590.
- Cleeves L. I. et al., 2018 *ApJ*, 865, 2, 155.
- Clegg R. E. S. et al., 1981 *ApJ*, 250, 262.
- Cockell C. S. et al., 2021 *Astrobiology*, 21, 4, 481.
- Coleman G. A. L. et al., 2019 *A&A*, 631, A7.
- Collier Cameron A., 2018 *The Impact of Stellar Activity on the Detection and Characterization of Exoplanets*, p. 23.
- Connelly J. N. et al., 2008 *ApJL*, 675, 2, L121.
- Connelly J. N. et al., 2012 *Science*, 338, 6107, 651.
- Cooke R. J. et al., 2018 *ApJ*, 855, 2, 102.
- Cordiner M. A. et al., 2020 *Nature Astronomy*, 4, 861.
- Cossou C. et al., 2013 *A&A*, 553, L2.
- Cossou C. et al., 2014 *A&A*, 569, A56.

- Costa Silva A. R. et al., 2020 *A&A*, 634, A136.
- Cresswell P. et al., 2007 *A&A*, 473, 1, 329.
- Crossfield I. J. M. and Kreidberg L., 2017 *AJ*, 154, 6, 261.
- Crowther P. A., 2007 *ARA&A*, 45, 1, 177.
- Curtis J. L. et al., 2018 *AJ*, 155, 4, 173.
- Cuzzi J. N. and Zahnle K. J., 2004 *ApJ*, 614, 1, 490.
- Czekala I. et al., 2021 *arXiv e-prints*, arXiv:2109.06188.
- da Silva R. et al., 2015 *A&A*, 580, A24.
- Daly R. T. and Schultz P. H., 2018 *Science Advances*, 4, 4, eaar2632.
- Danilovich T. et al., 2016 *A&A*, 588, A119.
- Danilovich T. et al., 2017 *A&A*, 606, A124.
- Danilovich T. et al., 2018 *ArXiv e-prints*.
- Dasgupta R., 2013 *Reviews in Mineralogy and Geochemistry*, 75, 1, 183.
- Dasgupta R. and Grewal D., 2019 *Origin and Early Differentiation of Carbon and Associated Life-Essential Volatile Elements on Earth*.
- Dauphas N., 2017 *Nature*, 541, 7638, 521.
- Dauphas N. and Pourmand A., 2011 *Nature*, 473, 7348, 489.
- Dauphas N. et al., 2014 *Philosophical Transactions of the Royal Society of London Series A*, 372, 2013.0244.
- Day J. M. D. et al., 2007 *Science*, 315, 5809, 217.
- de Sanctis M. C. et al., 2015 *Nature*, 528, 7581, 241.
- DeMeo F. E. and Carry B., 2014 *Nature*, 505, 7485, 629.
- DeMeo F. E. et al., 2014 *Icarus*, 229, 392.
- Des Marais D. J. et al., 2008 *Astrobiology*, 8, 4, 715.
- Desch S. J. et al., 2018 *ApJS*, 238, 1, 11.
- Desch S. J. et al., 2020 *The Volatile Content of Rocky Planets*.
- Dittkrist K. M. et al., 2014 *A&A*, 567, A121.
- Dodson-Robinson S. E. et al., 2009 *Icarus*, 200, 2, 672.
- Dominik C. and Tielens A. G. G. M., 1997 *ApJ*, 480, 2, 647.
- Dorn C. et al., 2015 *A&A*, 577, A83.
- Doyle A. E. et al., 2019 *Science*, 366, 6463, 356.
- Drążkowska J. and Alibert Y., 2017 *A&A*, 608, A92.
- Drążkowska J. et al., 2016 *A&A*, 594, A105.
- Drążkowska J. et al., 2021 *A&A*, 647, A15.
- Dressing C. D. et al., 2010 *ApJ*, 721, 2, 1295.
- Drozdovskaya M. N. et al., 2019 *MNRAS*, 490, 1, 50.
- Du F. et al., 2017 *ApJ*, 842, 2, 98.
- Duffau S. et al., 2017 *A&A*, 604, A128.
- Dukes D. and Krumholz M. R., 2012 *ApJ*, 754, 1, 56.
- Dullemond C. P. et al., 2006 *ApJL*, 640, 1, L67.
- Dumusque X. et al., 2017 *A&A*, 598, A133.
- Dutrey A. et al., 1997 *A&A*, 317, L55.
- Dutrey A. et al., 2011 *A&A*, 535, A104.
- Dwarkadas V. V. et al., 2017 *ApJ*, 851, 2, 147.
- Ecuivillon A. et al., 2004 *A&A*, 418, 703.
- Ehlmann B. et al., 2016 *Journal of Geophysical Research: Planets*, 121, 10, 1927.
- Elkins-Tanton L. T., 2012 *Annual Review of Earth and Planetary Sciences*, 40, 1, 113.
- Ercolano B. and Clarke C. J., 2010 *MNRAS*, 402, 4, 2735.
- Evans K., 2006 *Geology*, 34, 6, 489.
- Fabrycky D. C. and Murray-Clay R. A., 2010 *ApJ*, 710, 2, 1408.
- Facchini S. et al., 2021 *AJ*, 162, 3, 99.
- Fang J. and Margot J.-L., 2012 *ApJ*, 761, 2, 92.
- Fedoseev G. et al., 2015 *MNRAS*, 446, 1, 439.
- Fegley Bruce J. et al., 2020 *Chemie der Erde / Geochemistry*, 80, 1, 125594.
- Fischer D. A. and Valenti J., 2005 *ApJ*, 622, 2, 1102.
- Fischer W. W. et al., 2016 *Annual Review of Earth and Planetary Sciences*, 44, 647.
- Fischer-Gödde M. and Kleine T., 2017 *Nature*, 541, 7638, 525.
- Fitoussi C. and Bourdon B., 2012 *Science*, 335, 6075, 1477.
- Foley B. J. and Smye A. J., 2018 *Astrobiology*, 18, 7, 873.
- Fomenkova M. N., 1999 *SSRv*, 90, 109.
- Fomenkova M. N. et al., 1994 *GeoCoA*, 58, 20, 4503.
- Ford E. B. and Rasio F. A., 2008 *ApJ*, 686, 1, 621.
- Foster P. N. and Boss A. P., 1997 *ApJ*, 489, 1, 346.
- Franchi I. A. et al., 1999 *M&PS*, 34, 4, 657.
- Frank E. A. et al., 2014 *Icarus*, 243, 274.
- Fu R. R. and Elkins-Tanton L. T., 2014 *Earth and Planetary Science Letters*, 390, 128.
- Fu R. R. e. a., 2017 *Silicate Melting and Volatile Loss During Differentiation in Planetesimals*.
- Fuente A. et al., 2010 *A&A*, 524, A19.
- Fujii M. S. and Hori Y., 2019 *A&A*, 624, A110.
- Fulton B. J. et al., 2017 *AJ*, 154, 3, 109.
- Furuya K. et al., 2017 *A&A*, 599, A40.
- Gaidos E. et al., 2009 *ApJ*, 696, 2, 1854.
- Gaidos E. J., 2000 *Icarus*, 145, 2, 637.
- Gail H.-P. and Trialet M., 2017 *A&A*, 606, A16.
- Gao P. et al., 2021 *Journal of Geophysical Research (Planets)*, 126, 4, e06655.
- Garufi A. et al., 2018 *A&A*, 620, A94.
- Geiss J., 1987 *A&A*, 187, 1-2, 859.
- Genda H. and Abe Y., 2005 *Nature*, 433, 7028, 842.
- Genda H. et al., 2012 *ApJ*, 744, 2, 137.
- Gentile Fusillo N. P. et al., 2019 *MNRAS*, 482, 4, 4570.
- Giocalone S. et al., 2019 *ApJ*, 882, 1, 33.
- Gibb E. L. and Horne D., 2013 *ApJL*, 776, 2, L28.
- Gonzalez G., 1997 *MNRAS*, 285, 2, 403.
- Gounelle M. and Meynet G., 2012 *A&A*, 545, A4.
- Grewal D. S. et al., 2019 *Science Advances*, 5, 1, eaau3669.
- Grewal D. S. et al., 2019 *Geochimica et Cosmochimica Acta*, 251, 87.
- Grewal D. S. et al., 2021 *Nature Astronomy*, 5, 356.
- Grimm R. E. and McSween H. Y., 1993 *Science*, 259, 5095, 653.
- Grimm S. L. et al., 2018 *A&A*, 613, A68.
- Grossman L., 1972 *Geochimica et Cosmochimica Acta*, 36, 5, 597.
- Grundy W. M. et al., 2020 *Science*, 367, 6481, aay3705.
- Gundlach B. and Blum J., 2015 *ApJ*, 798, 1, 34.
- Gupta A. and Schlichting H. E., 2019 *MNRAS*, 487, 1, 24.
- Guzmán V. V. et al., 2021 *ApJS*, 257, 1, 6.
- Haenecour P. et al., 2016 *ApJ*, 825, 2, 88.
- Haffert S. Y. et al., 2019 *Nature Astronomy*, 3, 749.
- Haghighipour N. and Boss A. P., 2003 *ApJ*, 583, 2, 996.
- Haghighipour N. and Maindl T. I., 2022 *arXiv e-prints*, arXiv:2201.06702.
- Halliday A. N., 2013 *GeoCoA*, 105, 146.
- Hamano K. et al., 2013 *Nature*, 497, 7451, 607.
- Harper Charles L. J., 1996 *ApJ*, 466, 1026.
- Hartmann L. et al., 2016 *ARA&A*, 54, 135.
- Hartogh P. et al., 2011 *Nature*, 478, 7368, 218.
- Hasegawa Y. and Pudritz R. E., 2011 *MNRAS*, 417, 2, 1236.
- Haywood M. et al., 2013 *A&A*, 560, A109.
- Henning T. and Semenov D., 2013 *Chemical Reviews*, 113, 12, 9016.
- Herbert O. et al., 2020 *A&A*, 636, A71.
- Heritier K. L. et al., 2018 *Nature Communications*, 9, 2580.
- Hess B. L. et al., 2021 *Nature Communications*, 12, 1535.
- Hily-Blant P. et al., 2019 *A&A*, 632, L12.
- Hinkel N. R. et al., 2014 *AJ*, 148, 3, 54.

- Hirose K. et al., 2013 *Annual Review of Earth and Planetary Sciences*, 41, 657.
- Hirschmann M. and Kohlstedt D., 2012 *Phys. Today*, 65, 3, 40.
- Hirschmann M. M. et al., 2021 *Proceedings of the National Academy of Science*, 118, 13, 2026779118.
- Hoehler T. M. et al., 2020 *Life's Requirements, Habitability, and Biological Potential*.
- Holland H. D., 2002 *Geochimica et Cosmochimica Acta*, 66, 21, 3811.
- Homma K. A. et al., 2019 *ApJ*, 877, 2, 128.
- Hony S. et al., 2002 *A&A*, 390, 533.
- Huang J. et al., 2018a *ApJL*, 869, 2, L42.
- Huang J. et al., 2018b *ApJL*, 869, 2, L42.
- Hueso R. and Guillot T., 2005 *A&A*, 442, 2, 703.
- Huss G. R. et al., 2009 *GeoCoA*, 73, 17, 4922.
- Ilee J. D. et al., 2021 *ApJS*, 257, 1, 9.
- Iyer A. R. and Line M. R., 2020 *ApJ*, 889, 2, 78.
- Izidoro A. et al., 2015 *ApJL*, 800, 2, L22.
- Izidoro A. et al., 2017 *MNRAS*, 470, 2, 1750.
- Izidoro A. et al., 2021a *A&A*, 650, A152.
- Izidoro A. et al., 2021b *Nature Astronomy*.
- Izidoro A. et al., 2021c *ApJ*, 915, 1, 62.
- Jacobson S. A. et al., 2014 *Nature*, 508, 7494, 84.
- Jenkins E. B., 2009 *ApJ*, 700, 2, 1299.
- Jewitt D. and Luu J., 2019 *ApJL*, 886, 2, L29.
- Jiang H. et al., 2022 *ApJL*, 924, 2, L31.
- Jin S. and Mordasini C., 2018 *ApJ*, 853, 2, 163.
- Johansen A. and Lambrechts M., 2017 *Annual Review of Earth and Planetary Sciences*, 45, 1, 359.
- Johansen A. et al., 2014 *Protostars and Planets VI* (H. Beuther, R. S. Klessen, C. P. Dullemond, and T. Henning), p. 547.
- Johansen A. et al., 2021 *Science Advances*, 7, 8, eabc0444.
- Johnson B. and Goldblatt C., 2015 *Earth-Science Reviews*, 148, 150.
- Johnson J. A. et al., 2010 *PASP*, 122, 894, 905.
- Johnson J. L. and Li H., 2012 *ApJ*, 751, 2, 81.
- Jones A. P., 2016 *Royal Society Open Science*, 3, 12, 160221.
- Jones A. P. and Ysard N., 2019 *A&A*, 627, A38.
- Jordan S. et al., 2021 *arXiv preprint arXiv:2108.05778*.
- Jura M. and Young E. D., 2014 *Annual Review of Earth and Planetary Sciences*, 42, 1, 45.
- Jurić M. and Tremaine S., 2008 *ApJ*, 686, 1, 603.
- Kaib N. A. and Cowan N. B., 2015 *Icarus*, 252, 161.
- Kaib N. A. et al., 2013 *Nature*, 493, 7432, 381.
- Kaiser B. C. et al., 2021 *Science*, 371, 6525, 168.
- Kaltenegger L., 2017 *ARA&A*, 55, 1, 433.
- Kama M. et al., 2016 *A&A*, 588, A108.
- Kama M. et al., 2019 *ApJ*, 885, 2, 114.
- Kane S. et al., 2021 *Bulletin of the American Astronomical Society*, vol. 53, p. 208.
- Kasen D. et al., 2017 *Nature*, 551, 7678, 80.
- Kasting J. F. et al., 1993 *Icarus*, 101, 1, 108.
- Kaula W. M., 1999 *Icarus*, 139, 1, 32.
- Keller L. P. et al., 2010 *Lunar and Planetary Science Conference*, Lunar and Planetary Science Conference, p. 1172.
- Keppler M. et al., 2018 *A&A*, 617, A44.
- Kim H. J. et al., 2012 *ApJ*, 758, 1, 38.
- Kimura H. et al., 2015 *ApJ*, 812, 1, 67.
- Kimura H. et al., 2020 *MNRAS*, 498, 2, 1801.
- King P. L. and McLennan S. M., 2010 *Elements*, 6, 2, 107.
- Kita R. et al., 2010 *Astrobiology*, 10, 7, 733.
- Kite E. S. and Ford E. B., 2018 *The Astrophysical Journal*, 864, 1, 75.
- Kite E. S. et al., 2009 *ApJ*, 700, 2, 1732.
- Klahr H. and Schreiber A., 2020 *ApJ*, 901, 1, 54.
- Klahr H. and Schreiber A., 2021 *ApJ*, 911, 1, 9.
- Klarmann L. et al., 2018 *A&A*, 618, L1.
- Kleine T. et al., 2009 *GeoCoA*, 73, 17, 5150.
- Kley W. and Nelson R. P., 2012 *ARA&A*, 50, 211.
- Kokubo E. and Ida S., 1996 *Icarus*, 123, 1, 180.
- Kokubo E. and Ida S., 1998 *Icarus*, 131, 1, 171.
- Koo B.-C. et al., 2013 *Science*, 342, 6164, 1346.
- Kopparapu R. K. et al., 2013 *ApJ*, 765, 2, 131.
- Kornet K. et al., 2005 *A&A*, 430, 1133.
- Korth J. et al., 2019 *MNRAS*, 482, 2, 1807.
- Kouchi A. et al., 2002 *ApJL*, 566, 2, L121.
- Kral Q. et al., 2020 *Nature Astronomy*, 4, 769.
- Krijt S. et al., 2016a *A&A*, 586, A20.
- Krijt S. et al., 2016b *ApJ*, 833, 2, 285.
- Krijt S. et al., 2018 *ApJ*, 864, 1, 78.
- Krijt S. et al., 2020 *ApJ*, 899, 2, 134.
- Kruijjer T. et al., 2014 *Science*, 344, 6188, 1150.
- Kruijjer T. S. et al., 2017 *Proceedings of the National Academy of Science*, 114, 26, 6712.
- Kuchner M. J. and Seager S., 2005 *arXiv e-prints*, astro-ph/0504214.
- Kuchner M. J. and Seager S., 2005 *arXiv preprint astro-ph/0504214*.
- Lada C. J. et al., 2006 *AJ*, 131, 3, 1574.
- Laird J. B., 1985 *ApJ*, 289, 556.
- Lambrechts M. and Johansen A., 2012 *A&A*, 544, A32.
- Lambrechts M. et al., 2014 *A&A*, 572, A35.
- Lambrechts M. et al., 2019 *A&A*, 627, A83.
- Lammer H. et al., 2018 *A&A Rv*, 26, 1, 2.
- Lauretta D. S. et al., 1996 *Icarus*, 122, 2, 288.
- Law C. J. et al., 2021 *arXiv e-prints*, arXiv:2109.06210.
- Le Voyer M. et al., 2017 *Nature Communications*, 8, 1, 1.
- Lécuyer C. and Ricard Y., 1999 *Earth and Planetary Science Letters*, 165, 2, 197.
- Lécuyer C. et al., 1998 *Chemical Geology*, 145, 3-4, 249.
- Lee E. J. and Chiang E., 2015 *ApJ*, 811, 1, 41.
- Lee E. J. et al., 2022 *arXiv e-prints*, arXiv:2201.09898.
- Lee J.-E. et al., 2010 *ApJL*, 710, 1, L21.
- Lee J.-E. et al., 2019 *Nature Astronomy*, 3, 314.
- Leemker M. et al., 2021 *A&A*, 646, A3.
- Lehmer O. R. et al., 2020 *Nature communications*, 11, 1, 1.
- Leinhardt Z. M. and Stewart S. T., 2012 *ApJ*, 745, 1, 79.
- Lenz C. T. et al., 2019 *ApJ*, 874, 1, 36.
- Levison H. F. et al., 2009 *Nature*, 460, 7253, 364.
- Levison H. F. et al., 2010 *AJ*, 139, 4, 1297.
- Levison H. F. et al., 2011 *AJ*, 142, 5, 152.
- Levison H. F. et al., 2015 *Nature*, 524, 7565, 322.
- Lewis J. S., 1972 *Icarus*, 16, 2, 241.
- Li J. et al., 2021 *Science Advances*, 7, 14, eabd3632.
- Li R. and Youdin A., 2021 *arXiv e-prints*, arXiv:2105.06042.
- Li Y.-F. et al., 2016 *Geochemical Perspectives Letters*, 2.
- Libourel G. et al., 2003 *Geochimica et Cosmochimica Acta*, 67, 21, 4123.
- Lichtenberg T. and Krijt S., 2021 *ApJL*, 913, 2, L20.
- Lichtenberg T. et al., 2016 *MNRAS*, 462, 4, 3979.
- Lichtenberg T. et al., 2019 *Nature Astronomy*, 3, 307.
- Lichtenberg T. et al., 2021 *Science*, 371, 6527, 365.
- Lin D. N. C. and Papaloizou J., 1986 *ApJ*, 309, 846.
- Lipp A. et al., 2021 *Geochemical Perspectives Letters*, 7, 21.

- Liu et al., 2022 *Nature*, *in press*.
- Livingston J. H. et al., 2018 *AJ*, *155*, 3, 115.
- Lodato G. et al., 2019 *MNRAS*, *486*, 1, 453.
- Lodders K., 2003 *ApJ*, *591*, 2, 1220.
- Lodders K., 2019 *arXiv e-prints*, arXiv:1912.00844.
- Lombaert R. et al., 2012 *A&A*, *544*, L18.
- Lorand J.-P. et al., 2003 *Geochimica et Cosmochimica Acta*, *67*, 21, 4137.
- Lovell J. B. et al., 2021 *MNRAS*, *500*, 4, 4878.
- Lugaro M. et al., 2012 *M&PS*, *47*, 12, 1998.
- Lugaro M. et al., 2018 *Progress in Particle and Nuclear Physics*, *102*, 1.
- Luger R. and Barnes R., 2015 *Astrobiology*, *15*, 2, 119.
- Luhman K. L. and Mamajek E. E., 2012 *ApJ*, *758*, 1, 31.
- Lundin R. et al., 2007 *Space Science Reviews*, *129*, 1, 245.
- Lyra W. et al., 2010 *ApJL*, *715*, 2, L68.
- Machida M. N. and Matsumoto T., 2011 *MNRAS*, *413*, 4, 2767.
- Maher K. and Chamberlain C., 2014 *science*, *343*, 6178, 1502.
- Mahjoub A. et al., 2021 *ApJL*, *914*, 2, L31.
- Malmberg D. et al., 2011 *MNRAS*, *411*, 2, 859.
- Mamajek E. E., 2009 *Exoplanets and Disks: Their Formation and Diversity*, vol. 1158 of *American Institute of Physics Conference Series* (T. Usuda, M. Tamura, and M. Ishii), pp. 3–10.
- Manara C. F. et al., 2018 *A&A*, *618*, L3.
- Mandell A. M. et al., 2007 *ApJ*, *660*, 1, 823.
- Marino S. et al., 2016 *MNRAS*, *460*, 3, 2933.
- Marino S. et al., 2018 *MNRAS*, *479*, 2, 1651.
- Marois C. et al., 2008 *Science*, *322*, 5906, 1348.
- Marois C. et al., 2010 *Nature*, *468*, 7327, 1080.
- Marty B., 2012 *Earth and Planetary Science Letters*, *313*, 56.
- Marty B. et al., 2013 *Reviews in Mineralogy and Geochemistry*, *75*, 1, 149.
- Marty B. et al., 2016 *Earth and Planetary Science Letters*, *441*, 91.
- Marty B. et al., 2017 *Science*, *356*, 6342, 1069.
- Marty B. et al., 2020 *Earth and Planetary Science Letters*, *551*, 116574.
- Masset F. S. et al., 2006 *ApJ*, *642*, 1, 478.
- Mastrobuono-Battisti A. et al., 2015 *Nature*, *520*, 7546, 212.
- Matrà L. et al., 2017 *ApJ*, *842*, 1, 9.
- Matrozos E. et al., 2013 *A&A*, *559*, A115.
- Matsuura M. et al., 2017 *MNRAS*, *469*, 3, 3347.
- Maurice M. et al., 2020 *Science advances*, *6*, 28, eaba8949.
- Maury A. J. et al., 2019 *A&A*, *621*, A76.
- Mayor M. and Queloz D., 1995 *Nature*, *378*, 6555, 355.
- Mayorga L. C. et al., 2021 *The Planetary Science Journal*, *2*, 4, 140.
- McClure M. K., 2019 *A&A*, *632*, A32.
- McClure M. K. et al., 2010 *ApJS*, *188*, 1, 75.
- McClure M. K. et al., 2020 *A&A*, *642*, L15.
- McDonough W. F. and Sun S. s., 1995 *Chemical Geology*, *120*, 3–4, 223.
- McGovern P. J. and Schubert G., 1989 *Earth and planetary science letters*, *96*, 1–2, 27.
- McGuire B. A., 2018 *ApJS*, *239*, 2, 17.
- McGuire B. A. et al., 2021 *Science*, *371*, 6535, 1265.
- McKay A. J. et al., 2019 *AJ*, *158*, 3, 128.
- McKenzie D. P. and Parker R. L., 1967 *Nature*, *216*, 5122, 1276.
- McKinnon W. B. et al., 2020 *Science*, *367*, 6481, aay6620.
- Meech K. and Raymond S. N., 2019 *arXiv e-prints*, arXiv:1912.04361.
- Meech K. J. et al., 2017 *Nature*, *552*, 7685, 378.
- Meibom S. et al., 2013 *Nature*, *499*, 7456, 55.
- Meijerink R. et al., 2009 *ApJ*, *704*, 2, 1471.
- Meléndez J. et al., 2009 *ApJL*, *704*, 1, L66.
- Melis C. et al., 2018 *Research Notes of the American Astronomical Society*, *2*, 2, 64.
- Meyer B. S. and Clayton D. D., 2000 *SSRv*, *92*, 133.
- Michel A. et al., 2021 *arXiv e-prints*, arXiv:2104.05894.
- Miller S. L., 1957 *Biochimica et Biophysica Acta*, *23*, 480.
- Miller W. G. et al., 2019 *Earth and Planetary Science Letters*, *523*, 115699.
- Min M. et al., 2016 *A&A*, *593*, A11.
- Mininni C. et al., 2018 *MNRAS*, *476*, 1, L39.
- Misener W. et al., 2019 *ApJ*, *885*, 2, 118.
- Mishra A. and Li A., 2015 *ApJ*, *809*, 2, 120.
- Morbidelli A. and Wood B. J., 2015 *Washington DC American Geophysical Union Geophysical Monograph Series*, *212*, 71.
- Morbidelli A. et al., 2000 *M&PS*, *35*, 6, 1309.
- Morbidelli A. et al., 2009 *Icarus*, *204*, 2, 558.
- Morbidelli A. et al., 2012 *Annual Review of Earth and Planetary Sciences*, *40*, 1, 251.
- Morbidelli A. et al., 2015 *Icarus*, *258*, 418.
- Morbidelli A. et al., 2016 *Icarus*, *267*, 368.
- Morbidelli A. et al., 2022 *Nature Astronomy*, *6*, 72.
- Mordasini C. et al., 2012 *A&A*, *541*, A97.
- Morgan W. J., 1968 *Journal of Geophysical Research*, *73*, 6, 1959.
- Mortier A. et al., 2012 *A&A*, *543*, A45.
- Mortier A. et al., 2013 *A&A*, *557*, A70.
- Mousis O. et al., 2016 *ApJL*, *823*, 2, L41.
- Mousis O. et al., 2021 *The Planetary Science Journal*, *2*, 2, 72.
- Mulders G. D. et al., 2015 *ApJ*, *807*, 1, 9.
- Mulders G. D. et al., 2016 *AJ*, *152*, 6, 187.
- Mulders G. D. et al., 2021 *arXiv e-prints*, arXiv:2107.12520.
- Musiolik G. and Wurm G., 2019 *ApJ*, *873*, 1, 58.
- Musiolik G. et al., 2016 *ApJ*, *827*, 1, 63.
- Mustill A. J. et al., 2017 *MNRAS*, *468*, 3, 3000.
- Najita J. R. and Bergin E. A., 2018a *ApJ*, *864*, 2, 168.
- Najita J. R. and Bergin E. A., 2018b *ApJ*, *864*, 2, 168.
- Najita J. R. and Kenyon S. J., 2014 *MNRAS*, *445*, 3, 3315.
- Najita J. R. et al., 2013 *ApJ*, *766*, 2, 134.
- Nesvorný D., 2018 *ARA&A*, *56*, 137.
- Nesvorný D. et al., 2013 *ApJ*, *768*, 1, 45.
- Nesvorný D. et al., 2019 *Nature Astronomy*, *3*, 808.
- Nimmo F., 2002 *Geology*, *30*, 11, 987.
- Nimmo F. et al., 2018 *SSRv*, *214*, 5, 101.
- Nissen P. E., 2013 *A&A*, *552*, A73.
- Nissen P. E. and Schuster W. J., 2010 *A&A*, *511*, L10.
- Nissen P. E. and Schuster W. J., 2014 *Setting the scene for Gaia and LAMOST*, vol. 298 (S. Feltzing, G. Zhao, N. A. Walton, and P. Whitelock), pp. 65–70.
- Nissen P. E. et al., 2007 *A&A*, *469*, 1, 319.
- Nissen P. E. et al., 2014 *A&A*, *568*, A25.
- Nittler L. R. and Ciesla F., 2016 *ARA&A*, *54*, 53.
- Nutman A. P. et al., 2016 *Nature*, *537*, 7621, 535.
- Öberg K. I. and Bergin E. A., 2016 *ApJL*, *831*, 2, L19.
- Öberg K. I. and Bergin E. A., 2021 *PhR*, *893*, 1.
- Öberg K. I. and Wordsworth R., 2019 *AJ*, *158*, 5, 194.
- Öberg K. I. et al., 2009 *A&A*, *504*, 3, 891.
- Öberg K. I. et al., 2011 *ApJL*, *743*, 1, L16.
- Öberg K. I. et al., 2015 *Nature*, *520*, 7546, 198.
- Öberg K. I. et al., 2021 *arXiv e-prints*, arXiv:2109.06268.
- Ogihara M. and Ida S., 2009 *ApJ*, *699*, 1, 824.
- Okuzumi S. et al., 2016 *ApJ*, *821*, 2, 82.

- O'Neill H. S. C., 1991 *Geochimica et Cosmochimica Acta*, 55, 4, 1159.
- Ormel C. W., 2017 *The Emerging Paradigm of Pebble Accretion*, vol. 445, p. 197.
- Ormel C. W. et al., 2010 *ApJL*, 714, 1, L103.
- O'Rourke L. et al., 2020 *Nature*, 586, 7831, 697.
- Ortenzi G. et al., 2020 *Scientific reports*, 10, 1, 1.
- Osborn A. and Bayliss D., 2020 *MNRAS*, 491, 3, 4481.
- Ouellette N. et al., 2007 *ApJ*, 662, 2, 1268.
- Owen J. E. and Mohanty S., 2016 *MNRAS*, 459, 4, 4088.
- Owen J. E. and Murray-Clay R., 2018 *MNRAS*, 480, 2, 2206.
- Owen J. E. and Wu Y., 2013 *ApJ*, 775, 2, 105.
- Owen J. E. and Wu Y., 2017 *ApJ*, 847, 1, 29.
- Ozaki K. and Reinhard C. T., 2021 *Nature Geoscience*, 14, 3, 138.
- Pacheco-Vázquez S. et al., 2016 *A&A*, 589, A60.
- Palme H. and O'Neill H., 2014 Cosmochemical estimates of mantle composition. planets, asteroids, comets and the solar system, volume 2 of treatise on geochemistry . edited by andrew m. davis.
- Parker R. J., 2020 *Royal Society Open Science*, 7, 11, 201271.
- Parker R. J. et al., 2014 *MNRAS*, 437, 1, 946.
- Parvathi V. S. et al., 2012 *ApJ*, 760, 1, 36.
- Pascucci I. et al., 2009 *ApJ*, 696, 1, 143.
- Pascucci I. et al., 2016 *ApJ*, 831, 2, 125.
- Patel B. H. et al., 2015 *Nature chemistry*, 7, 4, 301.
- Pegues J. et al., 2021 *ApJ*, 911, 2, 150.
- Peslier A. H. et al., 2017 *Space Science Reviews*, 212, 1, 743.
- Petigura E. A. et al., 2018 *AJ*, 155, 2, 89.
- Pfalzner S. et al., 2014 *ApJL*, 793, 2, L34.
- Pian E. et al., 2017 *Nature*, 551, 7678, 67.
- Piani L. et al., 2020 *Science*, 369, 6507, 1110.
- Pierens A. et al., 2013 *A&A*, 558, A105.
- Pinilla P. et al., 2012a *A&A*, 545, A81.
- Pinilla P. et al., 2012b *A&A*, 538, A114.
- Pinilla P. et al., 2017 *ApJ*, 845, 1, 68.
- Pinilla P. et al., 2020 *A&A*, 635, A105.
- Piso A.-M. A. et al., 2015 *ApJ*, 815, 2, 109.
- Plotnykov M. and Valencia D., 2020 *MNRAS*, 499, 1, 932.
- Poch O. et al., 2019 *EPSC-DPS Joint Meeting 2019*, vol. 2019, pp. EPSC-DPS2019-1527.
- Poch O. et al., 2020 *Science*, 367, 6483, aaw7462.
- Pontoppidan K. M. et al., 2005 *ApJ*, 622, 1, 463.
- Pontoppidan K. M. et al., 2008 *ApJ*, 678, 2, 1005.
- Pontoppidan K. M. et al., 2014 *Protostars and Planets VI* (H. Beuther, R. S. Klessen, C. P. Dullemond, and T. Henning), p. 363.
- Pontoppidan K. M. et al., 2019 *ApJ*, 874, 1, 92.
- Poteet C. A. et al., 2013 *ApJ*, 766, 2, 117.
- Prantzos N., 2003 *arXiv e-prints*, astro-ph/0301043.
- Price E. M. et al., 2021 *ApJ*, 913, 1, 9.
- Prodanović T. et al., 2010 *MNRAS*, 406, 2, 1108.
- Pu B. and Wu Y., 2015 *ApJ*, 807, 1, 44.
- Quinn S. N. et al., 2012 *ApJL*, 756, 2, L33.
- Quirico E. et al., 2016 *Icarus*, 272, 32.
- Rackham B. V. et al., 2018 *ApJ*, 853, 2, 122.
- Rafikov R. R., 2003 *AJ*, 125, 2, 942.
- Raymond S. N. and Izidoro A., 2017 *Icarus*, 297, 134.
- Raymond S. N. and Nesvorný D., 2020 *arXiv e-prints*, arXiv:2012.07932.
- Raymond S. N. et al., 2006a *Science*, 313, 5792, 1413.
- Raymond S. N. et al., 2006b *Icarus*, 183, 2, 265.
- Raymond S. N. et al., 2008 *MNRAS*, 384, 2, 663.
- Raymond S. N. et al., 2009 *Icarus*, 203, 2, 644.
- Raymond S. N. et al., 2010 *ApJ*, 711, 2, 772.
- Raymond S. N. et al., 2011 *A&A*, 530, A62.
- Raymond S. N. et al., 2012 *A&A*, 541, A11.
- Raymond S. N. et al., 2014 *Protostars and Planets VI* (H. Beuther, R. S. Klessen, C. P. Dullemond, and T. Henning), p. 595.
- Raymond S. N. et al., 2018a *MNRAS*, 479, 1, L81.
- Raymond S. N. et al., 2018b *arXiv e-prints*, arXiv:1812.01033.
- Raymond S. N. et al., 2022 *Nature Astronomy*, 6, 80.
- Reiter M., 2020 *A&A*, 644, L1.
- Ribas Á. et al., 2015 *A&A*, 576, A52.
- Richter K. et al., 2018 *Geochimica et Cosmochimica Acta*, 232, 101.
- Richter K. et al., 2019 *Meteoritics & Planetary Science*, 54, 6, 1379.
- Rimmer P. et al., 2019 *Geochemical perspectives letters*, 9, 38.
- Rimmer P. B. and Shorttle O., 2019 *Life*, 9, 1.
- Roederer I. U. et al., 2014 *AJ*, 147, 6, 136.
- Rogers J. G. and Owen J. E., 2021 *MNRAS*, 503, 1, 1526.
- Romanova M. M. and Lovelace R. V. E., 2006 *ApJL*, 645, 1, L73.
- Rosenthal A. et al., 2015 *Earth and Planetary Science Letters*, 412, 77.
- Rubin M. et al., 2019a *MNRAS*, 489, 1, 594.
- Rubin M. et al., 2019b *MNRAS*, 489, 1, 594.
- Rudnick R. and Gao S., 2014 *Amsterdam, NL: Elsevier*.
- Rudnick R. L. et al., 1998 *Chemical Geology*, 145, 3-4, 395.
- Ruttenberg K., 2003 *Treatise on geochemistry*, 8, 682.
- Sagan C., 1997 *Pale blue dot: A vision of the human future in space*, Random House Digital, Inc.
- Sagan C. and Mullen G., 1972 *Science*, 177, 4043, 52.
- Sakuraba H. et al., 2021 *Scientific Reports*, 11, 20894.
- Salinas V. N. et al., 2016 *A&A*, 591, A122.
- Santos N. C. et al., 2004 *A&A*, 415, 1153.
- Sasselov D. D. et al., 2020 *Science Advances*, 6, 6.
- Schiller M. et al., 2018 *Nature*, 555, 7697, 507.
- Schlecker M. et al., 2021 *A&A*, 656, A71.
- Schlichting H. E. and Mukhopadhyay S., 2018 *SSRv*, 214, 1, 34.
- Schlichting H. E. et al., 2015 *Icarus*, 247, 81.
- Schoonenberg D. and Ormel C. W., 2017 *A&A*, 602, A21.
- Schoonenberg D. et al., 2018 *A&A*, 620, A134.
- Schoonenberg D. et al., 2019 *A&A*, 627, A149.
- Schopf J. W., 2006 *Philosophical Transactions of the Royal Society B: Biological Sciences*, 361, 1470, 869.
- Schulze H. et al., 1997 *From Stardust to Planetesimals*, vol. 122 of *Astronomical Society of the Pacific Conference Series* (Y. J. Pendleton), p. 397.
- Schwartz S. R. et al., 2018 *Nature Astronomy*, 2, 379.
- Schwarz K. R. and Bergin E. A., 2014 *ApJ*, 797, 2, 113.
- Segura-Cox D. M. et al., 2018 *ApJ*, 866, 2, 161.
- Semenov D. and Wiebe D., 2011 *ApJS*, 196, 2, 25.
- Semenov D. et al., 2018 *A&A*, 617, A28.
- Shi J. R. et al., 2002 *A&A*, 381, 982.
- Shorttle O. et al., 2015 *Earth and Planetary Science Letters*, 427, 272.
- Shorttle O. et al., 2021 *Elements*, 17, 4.
- Shu F. H. et al., 1996 *Science*, 271, 5255, 1545.
- Simon J. B. et al., 2016 *ApJ*, 822, 1, 55.
- Simon J. B. et al., 2017 *ApJL*, 847, 2, L12.
- Singh S. K. et al., 2021 *Nature Communications*, 12, 2690.
- Sirono S.-i., 2011 *ApJ*, 735, 2, 131.
- Sirono S.-i. and Ueno H., 2017 *ApJ*, 841, 1, 36.
- Sleep N. H., 2005 *Metal Ions in Biological Systems, Volume 43-*

- Biogeochemical Cycles of Elements*, pp. 97–122.
- Sleep N. H., 2009 *Geochemistry, Geophysics, Geosystems*, 10, 11.
- Sleep N. H. and Blanpied M. L., 1992 *Nature*, 359, 6397, 687.
- Sleep N. H. and Zahnle K., 2001 *Journal of Geophysical Research: Planets*, 106, E1, 1373.
- Som S. M. et al., 2012 *Nature*, 484, 7394, 359.
- Som S. M. et al., 2016 *Nature Geoscience*, 9, 6, 448.
- Sousa S. G. et al., 2011 *A&A*, 533, A141.
- Sozzetti A. et al., 2009 *ApJ*, 697, 1, 544.
- Spadaccia S. et al., 2022 *MNRAS*, 509, 2, 2825.
- Speedie J. et al., 2022 *MNRAS*, 510, 4, 6059.
- Spite M. et al., 2011 *A&A*, 528, A9.
- Stammler S. M. et al., 2017 *A&A*, 600, A140.
- Steinpilz T. et al., 2019 *ApJ*, 874, 1, 60.
- Stern S. A. et al., 2019 *Science*, 364, 6441, aaw9771.
- Suárez-Andrés L. et al., 2016 *A&A*, 591, A69.
- Suárez-Andrés L. et al., 2017 *A&A*, 599, A96.
- Suárez-Andrés L. et al., 2018 *A&A*, 614, A84.
- Symonds R. B. and Reed M. H., 1993 *American Journal of Science (United States)*, 293, 8.
- Tagawa S. et al., 2021 *Nature communications*, 12, 1, 1.
- Tanaka H. and Ida S., 1999 *Icarus*, 139, 2, 350.
- Tanaka H. et al., 2002 *ApJ*, 565, 2, 1257.
- Tang H. and Dauphas N., 2012 *Earth and Planetary Science Letters*, 359, 248.
- Taquet V. et al., 2016a *MNRAS*, 462, S99.
- Taquet V. et al., 2016b *ApJ*, 821, 1, 46.
- Terada H. et al., 2007 *ApJ*, 667, 1, 303.
- Terquem C. and Papaloizou J. C. B., 2007 *ApJ*, 654, 2, 1110.
- Teske J. K. et al., 2014 *ApJ*, 788, 1, 39.
- Teske J. K. et al., 2019 *AJ*, 158, 6, 239.
- Tosi N. et al., 2017 *Astronomy & Astrophysics*, 605, A71.
- Trail D. et al., 2011 *Nature*, 480, 7375, 79.
- Tychoniec L. et al., 2020 *A&A*, 640, A19.
- Tyrrell T., 1999 *Nature*, 400, 6744, 525.
- Unterborn C. et al., 2020 *The Composition of Rocky Planets*.
- Unterborn C. T. et al., 2014 *ApJ*, 793, 2, 124.
- Unterborn C. T. et al., 2018 *Nature Astronomy*, 2, 297.
- Urey H. C., 1952 *Proceedings of the National Academy of Sciences of the United States of America*, 38, 4, 351.
- van Boekel R. et al., 2004 *Nature*, 432, 7016, 479.
- Van Clepper E. et al., 2022 *arXiv e-prints*, arXiv:2202.00524.
- van der Marel N. and Mulders G. D., 2021 *AJ*, 162, 1, 28.
- van der Marel N. et al., 2013 *Science*, 340, 6137, 1199.
- van der Marel N. et al., 2021 *arXiv e-prints*, arXiv:2108.07679.
- van Dishoeck E. F. and Bergin E. A., 2020 *arXiv e-prints*, arXiv:2012.01472.
- van Dishoeck E. F. et al., 2014 *Protostars and Planets VI* (H. Beuther, R. S. Klessen, C. P. Dullemond, and T. Henning), p. 835.
- van Dishoeck E. F. et al., 2021 *A&A*, 648, A24.
- van 't Hoff M. L. R. et al., 2017 *A&A*, 599, A101.
- van 't Hoff M. L. R. et al., 2018 *A&A*, 613, A29.
- van 't Hoff M. L. R. et al., 2021 *arXiv e-prints*, arXiv:2110.08286.
- van 't Hoff M. L. R. et al., 2020 *ApJ*, 901, 2, 166.
- Veras D. and Armitage P. J., 2006 *ApJ*, 645, 2, 1509.
- Visser R. et al., 2009 *A&A*, 495, 3, 881.
- Visser R. et al., 2015 *A&A*, 577, A102.
- Visser R. G. et al., 2021 *A&A*, 647, A126.
- Volk K. et al., 2020 *Ap&SS*, 365, 5, 88.
- Wada K. et al., 2013 *A&A*, 559, A62.
- Wade J. et al., 2017 *Nature*, 552, 7685, 391.
- Wadhwa M., 2008 *Reviews in Mineralogy and Geochemistry*, 68, 1, 493.
- Walker J. C. et al., 1981 *Journal of Geophysical Research: Oceans*, 86, C10, 9776.
- Walsh R. J., 2009 *Chemie der Erde / Geochemistry*, 69, 2, 101.
- Walsh C. et al., 2016 *ApJL*, 823, 1, L10.
- Walsh K. J. et al., 2011 *Nature*, 475, 7355, 206.
- Walton C. R. et al., In press *Earth Science Reviews*.
- Wang H. et al., 2017 *Science*, 355, 6325, 623.
- Wang J. and Fischer D. A., 2015 *AJ*, 149, 1, 14.
- Wang W. et al., 2009 *A&A*, 496, 3, 713.
- Wang W. et al., 2020 *ApJ*, 889, 2, 169.
- Ward W. R., 1997 *Icarus*, 126, 2, 261.
- Warren P. H., 2011 *Earth and Planetary Science Letters*, 311, 1, 93.
- Wasserburg G. J. et al., 1996 *ApJL*, 466, L109.
- Wasson J. T. and Kallemeyn G. W., 1988 *Philosophical Transactions of the Royal Society of London Series A*, 325, 1587, 535.
- Weidenschilling S. J., 1977 *MNRAS*, 180, 57.
- Weidenschilling S. J. et al., 1997 *Icarus*, 128, 2, 429.
- Westphal A. J. et al., 2009 *ApJ*, 694, 1, 18.
- Wetherill G. W. and Stewart G. R., 1989 *Icarus*, 77, 2, 330.
- Wettlaufer J. S., 2010 *ApJ*, 719, 1, 540.
- White W. et al., 2014 *Treatise on geochemistry*, 4, 457.
- Whittet D. C. B., 2010 *ApJ*, 710, 2, 1009.
- Wiechert U. et al., 2001 *Science*, 294, 5541, 345.
- Wierzchos K. and Womack M., 2017 *Central Bureau Electronic Telegrams*, 4464, 1.
- Wierzchos K. and Womack M., 2018 *AJ*, 156, 1, 34.
- Williams C. D. and Mukhopadhyay S., 2019 *Nature*, 565, 7737, 78.
- Williams D. A. et al., 1992 *MNRAS*, 258, 3, 599.
- Windley B. F., 1977 *Nature*, 270, 5636, 426.
- Winter A. J. et al., 2020 *Nature*, 586, 7830, 528.
- Womack M. et al., 1992 *ApJ*, 401, 728.
- Woodward C. E. et al., 2021 *The Planetary Science Journal*, 2, 1, 25.
- Wordsworth R., 2016 *Earth and Planetary Science Letters*, 447, 103.
- Wordsworth R. and Pierrehumbert R., 2013 *science*, 339, 6115, 64.
- Workman R. K. and Hart S. R., 2005 *Earth and Planetary Science Letters*, 231, 1-2, 53.
- Wu J. et al., 2018 *Journal of Geophysical Research: Planets*, 123, 10, 2691.
- Wyatt M., 2020 *Extrasolar Kuiper belts*, pp. 351–376.
- Xu R. et al., 2017 *ApJ*, 835, 2, 162.
- Xu S. et al., 2014 *ApJ*, 783, 2, 79.
- Yasui C. et al., 2010 *ApJL*, 723, 1, L113.
- Youdin A. N. and Goodman J., 2005 *ApJ*, 620, 1, 459.
- Young E. D., 2014 *Earth and Planetary Science Letters*, 392, 16.
- Zahnle K. J. and Carlson R. W., 2020 *Creation of a Habitable Planet*.
- Zhang J. et al., 2012 *Nature Geoscience*, 5, 4, 251.
- Zhang K. et al., 2015 *ApJL*, 806, 1, L7.
- Zhang K. et al., 2019 *ApJ*, 883, 1, 98.
- Zhang K. et al., 2020a *ApJL*, 891, 1, L16.
- Zhang K. et al., 2020b *ApJL*, 891, 1, L17.
- Zhang S. et al., 2018 *ApJL*, 869, 2, L47.
- Zhang Y., 2017 *Lunar and Planetary Science Conference*, 1964, p. 1499.
- Zhang Z. et al., 2019 *Earth and Planetary Science Letters*, 520,

164.

Zhu W. and Wu Y., 2018 *AJ*, 156, 3, 92.

Zhu Z. et al., 2019 *ApJL*, 877, 2, L18.

Ziurys L. M., 1987 *ApJL*, 321, L81.